Establishment of new assays of exosome purification and microRNA isolation and quantification

Dissertation

with the aim of obtaining a doctoral degree (Dr. rer. nat.)

at the Department of Biology

Faculty of Mathematics, Informatics and Natural Sciences

University of Hamburg

Submitted by

Magdalena Grunt

Hamburg, 2019

Reviewers of the dissertation:

Priv.Doz. Dr. Heidi Schwarzenbach

University Medical Center Hamburg-Eppendorf (UKE)

Institute of Tumor Biology

Campus Forschung N27

Martinistraße 52

20246 Hamburg

Prof. Dr. Julia Kehr

University of Hamburg

Faculty of Mathematics, Informatics and Natural Sciences

Department of Biology

Institute of Plant Science and Microbiology

Molecular Plant Genetics

Otto-Warburg-Haus

Ohnhorststr. 18

22609 Hamburg

A part of this thesis was already submitted to Nucleic Acids Research:

Grunt M., Failla A.V., Stevic I., Hillebrand T., Schwarzenbach H. „Establishment of new assays of exosome purification and microRNA isolation and quantification". Nucleic Acids Research

Delta System Solutions

Delta System Solutions GmbH
Rathochstr. 6a
81247 München

12 August 2019

Robert Muirhead MSc BEng CEng MIET
Delta System Solutions GmbH
Zentrum für Luft- und Raumfahrt ZLR I
Freiheitstrasse 120C
15745 Wildau
Germany

Reference: English Language Thesis Certification for Magdalena Grunt

To whom it may concern,

Magdalena Grunt, who was born on 17.01.1987 in Słupsk, Poland, is submitting her doctoral dissertation in English. The title of the thesis is "Establishment of new assays of exosome purification and microRNA isolation and quantification".

I hereby certify as a native English speaker that I have read this thesis and that the English language used in this thesis is sufficiently correct for submission.

Kind regards,

Robert Muirhead
Managing Director

Tel.: + 49 (0)3375 5921 3381
Email: robert.muirhead@delta-system-solutions.com

TABLE OF CONTENTS

LIST OF TABLES

LIST OF FIGURES

LIST OF ABBREVIATIONS

µg	microgram
µl	microliter
µm	micrometer
3´UTR	3′-untranslated regions
A	adenine
Ago2	argonaute 2
ANOVA	analysis of variance
APP	amyloid precursor protein
APS	ammonium peroxodisulphate
ATPase	adenosine triphosphatase
Bcl-2	B-cell lymphoma 2
BHQ-1	black hole quencher 1
bp	basepair
BSA	bovine serum albumin
C	cytosine
C. elegans	*Caenorhabditis elegans*
Ca^{2+}	calcium ion
$CaCl_2$	calcium chloride
CD	C_q differences
CD9, CD63, CD81	tetraspanins
cDNA	complementary DNA
CO_2	carbon dioxide
CPD	citrate-phosphate-dextrose
C_q	quantitation cycle
CV	coefficient of variance
ddH_2O	double-distilled water
ddPCR	digital droplet PCR
DGCR8	DiGeorge syndrome chromosomal [or critical] region 8

DMEM	Dulbecco’s modified Eagle’s medium
DNA	deoxyribonucleic acid
dNTP	nucleoside triphosphate
DPBS	Dulbecco’s phosphate buffered saline
DTT	dithiothreitol
dTTP	deoxythymidine triphosphate
E	efficiency
EDTA	ethylenediaminetetraacetic acid
EE	early endosome
EpCAM	epithelial cell adhesion molecule
ESCRT	endosomal sorting complex required for transport
EV	extracellular vesicle
Exo-L	large exosomes
Exo-S	small exosomes
FAM	carboxyfluorescein
Fas	cell surface death receptor, also known as APO-1 or CD95
FBS	fetal bovine serum
FITC	fluorescein isothiocyanate
fM	femtomolar
G	guanine
g	gravitational force equivalent
GAPDH	glyceraldehyde 3-phosphate dehydrogenase
GSCN	guanidinium thiocyanate
GTPase	guanosine triphosphatase
h	hour
HCl	hydrochloric acid
HDL	high density lipoprotein
HRP	horseradish peroxidase
HSD	honest significant difference

Hsp	heat shock protein
IDT	interdigitated transducers
ILV	intraluminal vesicle
kb	kilobase
kDa	kilodaltons
LDL	low density lipoprotein
LOD	limit of detection
M	molar
mg	milligram
MGB	minor groove binder
$MgCl_2$	magnesium dichloride
MGP	mannuronate-guluronate polymer
MHC	major histocompatibility complex
min	minute
MIQE	minimum information for publication of quantitative real-time PCR experiments
miR	microRNA
miRISC	miRNA/multiprotein complex
miRNA	microRNA
miRNA-seq	miRNA sequencing
mM	millimolar
mRNA	messenger RNA
MVB	multivesicular body
MWCO	molecular weight cut-off
N	any nucleotide
N/A	not applicable
NaCl	sodium chloride
ncRNA	non-protein coding RNA
nd.	not determinable
NGS	next generation sequencing

NLS	N-lauroylsarcosine sodium salt
nm	nanometer
NPM1	nucleophosmin 1
nt	nucleotide
NTA	nanoparticle tracking analysis NTA
NTC	no template control
PAA	polyacrylamide
PAGE	polyacrylamide gel electrophoresis
PBS	phosphate-buffered saline
PCR	polymerase chain reaction
PEG	polyethylene glycol
pg	picogram
PP	polypropylene
pre-miRNA	precursor miRNA
pri-miRNA	primary miRNA
PROSPR	precipitation of proteins with organic solvent
PrP^{C}	nornal prion protein
PrP^{Sc}	scrapie prion protein
PVDF	polyvinylidene fluoride
PVDF	polyvinylidene fluoride
qPCR	quantitative polymerase chain reaction
R^2	coefficient of the standard curve, linearity
RBP	RNA binding protein
RIP3	receptor interacting protein kinase 3
RIPA	radioimmunoprecipitation assay
RISC	RNA-induced silencing complex
RNA	ribonucleic acid
RNase	ribonuklease
rpm	revolutions per minute

RT	reverse transcription
RT-qPCR	quantitative reverse transcription polymerase chain reaction
SD	standard deviation
SDS	sodium dodecyl sulphate
SEC	size exclusion chromatography
sec	second
SNARE	soluble NSF (N-ethylmaleimide-sensitive factor) attachment protein receptor
SOD1	superoxide dismutase
TEI	Total Exosome Isolation Reagent
TEMED	tetramethylethylenediamine
TE PC	track-etch polycarbonate
™	trademark
TRBP	TAR (trans-activation response) RNA binding protein
TSG101	tumor susceptibility gene 101
U	unit
UNG	uracil-N-glycosylase
UV	ultraviolet
V	voltage
vs.	versus
ΔG	Gibbs free energy

SUMMARY

MicroRNAs (miRNAs) are released into the bloodstream by all types of cells, either as cell-free molecules or inside of extracellular vesicles (EVs), such as exosomes. Exosomes play an important role in cell-to-cell communication by transferring a selection of miRNAs which then can influence the recipient cell. The use of disease-specific signatures of miRNAs in exosomes has become promising for clinical applications, either as biomarkers or direct therapeutic targets.

The most commonly used technique for exosome isolation is ultracentrifugation, but it is time-consuming and requires an expensive equipment. The second method of choice for exosomes separation is based on the precipitation with polyethylene glycol (PEG). Though this technique is fast, easy and non-laborious, it struggles with contaminations of plasma proteins and precipitation chemicals. For miRNAs isolation, most protocols are based on the use of hazardous chemicals, such as phenol/chloroform or guanidine thiocyanate for sample lysis. For these reasons, I developed a new method for the enrichment of exosomes with a subsequent miRNA extraction from different cell-free fluids (plasma, serum, urine and cell culture supernatant), followed by an improved RT-qPCR. For all developed methods, I examined numerous reagents and parameters as well as combinations thereof. For exosome extraction, I established a new method which is based on the mannuronate-guluronate polymer (MGP) technique which entraps exosomes, and so avoids the co-precipitation of plasma proteins providing vesicles of high purity. For miRNAs isolation, I applied a combination of chaotropic and non-chaotropic salts in low concentrations that are not hazardous to the health and environment and supported a fast and efficient extraction. For RT-qPCR, I optimized the chemistry and TaqMan probe of a previously published stem-loop primer-based protocol. Those modifications led to an improved efficiency of the miRNAs quantification method that is now faster and cheaper.

Quantity and integrity of exosomes isolated by my new MGP-based extraction method were determined by Western Blot, Nanoparticle Tracking Analysis (NTA) and confocal microscopy. RNA extraction was verified by an Agilent Bioanalyzer and RT-qPCR. Sensitivity, efficiency, linearity, as well as repeatability and reproducibility of RT-qPCR were tested on serial dilutions of synthetic miR-16 and miR-142. These findings showed that my newly established procedure covering all steps of miRNA analyses measures the levels of either cell-free and exosomal miRNAs in plasma, serum and cell culture supernatant with high performance. In addition, I compared my approach with commercial

techniques comprising PEG-based exosome precipitation, phenol/chloroform-based miRNA isolation and original stem-loop primer-based miRNA quantification. The MGP-based exosome separation method was much more efficient than the PEG-based kit to isolate polystyrene beads, commercial exosome standards and exosomes in a high purity and void of contaminated proteins from plasma and serum. The amplification of miR-16 and miR-142 with my optimized method resulted in a higher efficiency, repeatability and reproducibility than the commercial kit.

In summary, the application of the whole package of my newly established assays (exosome extraction, miRNA isolation and RT-qPCR) for miRNA measurements in exosomal and cell-free fractions showed that my method provided congruent data and was not influenced by the source (plasma or serum) used for the analysis, whereas the commercial assay delivered different data for plasma and serum. Moreover, my approach confirmed previous findings, that miR-16 circulates mostly as a cell-free form, while miR-142 is rather present in the exosomal fraction.

ZUSAMMENFASSUNG

MikroRNAs (miRNAs) werden von allen Arten von Zellen in den Blutkreislauf freigesetzt, entweder als zellfreie Moleküle oder innerhalb von extrazellulären Vesikeln (EVs), wie Exosomen. Exosomen spielen eine wichtige Rolle in der Zell-zu-Zell Kommunikation, indem sie eine Auswahl von miRNAs von Zelle zu Zelle transferieren, die dann die Empfängerzelle beeinflussen können. Die Verwendung krankheitsspezifischer Signaturen von miRNAs in Exosomen ist für klinische Anwendungen vielversprechend geworden, und zwar entweder als Biomarker oder direkte therapeutische Zielmoleküle. Die am häufigsten verwendete Technik für die Isolierung von Exosomen ist die Ultrazentrifugation, sie ist jedoch zeitaufwendig und erfordert eine teure Ausstattung. Die zweite Methode der Wahl für die Extraktion von Exosomen basiert auf der Präzipitation mit Polyethylenglykol (PEG). Obwohl diese Technik schnell, einfach und unkompliziert ist, hat sie mit Kontaminationen von Plasmaproteinen und Fällungschemikalien zu kämpfen. Die meisten Protokolle für die Isolierung von miRNAs basieren auf der Verwendung toxischer Chemikalien wie Phenol/Chloroform oder Guanidinthiocyanat für die Probenlyse. Aus diesen Gründen entwickelte ich eine neue Methode zur Anreicherung von Exosomen mit anschließender miRNA-Extraktion aus verschiedenen zellfreien Flüssigkeiten (Plasma, Serum, Urin und Zellüberstand), gefolgt von einer verbesserten RT-qPCR. Für alle entwickelten Methoden untersuchte ich zahlreiche Reagenzien und Parameter sowie Kombinationen davon. Für die Exosomenextraktion habe ich eine neue Methode entwickelt, die auf der Technik des Mannuronat-Guluronat-Polymers (MGP) basiert, bei der Exosomen eingeschlossen werden und so die gleichzeitige Ausfällung von Plasmaproteinen vermieden wird, wodurch Vesikel mit hoher Reinheit extrahiert werden. Für die Isolierung von miRNAs habe ich eine Kombination von chaotropen und nicht-chaotropen Salzen in geringen Konzentrationen angewendet, die nicht gesundheits- und umweltgefährdend sind und eine schnelle und effiziente Extraktion unterstützen. Für die RT-qPCR optimierte ich die Chemie und die TaqMan-Sonde eines zuvor veröffentlichten Stamm-Loop-Primer-basierten Protokolls. Diese Modifikationen führten zu einer verbesserten Effizienz der miRNA-Quantifizierungsmethode, die jetzt schneller und billiger ist. Menge und Integrität der mit meiner neuen MGP-basierten Extraktionsmethode isolierten Exosomen wurden durch Western Blot, Nanopartikel-Tracking-Analyse (NTA) und konfokale Mikroskopie bestimmt. Die RNA-Extraktion wurde mit einem Agilent Bioanalyzer und RT-qPCR verifiziert. Empfindlichkeit, Effizienz, Linearität sowie

Reproduzierbarkeit der RT-qPCR wurden an Serienverdünnungen von synthetischem miR-16 und miR-142 getestet. Diese Daten zeigten, dass mein neu etabliertes Verfahren, das alle Schritte der miRNA-Analyse abdeckt, mit hoher Performanz die Spiegel zellfreier und exosomaler miRNAs in Plasma, Serum und Zellüberstand misst. Darüber hinaus verglich ich meinen Ansatz mit kommerziellen Techniken, die die PEG-basierte Exosomenfällung, die Phenol/Chloroform-basierte miRNA-Isolierung und die ursprüngliche Stamm-Loop-Primer-basierte miRNA Quantifizierung umfassen. Das MGP-basierte Exosomen-Verfahren war viel effizienter als das PEG-basierte Kit, um Polystyrolkügelchen, kommerzielle Exosomenstandards und Exosomen in hoher Reinheit und ohne kontaminierte Plasmaproteine aus Plasma und Serum zu isolieren. Die Amplifikation von miR-16 und miR-142 mit meiner optimierten Methode führte zu einer höheren Effizienz, Wiederholbarkeit und Reproduzierbarkeit als das kommerzielle Kit.

Zusammenfassend zeigte die Anwendung des gesamten Pakets meiner neu etablierten Assays (Exosomenextraktion, miRNA-Isolierung und RT-qPCR) für miRNA-Messungen in exosomalen und zellfreien Fraktionen, dass meine Methode kongruente Daten lieferte und nicht von der Quelle (Plasma oder Serum) beeinflusst wurde, während der kommerzielle Assay unterschiedliche Daten für Plasma und Serum lieferte. Darüber hinaus bestätigte mein Ansatz frühere Erkenntnisse, dass miR-16 hauptsächlich als zellfreie Form zirkuliert, während miR-142 eher in der exosomalen Fraktion vorhanden ist.

I. INTRODUCTION

Physiological events, such as apoptosis, necrosis and active secretion, release nucleic acids, such as DNA, RNA and microRNAs (miRNAs), into the blood circulation. Since their deregulated levels correlate with various benign and malignant diseases, these molecules may be a promising class of potential liquid biomarkers. They can be obtained in real-time from blood, and their analyses could, consequently, facilitate treatment decisions. Notably, miRNA screening in liquid biopsies may provide information on the aberrant signaling pathway that should be blocked by a chosen targeted therapy.

1. Release of nucleic acids into the bloodstream

1.1. Cell death

Apoptosis

Apoptosis is a programmed cell death which is triggered when DNA damage is irreparable. It is characterized by rounding up and shrinkage of the cell, causing the reduction of cell volume, condensation of the chromatin, nuclear DNA fragmentation, and plasma membrane blebbing without the loss of integrity (Mehal and Imaeda, 2010). All morphological changes accompanying this type of cell death are induced by the activation of caspase proteases, which are responsible for decomposition of the cell. Apoptosis comprises two main signalling pathways: the death receptor (extrinsic) and the mitochondrial (intrinsic) pathway. The first one occurs when cell-surface death receptors, such as Fas interact with their ligands. In contrary, the intrinsic pathway is initiated autonomously by the cell, and is triggered by pro-apoptotic proteins from the Bcl-2 family which induce permeabilization of the mitochondrial outer membrane (Green and Llambi, 2015).

Immediately after activation of the apoptotic process, the plasma membrane starts to bleb and releases vesicles, called apoptotic bodies. Vesicles formed during the apoptosis can have a different protein and lipid cargo, and therefore, pathophysiological effects that are distinct from those of vesicles actively released by cells. The process of bleb formation is regulated by the caspase 3-induced Rho kinase I, and is mediated by contractions of the actin-myosin cytoskeleton. Rho kinase I also controls the process of the nuclear material packing into the plasmalemma blebs (Boulanger Chantal M. et al., 2006). Finally, apoptosis ended in a collapse of the cell producing apoptotic bodies and cellular residues,

consisting of proteins, lipids, short DNA fragments (the so-called apoptotic DNA ladder) and RNA transcripts, including miRNAs (Schwarzenbach et al., 2014). Among the released cellular components, there are Argonaute 2 (Ago2) proteins and high density lipoproteins (HDL). Both of them can carry miRNAs, and thus, protect them from intracellular environment (Boon and Vickers, 2013; Schwarzenbach et al., 2011; Vickers et al., 2011).

Necrosis

Necrosis is a type of cell death also caused by irreparable cell damage, and is usually spontaneous and uncontrolled. However, recently it was demonstrated that signal transduction pathways and catabolic enzymes are involved in this type of cell death, therefore, it seems to be highly regulated (Golstein and Kroemer, 2007). Necrosis is characterized by increase in the cellular volume, swelling and loss of organelles structure, lack of chromatin condensation, plasma membrane rupture, and loss of intracellular contents (Green and Llambi, 2015; Mehal and Imaeda, 2010). There is at least one type of active necrosis induction, called necroptosis. Necroptosis can be provoked by several pathways, which lead to activation of the receptor interacting protein kinase 3 (RIP3). RIP3-dependent necrosis can be induced by the ligation of cell-surface receptors, cellular DNA damage or presence of double-stranded virus DNA in the cytosol upon virus infection (Green and Llambi, 2015). Finally, cells disintegrate releasing their content into the extracellular space, among others long DNA strands, RNA and miRNAs in complexes with RNA-binding proteins, e.g. Ago2 (Cortez et al., 2011).

1.2. Active cell release

Besides the cell death, cells can also actively release their content in a form of extracellular vesicles (EVs) containing DNA, mRNA, miRNAs, proteins and lipids (Figure 1) (Osteikoetxea et al., 2016). The content of EVs is specifically sorted and packed by the donor cell (Cesselli et al., 2018).

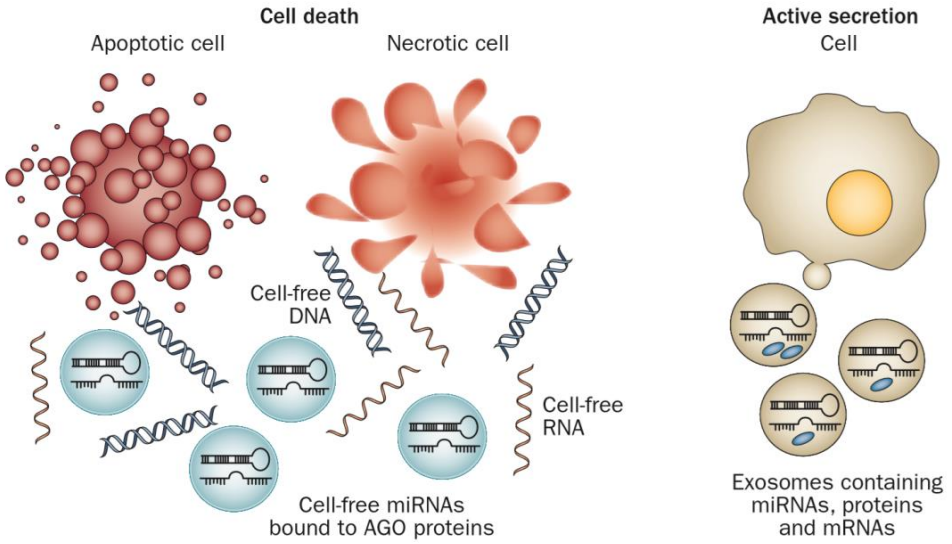

Figure 1: Mechanisms of the release of nucleic acids into the bloodstream (taken from Schwarzenbach et al., 2014)

There are three pathways of the release of nucleic acids from the cell into the extracellular space and subsequently into the bloodstream. Cell death, thus, apoptosis and necrosis release nucleic acids that circulate as cell-free molecules, in complexes with proteins, or inside of apoptotic bodies in the bloodstream. The third pathway relies on the active secretion of nucleic acids inside of EVs, such as exosomes, which can participate in the cell-to-cell communication.

2. Extracellular vesicles

EVs are small bubbles surrounded by a phospholipid membrane, and released by all cell types. They have been found in various body fluids, such as blood, urine, pleural effusions or saliva (Bayraktar et al., 2017). EVs are commonly divided into subgroups according to their size, mechanisms of their release, and their density. The most recent classification according to the EV size was presented by Zijlstra and di Vizio. They divided EVs into exomeres (~35 nm), small exosomes (Exo-S, 60-80 nm), large exosomes (Exo-L, 90-120 nm), microvesicles (≤1000 nm), exophers (~4 μm), migrasomes (≥1 μm) and large oncosomes (1-10 μm in diameter) (Figure 2) (Zijlstra and Di Vizio, 2018). A cell can release all classes of EVs.

Apart from heterogeneity of the EV size, they also display variations in their cargo. Different EV species exhibit different protein, lipid, DNA and RNA profiles (Bayraktar et al., 2017; Zhang et al., 2018; Zijlstra and Di Vizio, 2018). Recently, it has been proved that the heterogeneity of their cargo also affects a different organ-specific distribution of EVs, when injected into the blood of animals. The cargo of certain EVs species also variates between different cell types (Zhang et al., 2018). Thus, different classes of vesicles are

characterized by distinct nucleic acid profiles. However, reliable profiling of EVs, in particular exosomes and their cargo remains a challenge, because no optimized protocol is available, which allows to isolate exosomes of enough high purity and yield (Livshits et al., 2015).

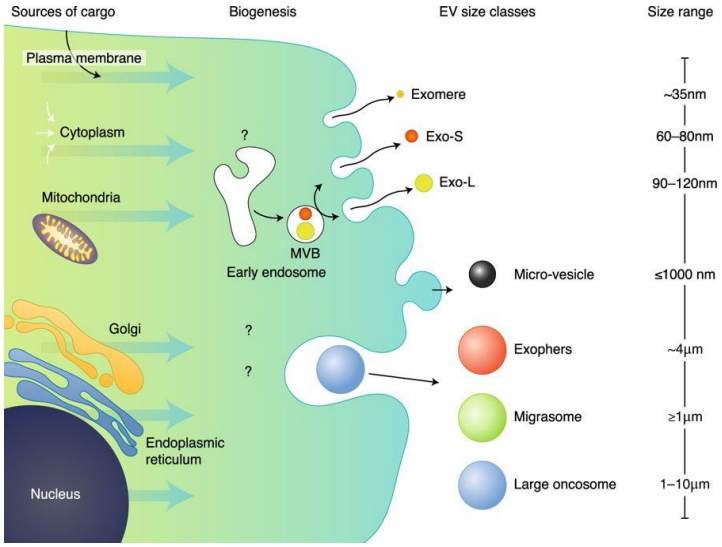

Figure 2: Classification of extracellular vesicles according to their size (taken from Zijlstra and di Vizio, 2018)

The recent classification of EVs is based on their size and includes exomeres, small and large exosomes, microvesicles, exophers, migrasomes and large oncosomes. To date, only the biogenesis of exosomes has been quite well defined, while the mechanism of release of other subclasses of EVs is largely unclear.

EVs are released from cells by diverse mechanisms (Zijlstra and Di Vizio, 2018). Cells under both physiological and pathological conditions shed EVs into the extracellular space, which can then be transported from a donor cell to an adjacent or a distant cell. Thus, EVs participate in the cellular communication. The EV content including among others miRNAs, can control many biological mechanisms, such as proliferation, angiogenesis, apoptosis, senescence, differentiation, immune signalling, and is involved in all benign and malignant diseases (Bayraktar et al., 2017; Li et al., 2017).

2.1. Exosome characteristics

Exosomes are the best characterized subpopulation of EVs. They are heterogenous, nanosized, phospholipid bilayer surrounded and non-self-replicating vesicles of endosomal origin. They are actively released by all cell types and can be detected in all body fluids. Although, at first, exosomes were considered as cellular waste, nowadays they are known to regulate an important event, notably to mediate the intercellular communication (Bayraktar et al., 2017; Kordelas et al., 2014; Zhang et al., 2018). Exosomes are enriched

in surface proteins, such as annexins, tetraspanins (CD9, CD63, CD81, CD82), and heat-shock proteins (Hsp60, Hsp70, and Hsp90). Moreover, the exosomal protein and lipid composition reveal their cellular origin, since exosomes carry the membrane from their origin cell (Bayraktar et al., 2017) (Figure 3). As already mentioned, there are 2 subpopulations of exosomes (Exo-S and Exo-L), which have different molecular and biophysical properties. Exo-S and Exo-L also contain diverse protein, lipid and nucleic acids profiles, and thereby possibly play different roles in the cell-to-cell communication (Zhang et al., 2018).

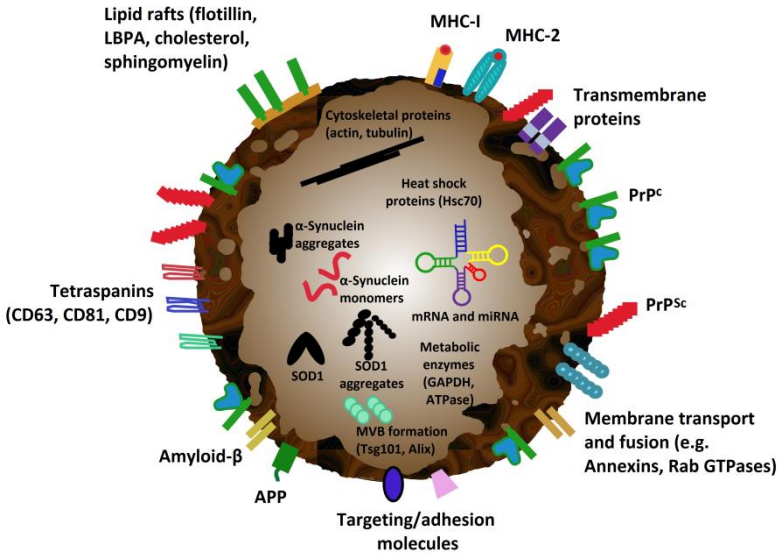

Figure 3: Schematic illustration of exosomal internal and external components (taken from Li et al., 2017; modified)

Most of exosomes display surface proteins that are common for all cell types from which they are released, and therefore, can serve as markers for the isolation and quantification of exosomes. Among those proteins are tetraspanins, flotilins, GTPases, heat shock proteins, membrane transport and fusion proteins, e.g. annexins, proteins involved in MVBs biogenesis, lactadherins, platelet derived growth factor receptors, transmembrane proteins and lysosome associated membrane protein-2B, or phospholipases. Besides, each exosome can harbor a specific set of proteins that reflect the origin cell type and its biological/physiological status. Moreover, exosomes contain nucleic acids, including DNA, mRNA and miRNAs, which are probably specifically incorporated during exosome biogenesis.

Despite increasing knowledge of the exosome content and biogenesis, it is still not well understood how the particular miRNAs are selective packaged into these vesicles and which mechanisms take part in this process. Probably, the sorting of miRNAs into exosomes is supported by RNA binding proteins (RBP). Ago2 might also be involved in this sorting mechanism, since it has been found near multivesicular bodies (MVBs) (Bebelman et al., 2018).

2.2. Exosome biogenesis

Exosomes, in contrary to the other microvesicles and apoptotic bodies, do not directly bud from the plasma membrane (Cesselli et al., 2018). The exosome biogenesis begins with the formation of an endosome from the plasma membrane. During the endosome maturation, the limiting membrane buds inward the endosome leading to the formation of intraluminal vesicles (ILVs). The endosomes containing ILVs are called multivesicular bodies (MVBs). After the maturation process, MVBs are either directed to lysosomes for degradation or to the plasma membrane, with which they fuse to release ILVs out of the cell as exosomes (Figure 4) (Bebelman et al., 2018; Bellingham et al., 2012; Raposo and Stoorvogel, 2013; Trajkovic et al., 2008).

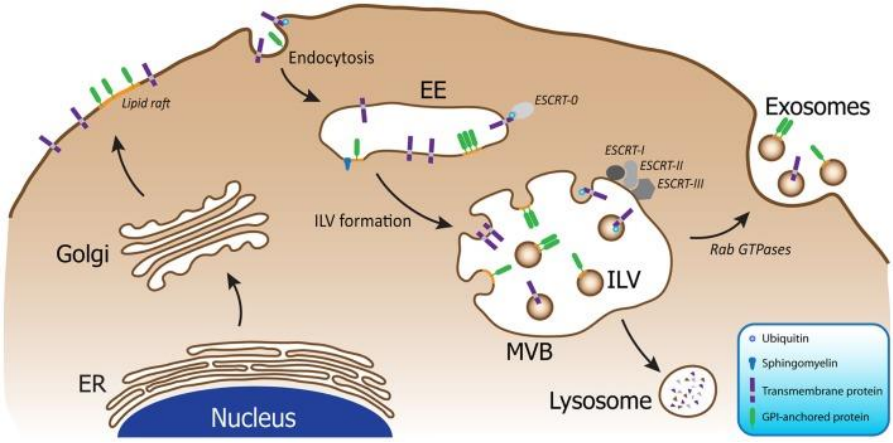

Figure 4: Exosome biogenesis (taken from Bellingham et al., 2012)
Exosome biogenesis starts from the endocytosis and formation of the early endosome (EE). Invagination of limiting membrane of the maturing endosome leads to packing the cargo into ILVs and to the formation of MVB. MVB together with its content can either be digested by a lysosome or be directed to the surface of the cell. The fusion with the plasma membrane leads to the release of ILVs into the extracellular space. Since this moment ILVs are called exosomes.

There are several pathways of MVB formation. A well described mechanism of the MVB biogenesis involves the Endosomal Sorting Complex Required for Transport (ESCRT) machinery. Sorting of the cargo and formation of ILVs require a consecutive action of different components of the ESCRT machinery. The process starts with the involvement of ESCRT-0 protein responsible for identification, preservation and accumulation of ubiquitinated proteins (the cargo) in the late endosomal membrane. Then, ESCRT-I/II cause the primary budding of the limiting membrane into the lumen of MVBs. ESCRT-III is responsible for involution of the limiting membrane into a neck. Subsequently, the ATPase VPS4 activates the final membrane detachment and formation of ILVs which are

released into the MVB lumen (Figure 5) (Bebelman et al., 2018; Henne et al., 2011; Raposo and Stoorvogel, 2013; Schöneberg et al., 2017).

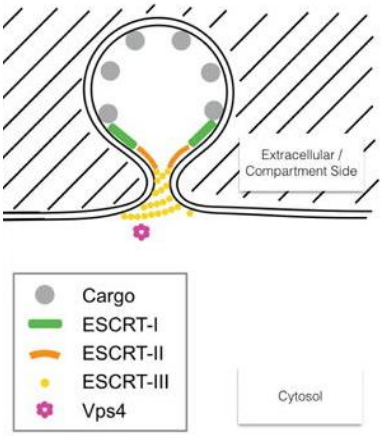

Figure 5: Budding of ILVs mediated by the ESCRT machinery (taken from Schöneberg et al., 2017; modified)

The cargo previously organized by ESCRT-0 is concentrated on the bottom of the inward bud created by ESCRT-I/II. ESCRT-III causes the constriction of the membrane neck, and ATPase VPS4 is subsequently responsible for the scission of the bud to complete vesicle formation.

An alternative mechanism of MVB formation is independent of the ESCRT machinery. It is the lipid raft-based segregation into micro-domains which contain a large number of sphingolipids. Trajkovic et al. showed that the sphingolipid ceramide, formed by hydrolytic removal of the phosphocholine moiety of sphingomyelin by sphingomyelinases, elicits the invagination of the limiting membrane into the lumen of MVBs. This mechanism is accomplished by the transformation of micro-domains into larger domains, leading to the domain-induced negative membrane curvature (Trajkovic et al., 2008).

It is still little known about the mechanisms involved in directing MVBs to the cellular surface, MVB docking, and fusion with the plasma membrane. These processes require the interaction of actin and microtubules of the cytoskeleton and are driven by kinesins and myosins. Finally, the molecular switches that are mediated by small GTPases, SNARE and tethering factors trigger the fusion with the plasma membrane. To date, different activators of exosome release have been found in different cell types, like plasma depolarization in neuronal cells, activation by liposaccharides in dendritic cells and thrombin receptor activation in platelets. However, there is one common activator for exosome shedding – the elevated intracellular Ca^{2+} concentration (Raposo and Stoorvogel, 2013).

2.3. Exosome cell-to-cell communication

Several cell-to-cell communication mechanisms have been described: the direct contact between cells, the interaction between signalling molecules and surface receptors on adjacent cells, the interplay between hormones and distinct cells, and the involvement of neurotransmitters via synapses and cells (Li et al., 2017; Valadi et al., 2007). Previously, another way of exchanging information between cells was discovered, namely the exosome shuttle. Exosomes circulating in body fluids can, thus, be uptaken by particular recipient cells in close or distant sites and can influence the behaviour of the host cell (Cesselli et al., 2018).

In 2012, Monteclavo et al. demonstrated that the exosome membrane can directly fuse with the plasma membrane of a recipient cell leading to release of the exosome content into the cytosol (Montecalvo et al. 2012). Another mechanism of exosome uptake is based on the endocytose of exosomes, trapping in cytosolic vesicles and transport to the perinuclear region (Tian et al. 2010). It is probable, that the exosome membrane fuses with the membrane of cytosolic vesicles, or exosomal proteins create pores in the limiting membrane of endocytic compartments to release the exosomal content into the cytosol (Bellingham et al. 2012).

Cells release exosomes to transfer various molecules to recipient cells. It has been demonstrated that exosomes can be used by cells to transfer their mRNAs and miRNAs to recipient cells, and upon the release into the recipient cell, those RNAs remain functional. Moreover, it seems that numerous of RNAs are selectively and exclusively packed into exosomes, and act as intercellular signals (Bayraktar et al., 2017; Escrevente et al., 2011; Valadi et al., 2007).

Apart from RNAs, exosomes are also responsible for the intercellular transport of proteins and pathogens, such as prions responsible for diseases, e.g. Creutzfeldt-Jakob, Alzheimer and Parkinson (Bellingham et al., 2012). Depending on their origin, exosomes can exhibit immune stimulatory or inhibitory functions (Kordelas et al., 2014). Thus, exosomes are involved in multiple biological and pathological processes.

Exosomes play a role in stroma-to-tumor and tumor-to-tumor cell communication, and thus, propagate cancer by transferring their oncogenic cargo from cell to cell (Nabet et al., 2017; Sansone et al., 2017; Zhang et al., 2015). Increased levels of exosomes are associated with tumor progression and metastasis (Hikita et al., 2019; Rajagopal and Harikumar, 2018).

2.4. Exosome isolation techniques

Differential centrifugation methods

Differential centrifugation is a method commonly used for separation of particles, such as organelles, viruses, proteins or nucleic acids, which differ by size and density. It comprises repeated centrifugation steps distinguished by an increasing speed and time, resulting in a consecutive separation of particles according to their weight and density (Li et al., 2017; Livshits et al., 2015). The particles of all sizes are usually equally distributed within the tube, but some smaller particles, that are closer to the bottom of the tube, can also be co-sedimented with bigger particles (Livshits et al., 2015; Witwer et al., 2013). Therefore, differential centrifugation is only efficient if particles differ significantly in their size. The successive differential centrifugation of exosomes results in consecutively fractioning cells, cell debris, bigger EVs, and finally exosomes (Livshits et al., 2015). A typical protocol for differential centrifugation includes the following steps: 1) 10 min at 300 g to pellet cells, 2) 10 min at 2,000 g to sediment cellular debris and apoptotic bodies, 3) 30 min at 10,000 g to pellet bigger EVs, 4) 70 min at 100,000 g to pellet exosomes, and 5) 70 min at 100,000 g to remove impurities (including proteins) from the resuspended exosome pellet (Figure 6) (Li et al. 2017; Livshits et al. 2015; Théry et al. 2006).

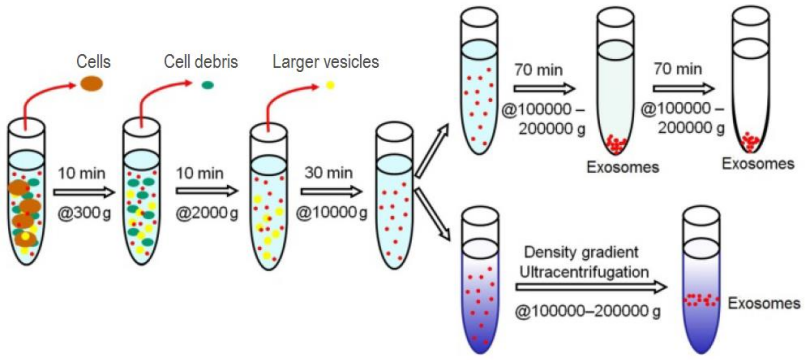

Figure 6: Schematic representation of differential centrifugation to obtain exosomes (taken from Li et al., 2017; modified)

After the first centrifugation step at 300 g, the supernatant is free of cells. The following centrifugation steps at 2000 g and 10000 g lead to the removal of cell debris and bigger vesicles, respectively. Subsequently, the supernatant is ultracentrifuged to collect the exosome fraction.

Remaining impurities and decreased yield of the isolated exosomes can be caused by the similarity in sedimentation properties of the different EV subgroups, by applying the same protocols for different types of rotors, and without considering the sample viscosity

(Livshits et al., 2015). Furthermore, ultracentrifugation can also cause vesicles aggregation (Linares et al., 2015).

Besides the classic ultracentrifugation, the discontinuous density gradient ultracentrifugation can also be applied for the separation of exosomes. This ultracentrifugation separates particles according to their density. Here, the ultracentrifugation tube is filled with layers of a matrix that density increases in the direction to the bottom of the tube. The sample containing the exosomes is applied as a narrowed layer on the top of the matrix, and then ultracentrifuged for an extended time. Particles of different densities move in the direction to the bottom of the tube with different sedimentation rates, and form individual zones. The exosomes located in a fixed interface between the specific matrix density layers do not move further, and can be easily collected after the centrifugation (Figure 7). This type of density gradient centrifugation is called as isopycnic because particles of a certain density are immobilized along the matrix layer of the same density (Li et al., 2017).

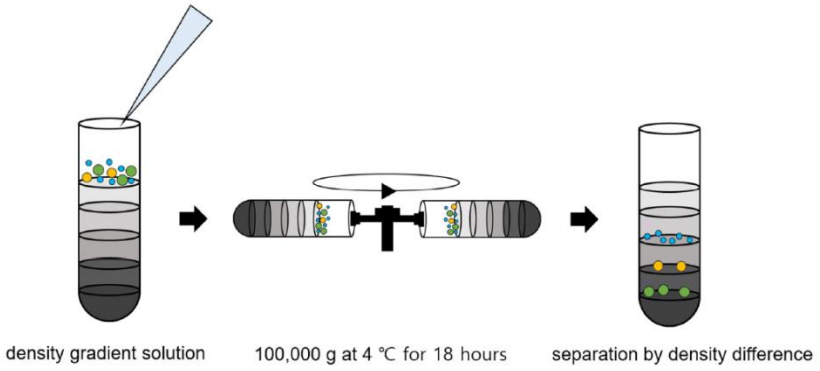

Figure 7: Exosome isolation by the isopycnic density gradient ultracentrifugation (taken from Yoo at al., 2018; modified)

First, the sample containing the exosomes and other EVs (shown as coloured balls) is applied on the top of the matrix consisting of multiple layers of different densities. After ultracentrifugation, the EVs are distributed to the layers that refer to their density, e.g., exosomes form an interface above the matrix layer that density corresponds to the density of the exosomes.

There is still another type of gradient density ultracentrifugation, called moving-zone ultracentrifugation. This technique, in contrary to the isopycnic density gradient centrifugation, is based on the separation of particles according to their size and mass, and allows separating vesicles that differ by mass, but display similar densities. The matrix of the tube has a lower density than any of a solute applied. Therefore, during centrifugation, particles do not stop moving at a certain density, but continue moving in the direction to the bottom of the tube. For this reason, the time of centrifugation has to be exactly

adjusted. Since the size and density of exosomes partially overlap with other EVs, the differential centrifugation is often combined with a further gradient density ultracentrifugation step to increase the purity of the isolated exosomes and decrease their loss (Li et al., 2017).

Size-dependent separation techniques

One of the simplest methods of exosomes isolation is ultrafiltration. Ultrafiltration is a membrane-based technique of separating particles according to their size or molecular weight. Exosomes are concentrated or separated by filtrating them through membranes with a defined size of pores or a molecular weight cut-off by applying pressure, centrifugation or vacuum forces. This method is relatively fast and does not require specialized equipment. However, it should be considered that by applying too high forces some exosomes may undergo deformation or breakage (Li et al., 2017). The use of filters harbouring pores with decreasing diameters, e.g, 0.65, 0.45, 0.22 and 0.1 μm, allows a selective isolation of individual fractions of EVs. Nonetheless, some exosomes can pass through the membrane, although the size of the pores should exclude and retain them on the filter. Contrariwise, some exosomes can also be lost together with bigger vesicles using a membrane with bigger pores. Ultrafiltrated exosomes often contain contaminations of non-exosomal proteins which are caused by the affinity of diverse proteins to the membrane material. Concentrated particles may also block pores of the membrane and do not allow smaller molecules to pass through them. Additionally, some exosomes may also stably bind to the filter, therefore it is necessary to implement an additional washing step for a proper recovery (Konoshenko et al., 2018; Witwer et al., 2013).

The sequential filtration technique relies on 3 consecutive steps. In the first step, a sample is passed through a 0.1-μm membrane filter to remove vesicles bigger than the cut-off of the filter. However, bigger and flexible vesicles can possibly pass through it at this stage. Then, the filtrate from the first step is subjected to the quintuple tangential flow filtration using hollow fibers of a molecular weight cut-off of 500 kDa. The aim of this step is to remove the majority of proteins, and to concentrate the exosomes. Finally, the retentate is filtrated through a 0.1 μm track-etch membrane to remove particles bigger than 100 nm in diameter (Figure 8) (Heinemann et al., 2014; Yoo et al., 2018).

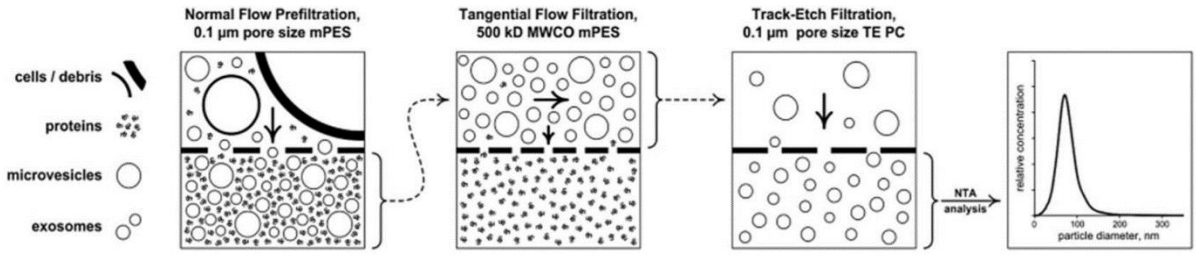

Figure 8: The principle of 3-step sequential filtration for the exosome isolation (taken from Yoo et al., 2018)

First, the sample is filtrated through a 0.1 µm filter to deplete cells, cell debris and bigger EVs. Second, the protein contaminants are removed by a tangential flow filtration. Then, the retentate is filtrated through a 0.1 µm track-etch filter to separate exosomes from bigger EVs.

Size exclusion chromatography (SEC) is a method of separation of particles of different size on a column filled with a material called stationary phase or adsorbent. The stationary phase consists of fine porous resin particles and has a pore size depending on the application. The sample is applied on the top of the stationary phase, is covered by an elution buffer, and migrates through the column provoked by the gravity force or a vacuum pump. During migration, smaller particles enter inside the pores of the resins, slowing their movement. Bigger particles, which cannot enter inside the pores, migrate between the grains of resins. During this procedure, fractions of a defined volume are collected from the bottom outlet of the column: the biggest particles, thus the biggest EVs are eluted in the first fractions, and the smaller particles, e.g. exosomes appear in the following fractions (Figure 9). Proteins of a small size that enter the pores of resin have the longest retention time and are eluted in the last fractions. The volume of a processed sample depends on the volume and diameter of the SEC column. SEC is able to separate exosomes of a high purity, but also dilutes them since the column is continuously covered with elution buffer until all particles are recovered. However, to narrow the volume, SEC can be combined with a further ultrafiltration step (Benedikter et al., 2017).

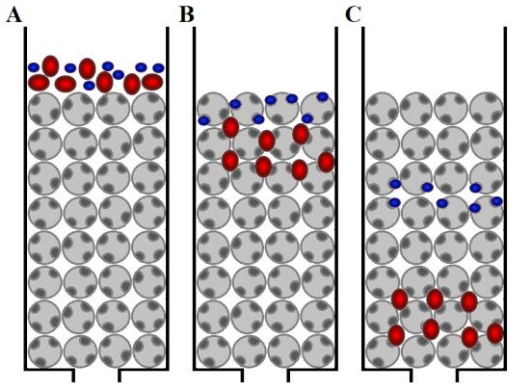

Figure 9: Principle of the size exclusion chromatography

A) A SEC column is filled with porous polymeric material (grey balls). The sample containing different sizes of particles (blue and red balls) is loaded on the top. B) Particles move through the column with different speed. Smaller particles (blue) move slower, because they enter the pores of resin beads, while bigger molecules (red) pass between the resin beads. C) The particles are fractionated in earliest fractions containing the bigger particles and later fractions containing smaller particles.

Affinity capture methods

Exosomes expose on their surface a number of various protein markers, e.g. tetraspanins (CD9, CD63, CD81), heat shock proteins, EpCAM and MHC antigens, as well as lipids and polysaccharides. There are multiple possibilities to separate exosomes using various affinity molecules, such as antibodies, lipid-binding proteins or lectins. Basically, the affinity molecules are coupled on a solid phase, including magnetic beads, membrane affinity filters, cellulose filters, plastic surfaces or highly porous monolithic silica microtips. Prior to the affinity separation, exosomes can be pre-isolated by precipitation techniques or ultracentrifugation. Then, the pre-isolated exosomes are incubated, allowing the interaction of the exosomal markers with specific immobilized affinity molecules leading to e.g. an antibody-ligand binding (Konoshenko et al., 2018).

An exemplary application of an affinity capture is the use of magnetic beads conjugated to monoclonal antibodies specific to proteins exposed on an exosomal membrane (Figure 10). Antibody-coated magnetic beads are added to the sample and incubated for several hours to allow binding between antibody and antigen, resulting in attaching exosomes to the surface of magnetic beads. Subsequently, a magnetic field is used to separate the magnetic bead-exosome conjugates from the sample (Greening et al., 2015; Théry et al., 2006). With this method, exosomes can be isolated either after pre-enrichment, e.g. with precipitation methods (Oksvold et al., 2015), or directly from an unprocessed sample, e.g. cell culture supernatant (Jeppesen et al., 2019).

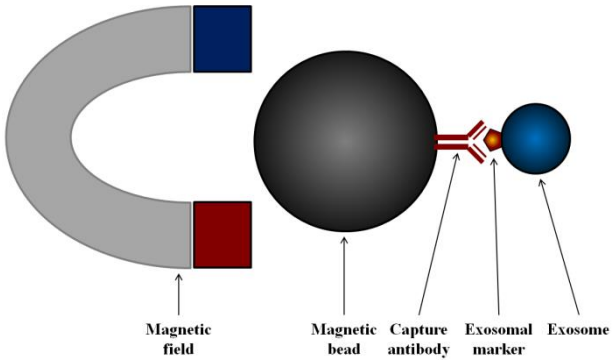

Figure 10: Immuno-magnetic extraction of exosomes

The magnetic beads are coupled with a capture antibody specific for an exosomal surface marker. After adding the sample, exosomes are caught via their marker by the antibody. The magnetic field is applied to pellet the magnetic beads and thus, separate the captured exosomes from the sample.

Affinity-based capture methods are relatively fast and simple, and allow isolating specific types of exosomes. Disadvantages can be that the solid phase may exhibit properties of a nonspecific binding of molecules different from the exosomes intended to extract, and that the separated exosomes cannot be easily eluted from the complexes of their affinity molecules, influencing their downstream applications, such as Western Blot, RT-qPCR, flow cytometry or electron microscopy (Konoshenko et al., 2018).

Microfluidic isolation techniques

This technology was developed in the 1980s, on the basics of microelectronics, and material and process engineering from a semiconductor industry. Microfluidics-based devices (called also chips or lab-on-chips) are compact and precise panels combining a network of channels of different microscale diameters. Depending on the application, these channels can be connected with each other and also with other specific units moderating the flow of the fluids supplied. Microfluidic devices allow reducing the process down to the microscale, and hence, decreasing the sample and reagent volumes from milliliters to microliters, and the procedure time from hours to seconds (He and Zeng, 2016). They were successfully adopted for the isolation of exosomes from different biological fluids, and are based on immunoaffinity capture, microporous filtration (sieving), trapping on porous micropillars or nanowires, or acoustic nanofiltration (Batrakova and Kim, 2015; Liga et al., 2015).

First, immunoaffinity-based chips were created for the exosome separation in 2010 by Chen et al. (Chen et al., 2010). Briefly, a sample is passed through microchannels which

are coated with an antibody against a selected exosomal marker. The exosomes representing the specific marker on their surface are captured and immobilized on the microfluidic device, leading to their separation from other membrane particles, proteins and lipids. After several washing steps, the immobilized exosomes can be characterized *in situ* by fluorescence measurement or plasmonic sensors, or lysed for nucleic acid isolation (Liga et al., 2015).

Microporous filtration-based chips can even separate exosomes from a whole blood sample. This type of a chip employs a filtration through a porous membrane driven by pressure or electrophoresis. The pressure driven filtration is less time consuming, and by applying electrophoresis a higher purity of isolated exosomes is reached, since phospholipidic vesicles have a lower negative charge and are more affected by the electric field than contaminating proteins (Figure 11) (Davies et al., 2012; Liga et al., 2015).

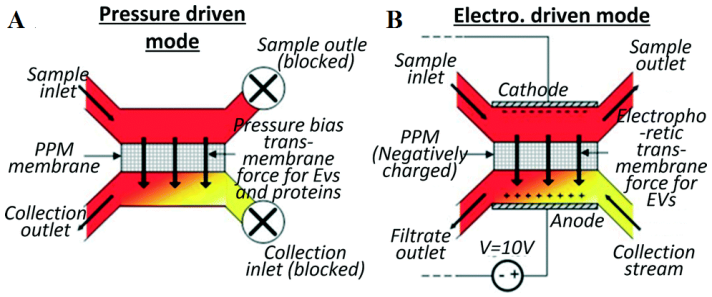

Figure 11: Principles of two types of microporous filtration-based microfluidic isolation techniques (taken from Liga et al., 2015)

A) Filtration through a porous membrane driven by pressure applied on an on-chip dead end filter. B) Electrophoresis-driven filtration. Transmembrane migration of negatively charged EVs, such as exosomes, under the applied voltage.

Microfluidic devices with porous microstructures able to selectively separate exosomes from other EVs and proteins according to their size were introduced in 2013 by Wang et al (Wang et al., 2013). These chips are made of porous silicon nano-wires etched in the sidewalls of micropillars. They can selectively capture vesicles at the size of 40-100 nm in just 10 min. However, for a further characterization of the intact exosomes, an overnight step is necessary to dissolve the silicon nano-wires and release the trapped vesicles , significantly increasing the total procedure time (Liga et al., 2015; Wang et al., 2013).

Microfluidic devices utilizing acoustic nanofiltration can be applied for a rapid, non-contact, label-free and size-tuneable separation of exosomes from sample volumes as small as 5-10 µl (Evander et al., 2015; Lee et al., 2015). Depending on the EV size and density,

ultrasound standing waves exert differential acoustic forces on EVs, leading to their fractionation (Figure 12) (Lee et al., 2015).

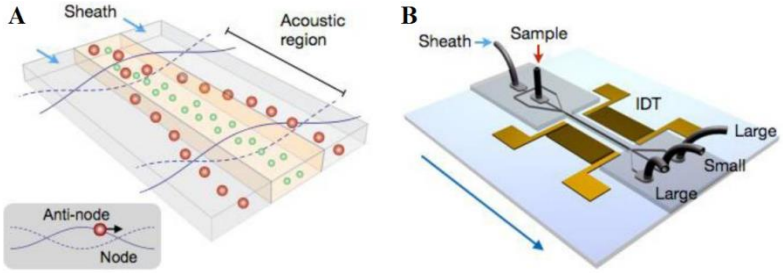

Figure 12: In-flow size-fractionation of EVs by an acoustic microfluidic device (taken from Lee et al., 2015)

A) Principle of chip operation. A sample containing vesicles of various sizes enters the acoustic region where the acoustic radiation pressure moves them towards nodes of the acoustic pressure region. The acoustic force is proportional to the EV volume, therefore, bigger EVs move faster to the pressure nodes than smaller ones. They are removed by sheath flows on both node regions. Smaller EVs remain in the centre flow. B) Schema of an acoustic microfluidic device. Two interdigitated transducers (IDT) electrodes create a standing surface acoustic wave across the flow direction. Smaller EVs are eluted in the outlet of the central channel, while bigger vesicles flow out of both lateral outlets.

To summarize, isolation of exosomes by microfluidic devices requires a shorter time and lower amounts of samples and reagents. It is possible to combine the isolation with a subsequent analysis of exosomes. Disadvantages limiting the utility of microfluidics chips are low exosomes yields, as well as channels blockage by the sample.

Precipitation-based methods

Polyethylene glycol (PEG) is a water soluble polymer that since decades is well known for its capabilities to precipitate proteins, nucleic acids, viruses and other small molecules in body fluids and other complex mixtures (Lis, 1980; Polson et al., 1964; Yamamoto et al., 1970). In the years 2014 till the first half of 2017, it was, after the ultracentrifugation, the second method of choice (26.4% of all original research papers) used to isolate exosomes (Konoshenko et al., 2018). PEG-based commercial kits, such as ExoQuick™ or Total Exosome Isolation™ are dedicated for specific body fluids or cell culture supernatants, and for a rapid isolation of relative high quantities of exosomes. However, PEG of different molecular weights and concentrations can be used directly, and is much cheaper than the commercial kits (Andreu et al., 2016; Rider et al., 2016; Weng et al., 2016). Briefly, PEG ties up water molecules, and reduces the solubility of suspended particles, causing their precipitation (Konoshenko et al., 2018; Li et al., 2017). The procedure of PEG-based

isolation of exosomes involves the following steps: mixing and incubation of PEG with the sample, pulling down the precipitate by low-speed centrifugation, and resuspension of precipitated exosomes in an appropriate buffer (Helwa et al., 2017; Karttunen et al., 2019; Sanz-Rubio et al., 2018; Van Deun et al., 2014). However, to isolate exosomes with less protein contaminations, either a further second precipitation with PEG or an ultracentrifugation step is necessary after the first exosome precipitation.

The method of protein purification by organic solvents is known since almost a century (Piettre and Vila, 1920). In this respect, the isolation of exosomes based on the precipitation of proteins with organic solvent (PROSPR) was recently proposed. This technique relies on the protein aggregation in the presence of acetone and the detainment of hydrophobic exosomes in the supernatant (Gallart-Palau et al., 2015). Briefly, the sample is mixed with a quadruple volume of cold acetone and centrifuged for 1 min at 3,000 g. The pellet containing the protein precipitate is discarded, and the supernatant containing exosomes is concentrated in a vacuum concentrator or by filtration through a 300 kDa filter. Then, the vacuum-dried pellet can be used directly for downstream applications (Gallart-Palau et al., 2015).

Precipitation techniques are fast, easy, scalable, and do not require specialized equipment or advanced technical knowledge (Batrakova and Kim, 2015). However, they struggle with several disadvantages. The isolated exosomes often contain non-soluble protein aggregates and polymers or chemicals used for the precipitation which might affect further analysis and the biological activity of exosomes (Konoshenko et al., 2018; Liga et al., 2015). For example, soluble proteins may interfere with downstream proteomic analyses of the exosomes. The total protein contents in isolated exosomes obtained by PEG-precipitation, PROSPR and SEC were compared by Gámez-Valero et al. by measuring the protein-specific absorbance at 280 nm. They found that PEG-precipitation resulted in the highest total protein quantity of ~21 mg, followed by the PROSPR protein yield of ~4 mg, and the undetectable protein content in the first SEC fractions (containing EVs), since most of soluble proteins are eluted in later SEC fractions (Gámez-Valero et al., 2016). Other experiments demonstrated that exosomes isolated by PEG-based kits (ExoQuick™ and Total Exosome Isolation™) co-precipitated up to 8-times more proteins than ultracentrifugation (Van Deun et al., 2014). Possibly, the excess of co-precipitated proteins and precipitation reagents may impede the detection of some exosomal markers by altering and masking their epitopes. Numerous experiments have demonstrated that precipitation-based techniques co-precipitate not only plasma proteins (albumin, apolipoprotein E) but

also cell-free riboprotein complexes, such as Ago2 (Arroyo et al., 2011; Liga et al., 2015) or HDL complexes (Vickers et al., 2011), affecting profiling of the exosomes content by simultaneous quantification of vesicle-free nucleic acids (Huang et al., 2013; Karttunen et al., 2019; Turchinovich et al., 2011; Van Deun et al., 2014). Moreover, it has been demonstrated that precipitation causes difficulties in the visualization of exosomes by cryo-electron microscopy. Exosomes isolated by PEG could not be visualized at all because dense aggregates contaminated the solution, while exosomes isolated by PROSPR changed their native structure and appeared to be merged in concentric multi-layer vesicles, probably a result of vesicular fusion (Gámez-Valero et al., 2016). Acetone has been ascribed to have a degradative influence on membranes increasing their fluidity, and probably causes the exosome membranes to merge (Posokhov and Kyrychenko, 2013). Furthermore, the administration of cell cultures with exosomes isolated by PEG or PROSPR can reduce the viability of the cultured cells, owing by the modifications of exosome properties and functions.

Table 1: Comparison of different exosome isolation approaches

Method	Advantages	Disadvantages
Differential centrifugation: ultracentrifugation	• isolation from large sample volumes • only a few reagents and consumables required	• time-consuming • expensive equipment required • trained personal required • no standardized protocol and low reproducibility • a low number of samples can be processed simultaneously • damage of exosomes • loss of exosomes • co-sedimentation of proteins and protein aggregates • aggregation of exosomes
Differential centrifugation: density gradient ultracentrifugation	• a higher purity than a standard ultracentrifugation • less protein aggregation than a standard ultracentrifugation • better morphological properties of exosomes than a standard ultracentrifugation	• time-consuming • complex and laborious • expensive equipment required • loss of exosomes • co-isolated EVs, proteins and viruses of a density similar to exosomes
Ultrafiltration	• fast • easy • no specialized equipment required • a possible parallel processing of multiple samples • unlimited sample volume	• loss of exosomes, lower yield than obtained by ultracentrifugation • contamination with proteins • possible exosome damage or deformation • possible membrane affinity • plugging of filter

Size exclusion chromatography	• fast • high reproducibility • high purity • no loss of exosomes • low content of non-exosomal proteins • little risk of aggregation • exosomes preserve their integrity and biological activity • scalable to process larger volumes (column diameter) and distinction of vesicles of close sizes (column length)	• complex • expensive • specialized equipment required • one sample can be processed at once • pretreatment and pre-concentration of exosomes required • processed sample volume should not exceed 1 ml of a 15-ml column volume • not efficient for diluted input material • exosomes are highly diluted • separation of large protein complexes, like LDL in the exosomal fractions
Affinity capture	• high purity • exosomes uniform in morphology, size and protein content • devoid of contamination with proteins of non-exosomal origin • possible to isolate tissue-specific exosomes • possible to scale up to 96 samples to process at once	• expensive • small amount of isolated exosomes • potential non-specific binding of exosomes and contaminants by solid material used • potential limitation of specificity of antibodies • difficult to separate exosomes from antibodies
Microfluidic isolation	• very fast • high purity • high efficiency • low amounts of samples and reagents • possible simultaneous isolation and analysis of exosomes on one chip/in one run • possible automation	• expensive • complex devices • low sample input and exosome yield • analyzed sample can block the channel
Precipitation	• fast • easy • no specialized equipment required • low cost by using in-house protocol • high quantity of isolated exosomes • no exosome deformation • scalable	• poor reproducibility • high costs of commercial kits • loss of properties and integrity of exosomes • co-precipitation of proteins of non-exosomal origin • contamination with chemicals used for precipitation • impeded detection of exosomal markers • hampering of microscope visualization • precipitated exosomes reduce viability of cultured cells

3. MicroRNAs

3.1. MicroRNA characteristics

MiRNAs are a class of small non-protein coding RNAs (ncRNAs) of 19–25 nucleotides (nt) in length. In 1993, the first miRNA, lin-4, was found in *Caenorhabditis elegans* by the group of Ambros (Lee et al., 1993). It was described as a small ncRNA that influences the development by negatively regulating LIN-14 protein expression. A further progress in the miRNA field was made 7 years later, when another miRNA in *C. elegans*, let-7, was discovered. Let-7 was identified to regulate developmental timing in *C. elegans* by inhibiting the protein expression of the lin-41 gene through specifically binding to the 3′-untranslated regions (3´UTR) of the lin-41 mRNA (Reinhart et al., 2000). Since that time, miRNAs have become of high interest in the scientific world, resulting in the discovery of numerous miRNAs across the species, and advances in understanding their biogenesis and functions. Just in the human genome, there are currently more than 1900 miRNA sequences ("miRBase: Homo sapiens miRNAs (1917 sequences) [GRCh38]," n.d.). To date, the specific functions of many miRNAs have still not been recognized (Peng and Croce, 2016).

MiRNAs are known to be well conserved across the species, where they play important roles in all biological signalling pathways (Bayraktar et al., 2017; Lee et al., 2007; Moss and Tang, 2003). MiRNAs represent around 1-5% of the animal genes, and it has been bio-informatically estimated that miRNAs can target more than 60% of mRNAs in the mammalian genome (Sohel, 2016). They can regulate the gene expression either at the transcriptional or posttranscriptional level by repressing their target genes (Bayraktar et al., 2017; Cheng et al., 2014b). Typically, miRNAs complementarily bind to the 3'UTR of their target mRNAs in the RNA-induced silencing complex (RISC), causing their degradation or the inhibition of their protein expression (Kehl et al., 2017; Schwarzenbach, 2017a). The binding of miRNAs to their target sequence must not be perfect. Already a partial binding of only 2-7 nucleotides at the 5´ end of the miRNA, called the "seed" region, leads to translational inhibition, compartmentalization or deadenylation, and therefore, destabilization of their target mRNAs. Because of this incomplete binding, a specific miRNA can potentially target hundreds of mRNA sequences (Bartel, 2009; Corcoran et al., 2011).

MiRNAs play an important role in the regulation of key processes in mammals. They control miscellaneous physiological processes in animals by interacting with diverse

targets. MiRNAs are responsible, among others, for cell death, differentiation and proliferation, development and regulation of developmental timing, or antiviral defence (Schwarzenbach, 2015; Wahid et al., 2010). They are crucial agents in controlling gene regulation, making them interesting as therapeutic targets. Their dysregulation causes the development of specific diseases in animals, including cancer (Wahid et al., 2010).

3.2. MicroRNA biogenesis

The miRNA biogenesis starts in the nucleus, where genomic DNA is transcribed by polymerase II, or rarely by polymerase III into a 1-3 kb long primary transcript called pri-miRNA (Corcoran et al., 2011; Sohel, 2016). Optimally, the pri-miRNA includes primary sequence motifs, like CNNC (cytosine/a nucleotide/a nucleotide/cytosine) distant from the base of the stem or UG (uracil/guanine) located in the base of the stem, a stem length of 33-39 nt, an apical loop of 3-23 nt, bulges positioned 5-9 nt from the stem base, near the Drosha processing site, and bulge depleted regions. These pri-miRNA characteristics provoke its further efficient processing (Adams, 2017; Roden et al., 2017). Subsequently, the pri-miRNA is cleaved by a microprocessor complex composed of the double-stranded RNA-specific ribonuclease III-type endonuclease Drosha, the protein binding double-stranded RNA DGCR8 and other proteins, such as DEAD box RNA helicases, or heterogenous nuclear ribonucleoproteins. First, DGCR8 identifies the loop of the pri-miRNAs consecutively ensuring the accurate cleavage into a precursor miRNA (pre-miRNA) by Drosha (Roden et al., 2017). The pre-miRNA is a double stranded, stem-loop, hair-pin shaped RNA molecule of around 70 nt in length. It is actively transported through the nuclear limiting membrane to the cytoplasm by the nuclear transport protein Exportin 5. The RNase enzyme Dicer in collaboration with a double-stranded RNA-binding protein TRBP processes the pre-miRNA into a miRNA/miRNA* duplex of around 22 bp in length. Finally, the duplex is separated into a mature miRNA which binds to two proteins (GW182 protein and either one of the proteins of the Argonaute family, mainly Ago2), and forms a miRNA/multiprotein complex called miRISC. The second strand is usually degraded in the cytoplasm. The miRISC specifically binds to partially complementary sequence motifs of the 3’UTR of their target mRNAs, resulting in its degradation or inhibition of translation (Figure 13) (Bayraktar et al., 2017; Sohel, 2016).

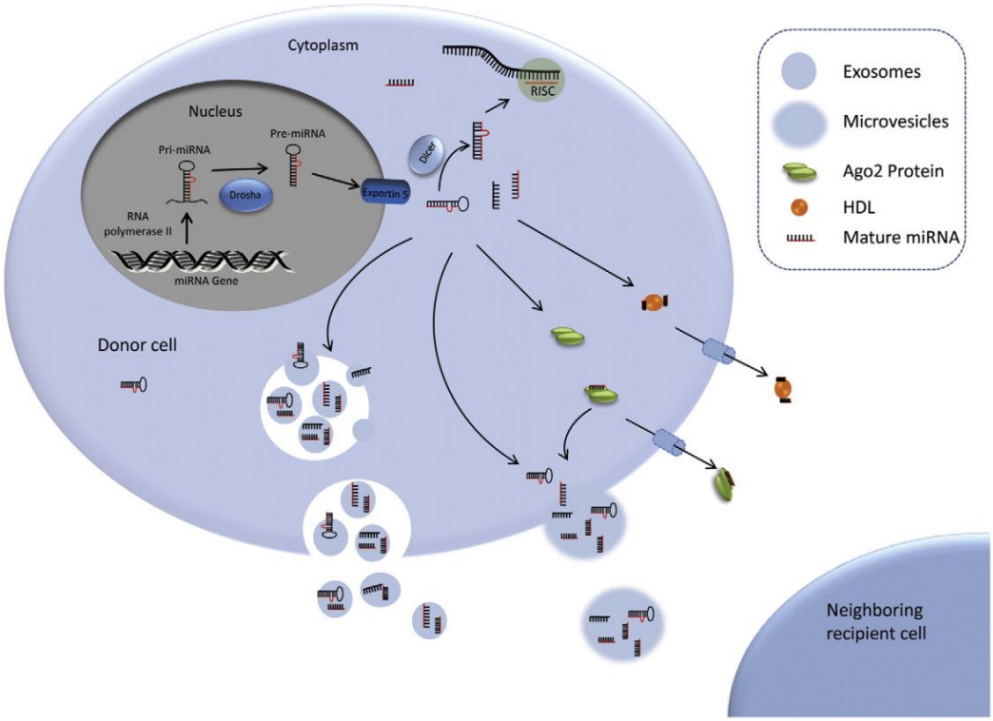

Figure 13: MiRNA biogenesis and release from the cell (taken from Sohel, 2016)

Genomic DNA is transcribed by RNA polymerase II into a pri-miRNA. The pri-miRNA is then processed by Drosha into a pre-miRNA, which is actively transported from the nucleus to the cytoplasm by Exportin 5. In the cytoplasm, the pre-miRNA is processed into a mature miRNA by Dicer, and integrated in the RISC complex. MiRNAs can be actively shed from the cell as a complex with Ago2 or HDL, or encapsulated in extracellular vesicles.

3.3. Exosomal and cell-free microRNAs

The presence of circulating, cell-free DNA in the bloodstream was first described by Mandel and Métais in 1948 (Mandel and Metais, 1948). Decades later, circulating RNA was observed in the plasma (Kamm and Smith, 1972; Stroun et al., 1977). However, only in 2002, it was proved that circulating RNA exists in a stable form in the blood and is protected from ribonuclease activity (Ng et al., 2002; Tsui et al., 2002). Then in 2008, the presence and stability of cell-free miRNAs were documented (Lawrie et al., 2008; Mitchell et al., 2008).

The majority of miRNAs are inside of the cell, however, they can also be found in the extracellular environment and the blood circulation, where they are called cell-free, extracellular and/or circulating miRNAs. Since extracellular miRNAs can be detected in a variety of body fluids, such as blood, urine, saliva, semen, cerebrospinal fluid, bronchial lavage or follicular fluid, they have been considered as a novel class of cellular messengers. Circulating miRNAs play important roles in the response to cellular stress,

disease, and environmental stress (Boon and Vickers, 2013; Sohel, 2016). Usually, foreign RNA in extracellular fluids is degraded by widespread RNases, as a defence response to the extraneous, pathogenic RNA (Koczera et al., 2016). However, circulating miRNAs are specifically protected by their carriers from degradation by endogenous RNase activity *in vivo* (Boon and Vickers, 2013; Vickers et al., 2011), as well as from harsh conditions, like high temperature, repeated freezing/thawing cycles or high/low pH in *in vitro* experiments (Sohel, 2016).

MiRNAs released by dying cells are enclosed in apoptotic bodies or complexed with lipoproteins [HDL and low density lipoproteins (LDL)] or ribonucleoproteins [nucleophosmin 1 (NPM1) and mainly Ago2)]. Actively secreted miRNAs enter the extracellular space encapsulated in bilayer membrane-enclosed EVs, such as exosomes (Boon and Vickers, 2013; Vickers et al., 2011). The RNA pool in exosomes differs from that in donor cells. It is enriched in small ncRNAs, e.g., miRNAs, and contains low levels of ribosomal RNA (Valadi et al., 2007). Presumably miRNAs are selectively packed into exosomes and exported to the extracellular space. They influence the recipient cell upon delivery, therefore they have been described as regulatory signals in the cell-to-cell communication (Boon and Vickers, 2013).

3.4. MiR-16 and miR-142

MiR-16 (hsa-miR-16-5p) has several target genes and is involved in AU (adenine/uracil)-reach element-mediated mRNA instability (Jing et al., 2005). Deregulated levels of miR-16 have been found in numerous benign and malignant diseases (Ardekani and Naeini, 2010; Lo Russo et al., 2018; Yan et al., 2019). For example, miR-16 has been found to be downregulated in Parkinson disease (Soreq et al., 2013). Moreover, one of miR-16 precursor, miR-16-2, allows to distinguish between treated and untreated Parkinson disease patients, because of its significant upregulation in patients after treatment (Margis et al., 2011). It is one of the most abundant miRNAs across various types of tissues (Chen et al., 2005), is highly abundant in human plasma (Ramón-Núñez et al., 2017) and is one of ten most highly expressed miRNAs in human urine (Cheng et al., 2014c). Based on its constant and steady expression, endogenous miR-16 is frequently used as a reference gene to normalize miRNA data derived from different isolation techniques (Schwarzenbach et al., 2011, p.), and applied to compare miRNA isolation methods (Lekchnov et al., 2016; McAlexander et al., 2013; Ramón-Núñez et al., 2017) or to check the influence of pre-analytical factors (Binderup et al., 2018; McDonald et al., 2011). However, there are

discrepant data on miR-16 expression. It is not only equally expressed across the tissues and diseases, but, as mentioned above, its deregulation has also been documented by numerous studies (Huang et al., 2015; Schwarzenbach, 2016a). Besides, miR-16 is the most expressed miRNA in erythrocytes, and therefore, pre-analytical factors, such as hemolysis can lead to a substantial increase in its levels (Vigneron et al., 2016).

Performing size-exclusion chromatography (SEC) of cell depleted serum and plasma samples, Arroyo et al. found that miR-16 is co-fractionated with relatively small plasma/serum proteins in late SEC fractions. They demonstrated that miR-16 is predominantly associated with ribonucleoprotein complexes, and is not significantly available in exosomes (Arroyo et al., 2011; Turchinovich et al., 2011). In contrast, other studies indicated that miR-16 is present in similar proportions inside, as well as outside of exosomes (Cheng et al., 2014c; Enderle et al., 2015). These discrepant data have also been complemented by inconsistent findings that miR-16 is either up- or downregulated in the same diseases (Huang et al., 2015; Schwarzenbach, 2016a).

MiR-142 (hsa-miR-142-3p) plays an emerging role in homeostasis, organogenesis and various diseases (Shrestha et al., 2017). For example, cell-free miR-142 has been indicated as a biomarker for Alzheimer disease (Chevillet et al., 2014; Kumar et al., 2013). Arroyo at al. demonstrated that circulating miR-142 is mostly present in exosomes and strongly reduced in protein fractions (Arroyo et al., 2011). However, as observed for miR-16, other studies showed that miR-142 can be found in both exosomes and protein complexes (Cheng et al., 2014a; Karttunen et al., 2019), with elevated levels in the exosomal fraction (Enderle et al., 2015).

MiRNA recovery by different isolation protocols depends on their abundance in the sample, their GC content, and the free energy (ΔG) of their most stable secondary structure. Structured miRNAs that fold into a stable secondary structure display a low ΔG. For example, phenol-based isolation techniques result in a poor recovery rate of structured miRNAs with a low GC content in samples with low RNA concentrations (Kim et al. 2012; Ramón-Núñez et al. 2017). Although both miR-16 and miR-142 are highly abundant in plasma and serum samples (Arroyo et al., 2011), miR-142 has a much lower GC content and folding ΔG (Table 2). As predicted by the mfold software ("RNA Folding Form | mfold.rit.albany.edu,"), the secondary structure of miR-142 is more stable than the conformation of miR-16 (Figure 14). For these reasons, miR-16 and miR-142 were used in the current work to compare commercial miRNA isolation and quantification techniques with my established techniques.

Table 2: Main characteristics of miR-16 and miR-142

miRNA	Sequence*	Length (nt)	%GC	ΔG**
hsa-miR-16-5p	uagcagcacguaaauauuggcg	22	45.45	-1.4
has-miR-142-3p	uguaguguuuccuacuuuaugga	23	34.78	-2.4

*****according to the miRBase 22.1, ** predicted by the mfold software

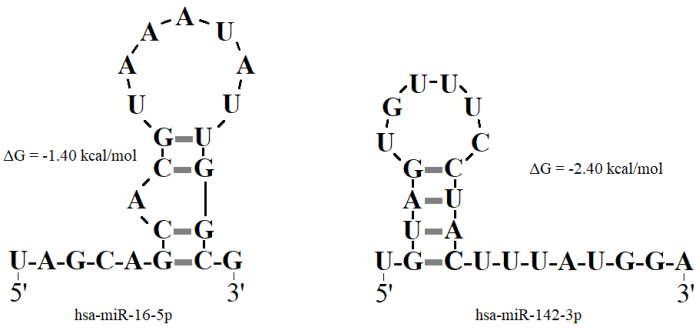

Figure 14: The most stable secondary structures of miR-16 and miR-142 predicted by the mfold software

MiR-142 has a lower GC content and a more stable secondary conformation than miR-16. These features are strong indicators of the miRNA loss during phenol-based isolation.

3.5. Different techniques used for microRNAs isolation

To isolate cell-free miRNAs from liquid biopsies, at first, samples should be handled to remove cells and cellular debris. This can be reached by several techniques, like a low speed centrifugation or filtration (Konoshenko et al., 2018). Subsequently, the supernatant has to be lysed to destroy all EV membranes and protein complexes carrying miRNAs, as well as to deactivate inhibitors and RNases. Then, the free miRNAs are bound on solid surfaces, comprising nylon, polysulphone, polyethersulphone, PVDF, acrylic polymer and ion exchange membranes, as well as polyethylene frits, filter papers, magnetic iron oxide particles, silicate particles and combinations thereof. MiRNAs stably bound on these solid surfaces are washed to remove remaining impurities. Finally, miRNAs are solved from the solid surface by elution and ready for downstream applications. Currently, most RNA isolation techniques are based on the use of chaotropic agents as a lysis components (acid phenol or guanidine thiocyanate/hydrochloride), which disrupt the hydrogen binding network between water molecules (Hillebrand, 2009).

The classic approach to isolate RNA, including miRNAs, is based on acid phenol/chloroform extraction (Chomczynski and Sacchi, 1987). This technique in

combination with silica-membrane spin columns is available as commercial kits, e.g. the Qiagen miRNeasy Serum/Plasma kit, or Invitrogen Total Exosome RNA and Protein Isolation kit. However, an acid phenol/chloroform extraction can also be successfully performed as an in-house method (Lekchnov et al., 2016; Tietje et al., 2014). First, samples are lysed and homogenized by the addition of acid phenol/guanidine thiocyanate lysis buffer. Then, lysed samples are mixed with chloroform, and after centrifugation, two phases separated by an interphase are formed in this mixture. The upper, aqueous phase contains RNA species, DNA molecules are in the interphase, and proteins are distributed in the lower, organic phase or in the interphase. Afterward, the upper phase containing RNAs is collected, mixed with alcohol (usually isopropanol or ethanol), and applied on a spin column with a filter harboring RNA binding capacity. The spin column is centrifuged at a low speed, so that phenol and other contaminants are removed. Subsequently, repeated washing steps and drying of the column lead to removal of the remaining impurities and alcohol. Finally, RNA is eluted from the filter, usually in RNase-free water (Endzeliņš et al., 2017; Turchinovich et al., 2011).

In the last years, new commercial techniques for cell-free miRNA isolation have been reported (Binderup et al., 2018; Lekchnov et al., 2016; McAlexander et al., 2013; Tiberio et al., 2015), and are available for example as a miRNeasy Serum/Plasma Advanced Kit (Qiagen), or a NucleoSpin® miRNA Plasma kit (Macherey-Nagel). These kits are free of phenol/chloroform extraction. At first, samples are lysed in the presence of guanidine thiocyanate and detergents to release RNAs. Then, contaminating proteins are precipitated and centrifuged. The supernatant is mixed with isopropanol to create proper binding conditions, and the mixture is applied on a spin filter made of a silica membrane. After centrifugation, the membrane is washed to remove impurities, and the RNA is eluted in water (Figure 15) (Alexander et al., 2015; “NucleoSpin miRNA Plasma,” n.d.).

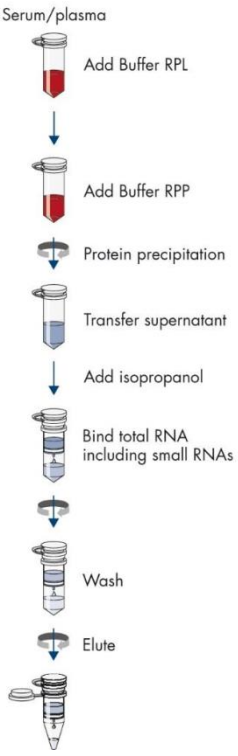

Figure 15: Principle of the Qiagen miRNeasy Serum/Plasma Advanced Kit (taken from the supplier's handbook, 2017)

In the first step, Buffer RPL is added to the sample to perform complete lysis. Then, the sample is incubated with precipitation buffer (Buffer RPP), and centrifuged to remove proteins. Next, the supernatant is mixed with isopropanol to create the binding condition. This mixture is applied on the spin filter. After RNA binding, the column is washed and pure RNA is eluted.

Another technique without the use of phenol/chloroform is offered by Applied Biosystems. The TaqMan™ miRNA ABC Purification Kits (Human Panel A and B) are based on two different sets of 377 anti-miRNA oligonucleotides conjugated on magnetic beads. In the first step, 50 µl of the sample is lysed with buffer containing guanidine hydrochloride. Then, the magnetic beads with the conjugated sequences complementary to one of the panels of 377 miRNAs are added to the sample, and incubated to allow hybridization of miRNAs to the beads. Finally, the beads-bound miRNAs conjugates are washed, and miRNAs are eluted (Figure 16).

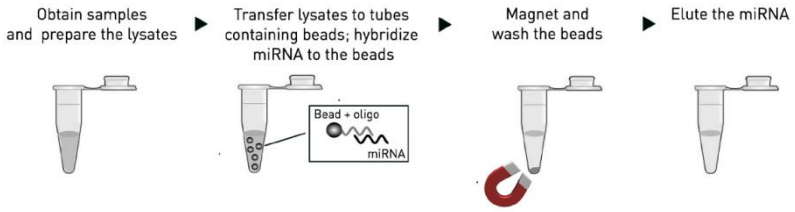

Figure 16: Overview of the TaqMan™ miRNA ABC Purification Kit (Applied Biosystems) procedure (taken from the supplier's user guide, 2012)

The sample is lysed to release nucleic acids, and magnetic beads prepared from Human Panel A or B are added to the sample. This mixture is incubated to allow hybridization of miRNAs to the beads. Subsequently, beads are attracted by a magnet and washed to remove contaminants. Finally, miRNAs are eluted in a small volume of elution buffer.

Although miRNA isolation methods based on the lysis with phenol are very efficient (Tiberio et al., 2015), contaminants and inhibitors are often present in the eluate (Ramón-Núñez et al., 2017), the protocol is time consuming, and most importantly, the chemicals used are hazardous to health (Lekchnov et al., 2016). Techniques involving post-lysis protein precipitation seem to overcome some of these problems. However, which of these two methods provides higher miRNA yields and quality is still under discussion, since the data differ among the research groups (McAlexander et al., 2013; Ramón-Núñez et al., 2017; Tiberio et al., 2015). These discrepant results can be caused by the influence of factors, such as miRNA GC content, free energy of the intra-molecular folding or the relative abundance of miRNAs in the sample that all affect the recovery rate. Therefore, a comparison of the different isolation techniques is difficult (Kim et al. 2012; Ramón-Núñez et al. 2017).

Thus, the isolation of endogenous miRNAs by anti-miRNA conjugated magnetic beads seems to be an interesting alternative. It does not involve the usage of hazardous components and allows a specific miRNA isolation in a sample volume as small as 50 µl. However, this small input volume can also be of a disadvantage, if a miRNA is low abundant. Moreover, the technique is expensive and the number of miRNAs is restricted by the anti-miRNA conjugated magnetic beads in the kit (Schwarzenbach, 2016b; Tiberio et al., 2015).

3.6. Methods of miRNAs quantification

MiRNAs are challenging targets to quantify, mainly because of their very short length, their GC content, similarities in sequences among miRNAs of the same family and the low abundance in the body fluids (Tiberio et al., 2015). Moreover, miRNAs only represent a small part of total RNA, and exist in three forms: the short, linear mature miRNA, the hairpin pre-miRNA and the long pri-miRNA (Shingara et al., 2005). Currently, several techniques are used for quantifying total or particular miRNAs. To the first group detecting the overall yield of miRNAs belong platforms, such as a fluorometer, e.g. the Invitrogen Qubit or an automated lab-on-chip electrophoresis, e.g. the Agilent Bioanalyzer. The second group includes hybridization-based miRNA microarrays, massively parallel miRNA sequencing (miRNA-seq) and quantitative reverse transcription polymerase chain reaction (RT-qPCR). All these methods significantly differ in specificity and sensitivity.

The Qubit is a benchtop device allowing fluorometric quantification, as well as a quality and an integrity assessment of nucleic acids. Prior to measurement, the sample is incubated with a fluorescent dye which binds specifically to the target and emits the signal. The Invitrogen Qubit miRNA Assay Kit is dedicated to selectively quantify as little as 0.5 ng of miRNAs that measurement does not seem to be influenced by long RNA and DNA molecules, free nucleotides, detergents or proteins. Moreover, the measurement is simple, rapid, and does not require specially qualified personal. A disadvantage is that the Qubit kit is not exclusively specific to miRNAs, but also to all other small RNAs species (Garcia-Elias et al., 2017).

The Agilent Bioanalyzer is a platform for a high-resolution, automated and microfluidic-based electrophoresis of nucleic acids and proteins. The Agilent small RNA Kit analyses up to eleven samples simultaneously, and only requires 1 µl of each sample. The analysis includes quantification and sizing of small RNAs in a size range from 6 to 150 nt. The whole procedure is fast, non-laborious and produces easy to analyse results. However, Garcia-Elias et al. found that the Agilent 2100 Bioanalyzer is not reliable for the quantification of miRNAs particularly in plasma samples, because of the high variability of data, especially if RNA concentrations are low (Garcia-Elias et al., 2017).

Hybridization-based miRNA microarrays are commercially available for several platforms, such as the Affymetrix GeneChip or the Agilent SurePrint Human miRNA microarray. Briefly, miRNAs are tailed by the poly(A) polymerase, labelled with e.g., biotin or amine reactive molecules, like Cy or Alexa dyes, and then, hybridized to the DNA probes on the

microarray surface. Afterwards, the microarray cartridge is washed to remove not-bound miRNAs, and the signal induced by the label is detected to confirm the presence of miRNAs (Figure 17) (Moody et al., 2017; Shingara et al., 2005). In one microarray assay, around two thousand miRNAs can be detected using 130 ng of total RNA. However miRNAs detection is limited to those sequences that are listed in the miRbase databank (Schwarzenbach, 2016b; Tiberio et al., 2015).

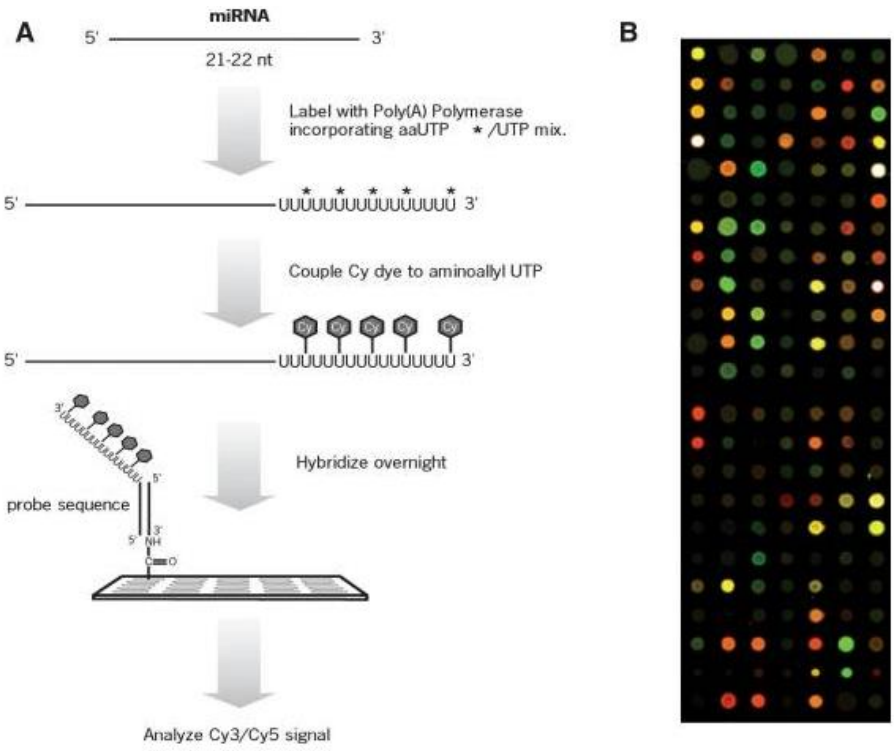

Figure 17: Exemplary approach of the miRNA microarray performance (taken from Shingara et al., 2011)

A) MiRNAs are tailed with amine-modified nucleotides (aaUTP), and Cy, an amine reactive dye is coupled to the aaUTP tail. Labelled miRNAs are added to the microarray coated with DNA probes complementary to miRNAs. After hybridization, microarrays are processes and analysed. B) Exemplary outcome from a scanned microarray.

Moreover, the method is time-consuming, laborious, requires specialized equipment and specific probes, and the data normalization is complicated (Moody et al., 2017). Additionally, microarrays have a restricted specificity and dynamic range, and a low relative correlation in the fold change of miRNAs as derived from the different platforms (Dong et al., 2013; Tiberio et al., 2015).

For miRNA-seq or next generation sequencing (NGS), several platforms are available, e.g. from Illumina or Life Technologies. Basically, the protocol consists of RNA isolation, RNA-adapter ligation, cDNA library preparation, PCR amplification and sequencing, and

data analysis (Schwarzenbach, 2016b). In contrary to the standard Sanger sequencing, these techniques allow sequencing multiple samples in parallel, can cover the entire genome, and thus, enable the discovery of new miRNAs (Moody et al., 2017). In particular, they are useful to detect miRNAs which differ by only one nucleotide, or isomiRs of different lengths (Tiberio et al., 2015). However, they are laborious and expensive, and the data analysis is still complicated and not standardized (Moody et al., 2017).

RT-qPCR is considered as a "golden standard" in miRNA quantification. Currently, the most sensitive and specific approach for PCR-based miRNA amplification involves the use of stem-loop primers and TaqMan probe labelled with minor groove binder (MGB) (Chen et al., 2005). The reaction starts with the reverse transcription using a specially designed stem-loop primer (Moody et al., 2017). Stem-loop primers have been proved to be more specific and efficient than linear ones, probably because the base-stacking of the stem increases the thermal stability of the RNA-DNA heteroduplex, and the special constraint of the loop increases their specificity (Chen et al., 2005). After reverse transcription, cDNA is used for qPCR, which engages TaqMan MGB probes that are dual labelled with a fluorescent reporter dye at the 5' end and a non-fluorescent quencher combined with MGB at the 3' end. MGB increases the melting temperature of the probe and the specificity of probe-target binding. Therefore, MGB probes can be significantly shorter than a usual probe with a quencher alone, and are important for the amplification of short miRNA sequences. The TaqMan MGB probe and primer hybridize to cDNA. Subsequently, the primer is elongated by the Taq polymerase, and while reaching the TaqMan MGB probe, the probe is degraded by the polymerase 5'-3' exonuclease activity. A fluorophore is released from the proximity of the quencher, increasing the fluorescence. The emitted signal refers to the amount of miRNAs in the sample (Figure 18) (Hackett et al., 2000; Kutyavin et al., 2000). Although the stem-loop primer-based RT-qPCR is very efficient, specific and sensitive, this technology is relatively expensive since it requires a separate primer set for each miRNA and allows to detect only annotated miRNAs (Moody et al., 2017; Tiberio et al., 2015).

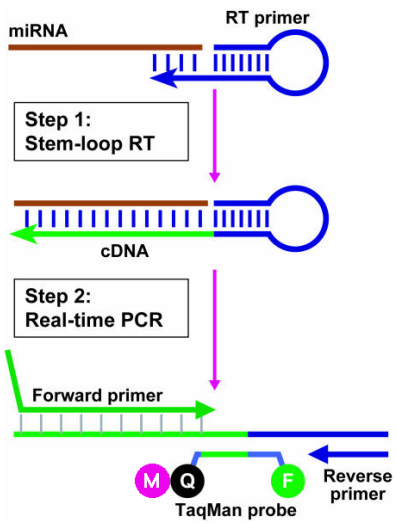

Figure 18: Schema of RT-qPCR using a stem-loop primer and a TagMan MGB probe (taken from Chen et al., 2005; modified)

First, during the reverse transcription, the stem-loop RT primer specifically binds to a miRNA, and is enzymatically elongated to produce cDNA. In a second step, cDNA is used as a template for PCR and amplified with a tailed forward primer, a universal reverse primer and a fluorescently labelled TaqMan MGB (M) probe. Q, black hole quencher 1 (BHQ-1); F, fluorophore.

Assays allowing the simultaneous quantification of multiple miRNAs are also available as microfluidic array cards, e.g. the Applied Biosystems TaqMan Advanced MicroRNA Human A and B Cards or the Qiagen miScript miRNA PCR Array. They offer the detection of more than 700 miRNAs starting from only 100 ng of input RNA. The generated data are easy to analyse and display high inter- and intra assay correlations between the platforms. However, PCR arrays can reach only medium throughput, and allow analysing only selected miRNAs (Tiberio et al., 2015).

Digital droplet PCR (ddPCR) is also a precise technique for miRNA quantification. ddPCR relies on sharing the sample into thousands of partitions of a defined volume through forming water-in-oil immersion droplets which hydrostatically separate the targets (Stein et al., 2017). After the PCR reaction, each droplet contains or does not contain a target molecule, facilitating the estimation of the absolute target copy number by applying the Poisson correction. In contrary to RT-qPCR, ddPCR allows an absolute quantification with immediate results without any need of preparation of a standard curve, excludes data normalization, and is more precise and sensitive for low abundant targets (Campomenosi et al., 2016). However, ddPCR has still some shortcomings in miRNAs amplification, like the influence of target nucleotide composition on the RT reaction or the lack of optimized reagents for miRNA measurements (Stein et al., 2017).

II. AIM OF THE STUDY

The current study aimed to develop a comprehensive workflow for separation of exosomes, isolation and quantification of exosomal miRNAs, as well as cell-free miRNAs. All methods should be efficient, non-time consuming, non-laborious, inexpensive and requiring only the common laboratory equipment.

The first goal was to optimize an existing method for miRNAs quantification (reverse transcription/real-time PCR) which uses the stem-loop primer-based approach. The optimization should result in a higher performance, less time consuming and less expensive technique, so it could be easily applied in a daily laboratory routine. This improved protocol was used for the verification of the further experiments: the establishment of the exosome purification and miRNA extraction techniques.

Exosomes with their cargo are a promising diagnostic marker and can also be applied for targeted treatment of multiple pathological conditions, such as various benign and malignant diseases. Therefore, an efficient and standardized method for such analyses that can be used among all research groups is urgently needed. For this reason, the main objective of this study was to develop a novel method for exosome extraction which should be as efficient as ultracentrifugation, as easy as a common precipitation by polymeric solutions and not influenced by the sample type (plasma with different anticoagulation agents, serum, cell culture supernatant, urine or any other cell-free fluid), sample volume (planned and achieved range from only 300 µl for plasma samples up to 10 ml for urine) or the sample dilution factor (like in SEC fractions).

The third aim was to establish a new technique for miRNA isolation. The protocol was subjected to efficiently extract miRNAs independent of their source (exosomes, cell-free miRNAs, cell culture supernatant, plasma, serum or urine) and sample volume. Alternative chemicals should replace the common use of hazardous chemicals, such as phenol/chloroform mixtures or guanidine thiocyanate. Moreover, the simplicity of the protocol should allow further automation of the method.

The complete workflow for exosomal and cell-free miRNA analysis should be compared with one of the most commonly used techniques, like the PEG-based exosome precipitation, the phenol/chloroform miRNA isolation, and the original stem-loop primer-based miRNA amplification.

III. MATERIALS

1. Commercially available chemicals, solutions and consumables

Chemical/Solution	Supplier
6x DNA Loading dye	Thermo Fisher Scientific, Waltham, USA
β -mercaptoethanol	Sigma-Aldrich, St. Louis, USA
Acetic acid	Carl Roth, Karlsruhe, Germany
APS (Ammonium Peroxodisulphate)	Carl Roth, Karlsruhe, Germany
BSA (Bovine Serum Albumin)	Sigma-Aldrich, St. Louis, USA
Bromophenol Blue	Bioatlas, Tartu, Estonia
DMEM-Dulbecco's Modified Eagle's Medium	Life Technologies, Carlsbad, USA
DPBS (Dulbecco's Phosphate Buffered Saline)	Life Technologies, Carlsbad, USA
EDTA	Carl Roth, Karlsruhe, Germany
Ethanol	Th. Geyer, Renningen, Germany
Ethidium bromide 5 mg/ml	Carl Roth, Karlsruhe, Germany
Exosome-depleted FBS	Life Technologies, Carlsbad, USA
Gene Ruler DNA Ladder Mix 0.5 µg/µl	Thermo Fisher Scientific, Waltham, USA
Glycerol	Sigma-Aldrich, St. Louis, USA
Glycine	Carl Roth, Karlsruhe, Germany
HCl	Carl Roth, Karlsruhe, Germany
Honeywell Fluka Magnesium Chloride Solution, 1M	Honeywell International, Charlotte, USA
LE Agarose	Biozym Scientific, Hessisch Oldendorf, Germany
L-Glutamine 200 mM	Life Technologies, Carlsbad, USA
Methanol	Carl Roth, Karlsruhe, Germany
NaCl	VWR International, Randor, USA
PageRuler Prestained Protein Ladder, 10 to 180 kDa	Thermo Fisher Scientific, Waltham, USA
SDS (Sodium Dodecyl Sulphate)	Carl Roth, Karlsruhe, Germany
Sephacryl S-500 High Resolution	GE Healthcare, Chicago, USA

Streptomycin/Penicillin (200 U/mL)	Life Technologies, Carlsbad, USA
Sucrose	Serva, Heidelberg, Germany
TEMED (Tetramethylethylenediamine)	AppliChem, Darmstadt, Germany
Tris	Carl Roth, Karlsruhe, Germany
Triton X-100	Sigma-Aldrich, St. Louis, USA
Trypsin/EDTA (0.25%)	Life Technologies, Carlsbad, USA
Tween 20	Carl Roth, Karlsruhe, Germany
RNase-free water	Analytik Jena, Jena, Germany
RNase ZAP	Invitrogen, Carlsbad, USA
Roti-Blue 5x Konzentrat	Carl Roth, Karlsruhe, Germany
Roti-Lumin	Carl Roth, Karlsruhe, Germany
Roti-Quant 5x Konzentrat	Carl Roth, Karlsruhe, Germany
UltraPure ProtoGel	National Diagnostics, Patton Drive, USA

2. Commercially available plastics and consumables

Plastics/Consumable	**Supplier**
µ-Slide 8 Well Glass Bottom chamber	Ibidi, Gräfelfing, Germany
CB Collect	Fresenius Kabi, Bad Homburg, Germany
Centaur PP 1.75 mm	Forum Futura, Nijmegen, Netherlands
Immobilion-P 0.45 µm PVDF transfer membrane	Merck, Darmstadt, Germany
Porex PP-Platte, 2 mm	Porex, Fairburn, USA
Serological pipette 25 ml	Sarstedt, Nümbrecht, Germany
S-Monovette 9 ml K3E	Sarstedt, Nümbrecht, Germany
S-Monovette 9 ml Z	Sarstedt, Nümbrecht, Germany
Unifrom Dyed Microspheres DS02B	Bangs Laboratories, Fishers, USA
Whatman® Puradisc 25 syringe filters 0.2 µm	GE Healthcare Life Sciences, Chicago, USA

3. Commercially available kits

Kit	Supplier
20X TaqMan MicroRNA Assay (for miR-16 and miR-142)	Applied Biosystems, Foster City, USA
2X TaqMan Universal PCR Master Mix II, no UNG	Applied Biosystems, Foster City, USA
Agilent Small RNA Assay	Agilent Technologies, Santa Clara, USA
Exo-Glow Exosome Labeling Kit	System Biosciences, Palo Alto, USA
HRP Conjugation Kit	Abcam, Cambridge, Great Britain
PKH26 Red Fluorescent Cell Linker Kit for General Cell Membrane Labeling	Sigma-Aldrich, St. Louis, USA
TaqMan MicroRNA Reverse Transcription Kit	Applied Biosystems, Foster City, USA
Total Exosome Isolation Reagent (from plasma)	Invitrogen, Carlsbad, USA
Total Exosome Isolation Reagent (from serum)	Invitrogen, Carlsbad, USA
Total Exosome RNA and Protein Isolation Kit	Invitrogen, Carlsbad, USA
Venor GeM Classic Mycoplasma Detection Kit for Conventional PCR	Minerva Biolabs, Berlin, Germany

4. Synthetic microRNAs

MiRNA	Supplier
cel-miR-39-3p 5’-uca ccg ggu gua aau cag cuu g-3’	Metabion, Planegg, Germany
hsa-miR-140-3p 5’-uac cac agg gua gaa cca cgg-3’	Metabion, Planegg, Germany
hsa-miR-142-3p 5’-ugu agu guu ucc uac uuu aug ga-3’	Metabion, Planegg, Germany
hsa-miR-16-5p 5’-uag cag cac gua aau auu ggc g-3’	Metabion, Planegg, Germany
hsa-miR-483-5p 5’-aag acg gga gga aag aag gga g-3’	Metabion, Planegg, Germany
hsa-miR-484 5’- uca ggc uca guc ccc ucc cga u-3’	Metabion, Planegg, Germany
hsa-let-7b-5p 5’-uga ggu agu agg uug ugu ggu u-3’	Metabion, Planegg, Germany

5. Antibodies

Antibody	Supplier
CD63 Antibody (H5C6), monoclonal	Novus Biologicals, Centennial, USA
FITC anti-human CD326 (EpCAM)	BioLegend, San Diego, USA

6. Prepared buffers and solutions

Erythrocyte lysis buffer	
Components	**Concentrations**
Sucrose	0.3 M
Tris-HCl pH 7.5	10 mM
MgCl2	5 mM
Triton X100	1%

4x Loading buffer (reducing)	
Components	**Concentrations**
Tris-HCl pH 6.8	240 mM
SDS	4% (w/v)
Bromopenol Blue	0.1% (w/v)
Glycerol	40% (w/v)
β -mercaptoethanol	2.85 M

5x Laemmli running buffer	
Components	**Concentrations**
Glycine	960 mM
Tris-base	125 mM
SDS	17 mM

10x TBS buffer	
Components	**Concentrations**
Tris-base	50 mM
NaCl	150 mM
HCl	To set pH to 7.6

1x TBST buffer	
Components	**Volumes**
10x TBS buffer	100 ml
ddH_2O	899 ml
Tween 20	1 ml

1x TAE buffer	
Components	**Concentrations**
Tris-base	40 mM
Acetic acid	20 mM
EDTA pH 8.0	1 mM

7. Devices

Device	**Supplier**
Agilent 2100 Bioanalyzer	Agilent Technologies, Santa Clara, USA
Analytical balance APX-100	Denver Instrument, Bohemia, USA
BioShake IQ	SIRS-Lab, Jena, Germany
Bio-Vision+1000/26MIX Transiluminator	Vilber Lourmat, Collégien, France
Centrifuge with vortex	neoLab, Heidelberg, Germany
CFX96 Touch Real-Time PCR Detection System	Bio-Rad Laboratories, Hercules, USA
ChemStudio SA^2	Analytik Jena, Jena, Germany
Compact S electrophoresis system	Biometra, Göttingen, Germany
Extend BD ED 200 balance	Sartorius, Göttingen, Germany

Freezer -20°C	Indesit, Fabriano, Italy
Freezer -20°C	Liebherr, Kirchdorf, Germany
Freezer -80°C	Kryotec-Kryosafe, Hamburg, Germany
Freezer -80°C	Thermo Fisher Scientific, Waltham, USA
Fridge 4°C	Bosch, Gerlingen, Germany
Fridge 4°C	Liebherr, Kirchdorf, Germany
Heraeus Megafuge 40R Centrifuge	Thermo Fisher Scientific, Waltham, USA
Heraeus Multifuge 3 S-R	Thermo Fisher Scientific, Waltham, USA
Hybridisation Oven OV500	Biometra, Göttingen, Germany
Incubation Bath 1003 GFL	GmbH für Labortechnik, Burgwedel, Germany
Inkubator HeraCell 150i CO_2	Thermo Fisher Scientific, Waltham, USA
Leica TCS SP5	Leica Microsystems, Wetzlar, Germany
Leica TCS SP8	Leica Microsystems, Wetzlar, Germany
MC 6, Centrifuge	Sarstedt, Nümbrecht , Germany
Microcentrifuge, MiniStar	VWR Radnor, Pennsylvania, USA
Microplate reader	Tecan, Männerdorf, Switzerland
Microwave M1727	Samsung, Seoul, South Korea
Mini Centrifuge	Bio-Rad Laboratories, Hercules, USA
MJ Research PTC-200 Peltier Thermal Cycler	Bio-Rad Laboratories, Hercules, USA
NanoSight LM10	Malvern Panalytical, Malvern, Great Britain
neoMag magnetic stirrer with heater	neoLab, Heidelberg, Germany
Optima LE-80K Ultracentrifuge	Beckman Coulter, Brea, USA
PAGE Eco-Mini System EBC	Biometra, Göttingen, Germany
pH-Meter SevenEasy	Mettler Toledo, Columbus, USA
Power supply PS 300TP	Biometra, Göttingen, Germany
ProJet 1200 SLA 3D printer	3D Systems, Rock Hill, USA
ScanDrop 250	Analytik Jena, Jena, Germany
Table centrifuge 5415R	Eppendorf, Hamburg, Germany

Thermomixer comfort	Eppendorf, Hamburg, Germany
Tilting laboratory shaker, TT30	Biometra, Göttingen, Germany
Vortex-Genie 2	Scientific Industries, New York, USA
Vortexer MS2 S8 Minishaker	IKA Works, Wilmington, USA

8. Biological materials

Biological material	**Supplier**
Blood CPD	Clinical Transfusion Medicine Jena gGmbH, Jena, Germany
Blood EDTA	UKE Transfusion Medicine, Hamburg, Germany
Blood without anticoagulant	UKE Transfusion Medicine, Hamburg, Germany
Lyophilized exosome standards from plasma of healthy donors	HansaBioMed Life Sciences, Tallinn, Estonia
MDA-MB-468	Adenocarciroma, triple negative breast cancer cell lines

IV. METHODS

1. Sample proceedings

1.1. Preparation of plasma and serum

Blood samples were obtained from UKE Transfusion Medicine (serum, plasma EDTA) and Institute of Clinical Transfusion Medicine Jena gGmbH (plasma CPD), namely from volunteers who signed donor informed consent. For preparation of serum, plasma EDTA and plasma CPD, blood was collected by S-Monovette Z, S-Monovette K3E and CB Collect, respectively. Then, all samples were centrifuged at 300 g for 10 min to remove cells. Supernatants were transferred into new tubes.

1.2. Verification of hemolysis

Hemolysis of the blood falsely alters the level of cell-free miRNAs (Kirschner et al., 2011). To prevent the measurement of miRNA of cellular origin, all plasma and serum samples were measured for hemolysis according to the method previously established in our lab (Stevic et al., 2018). Briefly, blood cells of 7 ml whole blood were lysed by erythrocyte lysis buffer containing 0.3 M sucrose, 10 mM Tris pH 7.5, 5 mM $MgCl_2$ and 1% Triton X100. A serial dilution of lysed blood cells was used to prepare a standard curve that was used for measurement of hemolysis in all plasma and serum samples. Fifty µl of all samples, including standard and samples of interest, were measured in duplicate on a Microplate reader. The average values and standard deviations were calculated from the duplicates. Free haemoglobin results in the highest absorbance at 414 and two additional peaks at 541 and 576 nm. The absorbance value is directly proportional to the level of hemolysis. Samples of interest with absorbance exceeding 0.25 were excluded from the experiment.

1.3. Pre-analytical treatment of samples

To avoid contaminations, cell debris and apoptotic bodies were removed from all samples, including serum, plasma and cell culture supernatants by centrifugation at 2.000 g for 10 min. Then, the supernatants were carefully transferred into new tubes without disturbing the pellets. Subsequently, large vesicles were removed by centrifugation at 10.000 g for 10 min. Finally, the supernatants were filtrated through Whatman® Puradisc 25 syringe filters

to remove EVs bigger than 0.2 µm in diameter, resulting in a flow-through containing mainly vesicles in a size referring to exosomes (Figure 19).

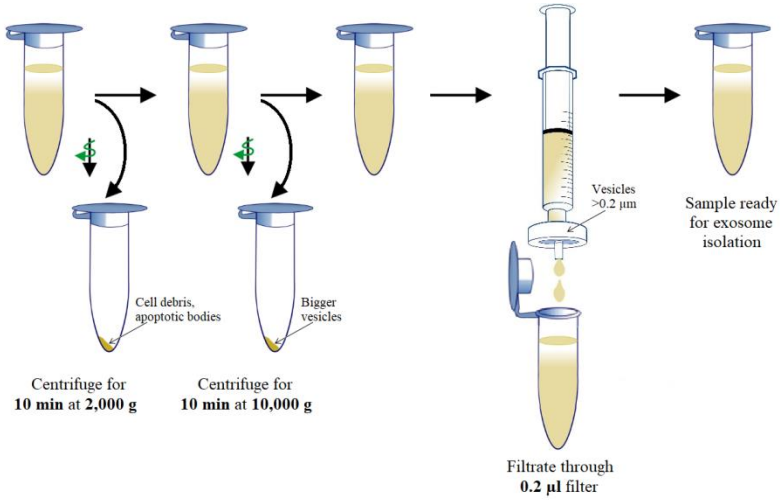

Figure 19: Sample pre-analytical treatment

In order to remove cell debris and apoptotic bodies, the sample was centrifuged for 10 min at 2,000 g. Then, the supernatant was centrifuged for 10 min at 10,000 g and bigger vesicles were pelleted. Finally, to remove vesicles bigger than 0.2 µm, the sample was filtrated through a Whatman filter with a cut-off of 0.2 µm.

2. Cell line culture

The breast cancer cell line MDA-MB-468 was used in this study. It was cultured at 37°C, 10 % CO_2, and in the humidified atmosphere, in DMEM with 10% exosome-depleted FBS, enriched with 200 U/mL of Streptomycin/Penicillin and 200 mM L-Glutamine. To improve overall cell viability and speed of growth, the cell line was passaged when it reached 90% confluence, still before the end of the logarithmic growth phase. Briefly, cells were washed with PBS, detached with 0.05%/0.02% solution of Trypsin-EDTA warmed up to 37°C, and finally centrifuged for 3 min at 250 g. To ensure that cells are free of contaminations, a mycoplasma test was performed every month.

3. Isolation of exosomes from plasma using the Total Exosome Isolation Reagent kit from Invitrogen

The polyethylene glycol-based kit Total Exosome Isolation Reagent (TEI, for plasma and for serum, Invitrogen) was used as a reference technique for the comparison with the self-developed MGP-based exosome enrichment method. Exosomes were isolated according to the manufacturer's instructions. Briefly, 500 µl of pre-analytically treated plasma was mixed with 250 µl of PBS and 150 µl of TEI (for plasma). After 10 min incubation at room

temperature, the sample was centrifuged at 10,000 g for 5 min at room temperature. Differently, 500 µl of pre-analytically treated serum was directly mixed with 100 µl TEI (for serum), incubated at 4°C for 30 min, and centrifuged at 10,000 g for 10 min at room temperature. For both, plasma and serum, the supernatant was separated from the created pellet and transferred into a new tube. The pellet was then centrifuged for 30 sec at 10,000 g to collect and remove the residual supernatant. Subsequently, the pellet was dissolved in PBS to a final volume of 200 µl.

4. Re-isolation of exosomes by ultracentrifugation

Ultracentrifugation is recognized as the gold standard, and therefore the most frequently applied technique of separation of exosomes. In this thesis, ultracentrifugation was used to re-isolate exosomes from a dilution of lyophilized exosome standards from plasma of healthy donors (>3 x 10^9 exosomes/ml, HansaBioMed). One ml of exosomes was added to the centrifugation tube, and the tube was filled with PBS. The sample was centrifuged for 1 h at 100,000 g and 21°C with maximal acceleration and slow deceleration. The supernatant was carefully removed and discarded, and the pellet was dissolved in 1 ml of PBS.

5. Size Exclusion Chromatography

Sephacryl S-500 High Resolution resin was used for size exclusion chromatography (SEC). A 25 ml serological pipette, from which both ends were removed, was used to build a column. A 2 mm thick round plate made of polypropylene (PP) was placed tightly at the outlet of the pipette and served as a bed (sephacryl beads) support. The PP used is porous (7-12 µm) and a hydrophobic material which stops the column bed (particles size of ~50 µm) from running out of the column, and simultaneously allows an easy passage of all particles suspended in the sample (e.g. proteins and exosomes of <7 µm). The outlet of the column was then secured with a 3D-printed cap with a plug. The special design of the cap limited the dead space at the column outlet to avoid re-mixing of already separated fractions. PBS was passed through the column and after ensuring that there were no air bubbles trapped under the PP ring, the column was closed with the plug leaving ~2 cm of PBS in the column. Twenty-four ml of Sephacryl S-500 High Resolution resin was washed five times with two column volumes of 0.2 µm filtrated PBS and diluted to form an 60% slurry. The stirred and homogenous slurry was poured at once along the inside wall of the column using a glass rod. The column was carefully filled with PBS up to the top, and the

resin was allowed to sediment for 10 min. The top of the column was secured with a second PP plate, to avoid any disturbances of the bed surface when pouring the PBS for bed sedimentation and later for sample elution. The outlet of the column was opened, and the PBS flow was allowed until the bed was completely packed. The second PP plate was carefully pushed down the column until it reached the surface of the bed (Figure 20A). The final bed height was 14 cm with a volume of 19 ml and elution speed of ~0.5 ml/min. To check the quality of the packing, 0.5 ml of 0.124% (w/v) dilution of blue-dyed Uniform Dyed Microspheres of a mean diameter of 53 nm, suspended in RNase-free water, was mixed with 50 µl of glycerol and applied on the top of the bed. Immediately after the sample entered the bed, the top of the column was filled with PBS until the column top and remained filled until the end of the sample elution. A blue, narrow zone of the Uniform Dyed Microspheres progressing through the bed was observed, and the 1 ml factions containing PBS were collected at the outlet of the column, while the fractions 7-9 contained the blue Uniform Dyed Microspheres.

A

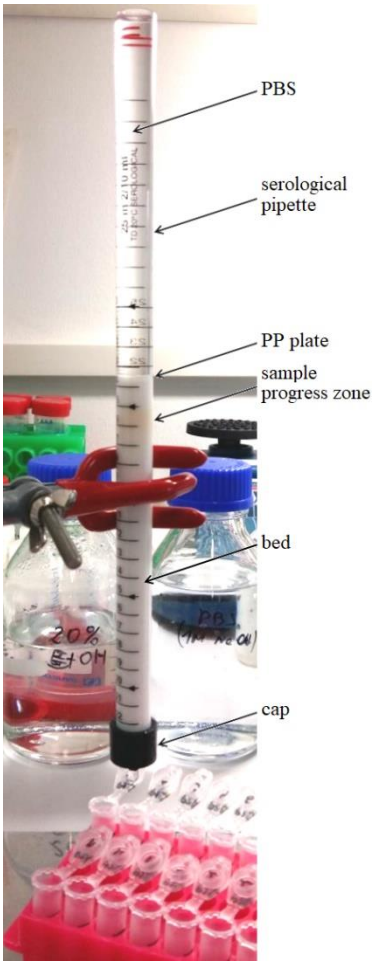

B

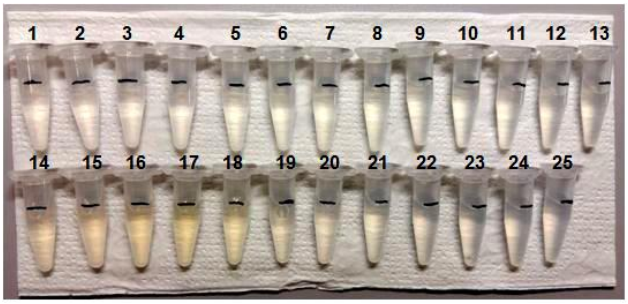

Figure 20: SEC of plasma samples

A) Construction of the SEC column. The column was built with a serological pipette, filled with bed and protected by 2 PP rings (the lower ring covered by the cap is not visible). The bed was permanently covered with PBS for elution of the sample which can be visible as a progressing zone. B) 500 µl of plasma fractionated into 25 fractions of 1 ml volume each (1-25). The highest plasma protein presence was observed in fractions 14-20.

After washing the column 3 times with two column volumes of PBS, 500 µl serum or plasma sample mixed with 50 µl of glycerol was run through the column. Twenty-five fractions of 1 ml were collected from each sample and further analyzed (Figure 20B).

6. Visualization of exosomes using confocal microscopy

Exosomes isolated from 500 µl of plasma by my MGP-based method were labelled with the Exo-Glow Exosome Labelling kit. Exo-Red is a fluorescent cationic dye based on the acridine orange chemical, is membrane-permeable and selectively binds to nucleic acids. It associates with exosomal RNA by electrostatic attraction, and emits a red fluorescence by excitation at 460 nm and has the emission maximum at 650 nm. Briefly, the exosome/MGP pellet was resuspended in PBS up to a final volume of 150 µl. Seven and half µl of 10x Exo-Red was added to 75 µl of exosome suspension and gently mixed. The mixture was incubated for 10 min at 37°C, and the reaction was stopped by mixing 16.5 µl of ExoQuick-TC reagent and incubation for 30 min on ice. After incubation, the sample was centrifuged for 3 min at 16,000 g, and the supernatant was discarded. The pellet containing labelled exosomes was dissolved in 50 µl of PBS, and visualized under a confocal microscope Leica TCS SP5, with a 63x NA=1.4 oil objective lens employed for excitation and detection of fluorescence light.

7. Observation of the biological activity of MGP-isolated exosomes under the confocal microscope

The biological activity of MGP-isolated exosomes was determined by the observation of their cellular uptake under the confocal microscope. For this reason, PKH26 Red Fluorescent Cell Linker Kit was used to dye exosomes for life imaging. PKH26 is a highly fluorescent lipophilic dye that stains membranes by incorporating its aliphatic portions into the lipid bilayer. This dye is a red fluorochrome, which is excited at 551 nm and emits the fluorescence light at 567 nm.

Briefly, exosome/MGP pellets isolated from 2 ml of plasma or serum were dissolved in 50 mM EDTA up to a final volume of 200 µl. Then, 1.2 µl of PKH26 was added to each sample, gently mixed and incubated for 5 min at room temperature. The reaction was stopped by addition of 1 ml of exosome-depleted FBS. Samples were then ultracentrifuged at 100,000 g for 1 h to pellet the stained exosomes. A second ultracentrifugation step was introduced to remove the excess of fluorescent dye.

For the examination of the cellular uptake of these exosomes, the breast cancer cell line MDA-MB-468 was seeded in a µ-Slide 8 Well Glass Bottom chamber containing an exosome-depleted medium and incubated for 1 day in a humidified atmosphere of 37°C and 10 % CO_2. Then, the cell culture supernatant was removed, cells were washed with PBS and stained with FITC-conjugated EpCAM monoclonal antibody (green fluorescence). Fifty µl of the antibody diluted 1:50 in PBS was added to each well and incubated for 1 h at room temperature, protected from light. Afterward, cells were washed with PBS and supplemented with an exosome-depleted medium. The PKH26-stained exosomes were added to the FITC-dyed cells in the wells of the life imaging chamber and incubated for 1.5 hours in a humidified atmosphere of 37°C and 10 % CO_2. The cells were visualized under the Leica TCS SP8 confocal microscope with a 63x NA=1.4 oil objective lens, and lasers of 488 nm and 561 nm were used for excitation of the green (FITC) and red (PKH26) dye, respectively. The image pixel size ranged between 120 and 190 nm, the interplane distance was set to be 500 nm, and the acquisition speed was between 2.6 to 2.8 frames per second.

8. Protein concentration measurement by the Bradford assay

Proteins were quantified by the measurement of absorbance of protein-Coomassie Brilliant Blue Dye-G250 complexes which was first described by Bradford (Bradford, 1976). The Coomassie Brilliant Blue Dye-G250 displays 3 different states which absorb light at different wavelengths: cationic (470 nm, red), neutral (650 nm, green) and anionic (595 nm, blue). Binding to the proteins changes its state from cationic to anionic. The increase in absorbance at 595 nm is proportional to the protein concentration which can be measured over a wide concentration range.

To measure the protein concentration in SEC fractions, as well as in MGP and TEI pellets and supernatants, first, a calibration curve using a serial dilution of BSA (0-2 mg/ml) was prepared. Both, serial dilutions of BSA and samples were mixed with 1X Roti-Quant staining solution and incubated for 5 min at room temperature. The absorbance at 595 nm was measured in respect to the reference (sample buffer in 1x staining solution) on a ScanDrop spectrophotometer. The BSA calibration curve was prepared, and the protein concentrations were calculated.

9. SDS-PAGE protein separation and Coomassie Blue staining

To evaluate the total protein of MGP and TEI pellets, as well as of SEC fractions, and compare them to the total protein in the plasma and serum samples prior to exosome/fraction separation, proteins of the SDS-PAGE were visualized by staining with Coomassie Blue. SDS-PAGE is an electrophoresis method that separates proteins according to their mass. Coomassie Blue is a blue-coloured dye that electrostatically interacts with the protein carboxyl- and amino-groups.

In this thesis, the SDS-PAGE gels were composed of the 5% stacking gel in the upper layer and 12% resolving gel in the lower layer. Gels were prepared according to the receipt as described in the table below:

Components	Stacking gel	Resolving gel
ddH_2O	992.5 µl	37 µl
30% PAA	335 µl	2.72 ml
1 M Tris-HCl pH 6.8	250 µl	N/A
1.5 M Tris-HCl pH 8.8	N/A	1.4 ml
0.5% SDS	400 µl	2.8 ml
TEMED	2.5 µl	7 µl
10% APS	20 µl	46.7 µl

MGP and TEI pellets were dissolved up to a final volume of 150 µl in 50 mM EDTA for MGP and in Exosome Resuspension Buffer (Invitrogen) for TEI. Mixtures containing 0.5 µl of dissolved pellet, 12 µl of 50 mM EDTA or Resuspension Buffer and 2.5 µl of 6x loading buffer were prepared. For SEC fractions, 5 µl of each fraction was mixed with 7.5 µl of PBS and 2.5 µl of loading buffer. All samples were denatured for 5 min at 95°C and loaded on the gels. Gels were placed in the PAGE Eco-Mini System EBC Electrophoresis Module filled with 1x Laemmli running buffer, and run for several min at 100 V to collect all proteins in a narrow belt on the resolving gel, and then run for 1.5 h at 150 V to separate proteins according to their molecular weight. Afterward, gels were gently removed from the gel cassette, placed in a cuvette containing the staining mixture and incubated for 1 h at room temperature with gentle agitation. To remove the dye from the background of the gel, the gel was incubated for 1 h in a de-staining solution 1, 2 h in a de-staining solution 2, and 2 h in a de-staining solution 3. The compositions of staining and de-staining solutions are listed in the table below:

Staining solution	De-staining solution 1	De-staining solution 2	De-staining solution 3
50% methanol	5% methanol	15% methanol	25% methanol
20% Roti-Blue	7.5% acetic acid	7.5% acetic acid	7.5% acetic acid
10% acetic acid			

10. Western Blotting

A Western Blot for detection of CD63, a recognized exosomal marker, was performed to verify if my MGP-based technique is able to isolate exosomes from different types of samples. For this purpose, MGP pellets derived from 500 µl of plasma, 500 µl of serum and 10 ml of urine were dissolved in 100 µl of 50 mM EDTA. In parallel, a negative control, i.e. a MGP pellet derived from 500 µl of RNase-free water was prepared and dissolved in 100 µl of 50 mM EDTA. The protein concentration of the pellets was measured by the Bradford Assay, and equal quantities of proteins were used for the Western Blot. Proteins were not detected in the negative control.

First, SDS-PAGE was used to separate the proteins according to their mass. The gel was composed of a 5% stacking gel and a 12% resolving gel, as described above. Thirty µg of proteins of the MGP pellets derived from plasma, serum and urine, 4 µg of exosome standards from plasma of healthy donors, 10 µl of the negative control and 8 µl of PageRuler Prestained Protein Ladder (10 to 180 kDa) were loaded on the stacking gel. The gel electrophoresis of the un-denatured (no incubation at 95°C) samples under non-reducing conditions (no ß-mercaptoethanol or DTT) was performed in the PAGE Eco-Mini System EBC Electrophoresis Module, first at 100 V to collect all the proteins on the resolving gel, then at 150 V until the 10 kDa protein band of the protein ladder reached the bottom of the gel (within approximately 1.5 h). Subsequently, the proteins were transferred onto an 0.45 µm PVDF transfer membrane by the PAGE Eco-Mini System EBC Blot Module. The gel sandwich was assembled as depicted in Figure 21. The transfer was carried out at 25 V for 1.5 h.

After blotting, the membrane was carefully removed from the sandwich and placed in the blocking buffer (4% BSA in TBST buffer). To prevent unspecific antibody binding, blocking was performed for 45 min, at room temperature, with agitation. The monoclonal antibody specific to the CD63 exosomal marker was labelled with horseradish peroxidase (HRP, Abcam) according to the manufacturer's instructions. Briefly, 5 µl of Modifier reagent was added to 50 µl (1 µg/µl) of antibody and mixed gently.

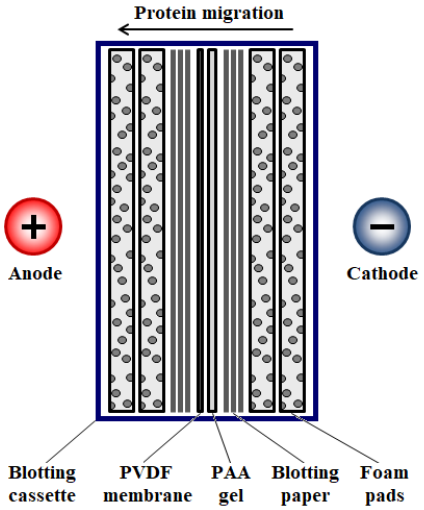

Figure 21: Schema of the blotting sandwich

Polyacrylamide (PAA) gel and polyvinylidene fluoride (PVDF) membrane were placed between 6 layers of blotting paper and 4 layers of foam pads. Negatively charged proteins migrate in the direction to the positively charged anode, and therefore they are transferred from the PAA gel to the PVDF membrane.

The mixture was added to the vial containing the lyophilized HRP Mix and gently resuspended by pipetting up and down. Then, it was incubated for 3 hours at room temperature in the dark. Five µl of Quencher reagent was added, gently mixed and incubated for 30 min at room temperature. The HRP-conjugated antibody was stored at 4°C for further usage. For staining, the transfer membrane was placed in a 50-ml falcon tube and covered with 5 ml of 1% BSA in TBST buffer supplemented with 7 µl of HRP-conjugated antibody (dilution of ~1:1,000). The tube was placed in a Hybridization Oven OV500 and incubated at 4°C overnight with rotation. After the incubation, the membrane was washed 3 times for 10 min in TBST buffer on a Tilting laboratory shaker TT30. For producing a chemiluminescence signal, HRP requires a substrate, such as luminol and the presence of hydrogen peroxide. Therefore, 4 ml of Roti-Lumin 1 and 4 ml Roti-Lumin 2 solutions were mixed and warmed up to the room temperature. The mixture was applied on the surface of the membrane and incubated for 1 min. The excess of Roti-Lumin substrate was removed and the chemiluminescence signal was detected in a ChemStudio SA^2 imager. The membrane was exposed for 5 min, and the image was captured at manual exposure, 100% focus, aperture f1.2, and 4x4 bin.

11. Nanoparticle tracking analysis

Nanoparticle tracking analysis (NTA) is a technique that exploits dynamic light scattering and Brownian motion to characterize the size and concentration of particles between 10 nm and 2,000 nm in diameter suspended in a solution. The particle suspension is placed in the sample chamber and the laser beam is passed through it. The particles which move in the path of the beam scatter light are detected, visualized and recorded by the 20x magnification microscope connected with a video camera. The camera records a movie with a speed of 30 frames per second. The NTA software tracks many particles simultaneously, and the diffusion events are analyzed individually for each of them. The Stokes-Einstein equation is used to recalculate the diffusion coefficient to the hydrodynamic diameter of the tracked particles.

In this PhD thesis, NTA was used to determine the size distribution and concentration of particles isolated with MGP technique from plasma, serum, and cell culture supernatant, as well as of unprocessed, re-isolated by MGP and by ultracentrifugation lyophilized exosome standards from plasma of healthy donors. In order to reduce the number of particles in the field of view, all samples depending on their primary particle concentrations were diluted 10-100 times with 50 mM EDTA or PBS. NTA was performed on the NanoSight LM 10 instrument and by the NTA 3.0 software. For each sample, 10 videos with a duration of 10 sec were recorded at 23.5°C, and with a camera level 16, a minimum track length, a minimal expected particle size and all blur settings set to automatic. The 10 videos were analyzed in a batch-processing mode.

12. Isolation of microRNAs using the Invitrogen kit

Total Exosome RNA and Protein Isolation Kit (Invitrogen) was used to isolate miRNAs from exosome pellet and exosome-depleted supernatant derived from 10 plasma EDTA and 10 serum samples of healthy donors as prepared by the TEI kit (Figure 22). Briefly, 200 µl of 2x Denaturation Buffer was added to 200 µl of the dissolved exosome pellet, mixed and incubated on ice for 5 min. Four hundred µl of Acid Phenol:Chloroform was added to the sample and vortexed for 60 sec. The sample was centrifuged for 5 min, at 16,000 g, at room temperature to create 3 phases, including a compact interphase. The upper phase was transferred into a new tube without disturbing the lower phase or interphase. The lower phase and interphase were discarded. Then, 1.25 volumes of absolute ethanol were added to the upper phase and mixed. The mixture was added to a

Filter Cartridge and centrifuged for 15 sec at 10,000 g. The flow-through was discarded, and the Filter Cartridge was washed once with 700 µl of Wash Solution 1 and twice with 500 µl of Wash Solution 2/3. Between each washing step, the Filter Cartridge was centrifuged for 15 sec at 10,000 g, and the flow-through was discarded. Subsequently, the Filter Cartridge was centrifuged for 1 min at 10,000 g to remove the residuals of ethanol. To elute the miRNAs, 50 µl of Elution Buffer preheated up to 95°C was added to the top of the filter, and the Filter Cartridge was centrifuged for 30 sec at 10,000 g. The elution step was repeated with another 50 µl Elution Buffer to obtain a final eluate volume of 100 µl. A similar protocol was applied for the isolation of miRNAs from the exosome-depleted supernatant, with an exception that the volumes of 2x Denaturation Buffer and Acid Phenol:Chloroform were increased proportionally to the volume of the supernatant.

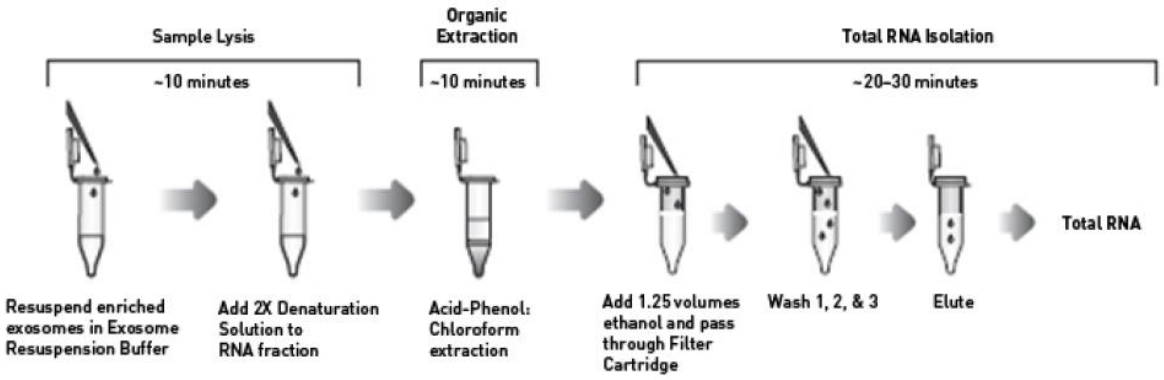

Figure 22: Schematic representation of the procedure for exosomal RNA isolation as recommended by the Invitrogen kit (taken from the Invitrogen protocol, modified)

13. Conversion of microRNAs into cDNA using the Applied Biosystems kit

TaqMan MicroRNA Reverse Transcription Kit was used as a reference technique for my optimized method of reverse transcription of miRNAs (miR-16 and miR-142 in 10-fold serial dilutions). The master mix for cDNA synthesis was prepared on ice according to the Applied Biosystems protocol, and its composition for a 15-µl reaction is listed in the table below:

Master mix component	Volume
Nuclease-free water	4.16 µl
10X Reverse Transcription Buffer	1.50 µl
MultiScribe Reverse Transcriptase, 50 U/µl	1.00 µl
RNase Inhibotor, 20 U/µl	0.19 µl
100 mM dNTPs (with dTTP)	0.15 µl
5X RT primer (for miR-16 or miR-142)	3.00 µl

All components of the master mix were gently mixed and centrifuged shortly to bring the solution to the bottom of the tube. Then, 10 µl of the master mix was dispensed into 0.2-ml tubes, and 5 µl of the template (miRNA) was added. To avoid false-positive results, potentially obtained from master mix contamination, formation of primer-dimers or unspecific products, a negative control containing nuclease-free water instead of the template was prepared in parallel with the miRNA samples. The RT mixtures were put on ice until loading them into the thermal cycler. The reverse transcription was performed on a MJ Research PTC-200 Peltier Thermal Cycler under the following parameters:

Step type	Time	Temperature
Hold	30 min	16°C
Hold	30 min	42°C
Hold	5 min	85°C
Hold	∞	4°C

The cDNA samples were stored at 4°C and used for a real-time PCR on the same day.

14. Quantitative real-time PCR using the Applied Biosystems kits

TaqMan MicroRNA Assays (Applied Biosystems) for miR-16 and miR-142 were used as a reference technique for my optimized method of real-time PCR. For this purpose, cDNA generated by the TaqMan MicroRNA Reverse Transcription kit was amplified in a 20-µl reaction consisted of the following master mix components:

Component	Volume
2X TaqMan Universal PCR Master Mix II, no UNG	10.00 µl
Nuclease-free water	7.67 µl
20X TaqMan MicroRNA Assay (for miR-16 or miR-142)	1.00 µl

The master mix with a volume of 18.67 µl was aliquoted on a PCR reaction plate and 1.33 µl of the template cDNA was added. The real-time PCR amplification was performed on a CFX96 Touch Real-Time PCR Detection System under the following conditions:

Step type	Time	Temperature
Hold	10 min	95°C
Cycle (x40)	15 sec	95°C
	60 sec	60°C

Fluorescence data were collected at 60°C and analyzed with the Bio-Rad CFX Manager 3.1 software.

15. Agarose gel electrophoresis of PCR products

To test the accuracy of the real-time PCR, an agarose gel electrophoresis of the amplification products of synthetic miR-16 and miR-142, as well as of the negative control (RNase-free water instead of miRNA) were prepared. A 2% w/v agarose gel was prepared according to the table below:

Component	Amount
Agarose	2 g
1x TAE buffer	100 ml
Ethidium bromide 5 mg/ml	2 µl

The mixture of agarose and TAE buffer was warmed up in a microwave until the agarose was completely dissolved. Ethidium bromide was added to the solution under gentle mixing. The gel tray and the comb were assembled in the casting apparatus, and the agarose mixture was poured into the formed gel mold. The mixture was left at room temperature to allow polymerizing the gel. The ready gel was placed in the gel box, was covered by 1x TAE buffer, and the comb was removed. Two µl of 6x loading dye was added to 10 µl of each sample. Samples and 8 µl of DNA ladder were loaded onto the gel which was run for 20-30 min at 130 V until the dye migrated far enough through the gel. After that, the gel was removed from the gel box, placed in the Bio-Vision gel documentation system equipped with the VisionCapt software, exposed for 1.2 sec with UV light, and a picture of the fluorescent bands containing the PCR products was taken.

16. MiRNA analysis on a bioanalyzer

In order to analyze the yield and size distribution of small RNAs extracted from 500 µl of plasma or serum, the Agilent Small RNA assay was run on the Agilent 2100 Bioanalyzer according to manufacturer's instructions. The kit allows analyzing small RNAs in a size range of 6-150 nt, and miRNAs in a concentration of 50-2000 pg/µl. Briefly, the lever of the syringe clip was adjusted to the lowest position, and the syringe plunger to the 1-ml position. Prior to and after the assay, the electrodes were cleaned with RNase ZAP and RNase-free water. Before use, all kit reagents were equilibrated for 30 min at room temperature, RNA ladder and samples were denatured for 2 min at 70°C and put on ice until loading them on the chip. Six hundred and fifty µl of the Small RNA gel matrix was loaded onto the spin filter and centrifuged for 15 min at 10,000 g. Two µl of dye concentrate was added to 40 µl of filtered gel, and the mix was centrifuged for 10 min at

13,000 g. Nine µl of the gel-dye mix was loaded into the "G"-marked well of the Small RNA chip, and the chip was placed in the chip priming station with the plunger positioned at 1 ml. The chip priming station was closed, and the plunger of the syringe was pulled down until it was held by the clip. After 60 sec, the clip was released and the plunger was slowly moved back to the start position. Afterward, 9 µl of the gel-dye mix was loaded in 2 other "**G**"-marked wells of the chip. Nine µl of Small RNA condition solution was pipetted in the well marked with "CS", and 5 µl of Small RNA marker was loaded in the well marked with the ladder symbol as well as in each of the 11 sample wells marked with "1-11". One µl of Small RNA ladder was applied in the ladder well. Finally, 1 µl of each sample was pipetted in each of the 11 sample wells. The chip was placed in the IKA vortex mixer and vortexed for 60 sec at 2400 rpm. After that, the chip was inserted in the bioanalyzer and the Small RNA Series II chip run was started. Gel images and electropherograms were generated by the Agilent 2100 expert software, version B.02.06.SI418.

17. Statistical analysis

The statistical analyses were performed using the SPSS software package, version 22.0 (SPSS Inc, Chicago, USA). Statistical differences of miRNA levels were calculated using the ANOVA with Tukey´s HSD test for all pairwise comparisons that correct for experiment-wise error rate. A p-value <0.05 was considered as statistically significant. All p-values are two-sided.

V. RESULTS

1. Study workflow

My Ph.D. work was composed of two parts: A) development and validation of methods for miRNA quantification, as well as for exosome enrichment and isolation of exosomal and cell-free miRNA, and B) comparison of the self-developed techniques with the commercially available kits.

Part A of my study was divided into three subparts (Figure 23). In subpart 1, a RT-qPCR-based method for miRNA quantification was optimized. For this purpose, synthetic miR-16 and miR-142 were used. Ten-fold serial dilutions of the known number of miRNA copies (from 4 x 10^2 to 4 x 10^9 copies per reaction) were amplified to determine method acceptance and performance parameters according to the Minimum Information for Publication of Quantitative Real-Time PCR Experiments (MIQE) guidelines (Bustin et al. 2009). In subpart 2, a method for isolation of exosomes from different starting materials was developed. This technique was tested in biological fluids, such as blood plasma, blood serum, urine, cell culture supernatant, and a sample of commercially available lyophilized exosome standards from plasma of healthy donors. Method efficiency, specificity, and integrity of separated exosomes were verified by NTA, Western Blot, confocal microscopy and SEC.

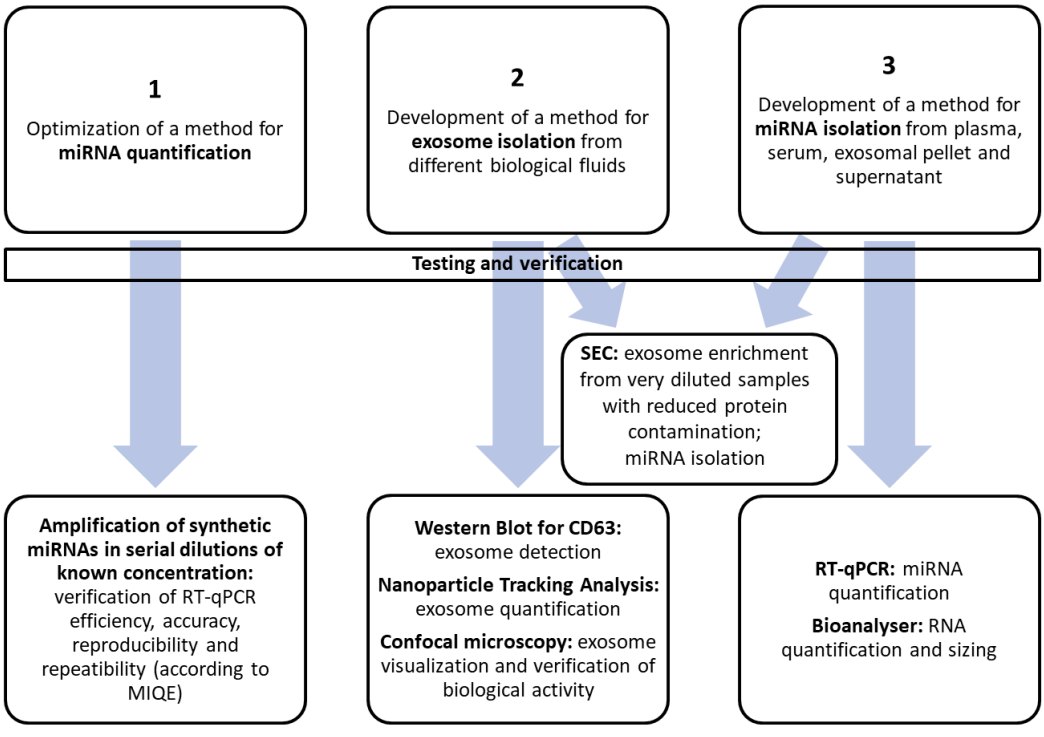

Figure 23: The workflow of part A - development and validation study

The subpart 3 of section A refers to the development of a method for miRNA isolation from plasma, serum, exosome pellet, as well as from exosome-depleted supernatant. The performance of this method was checked by RT-qPCR for miRNA quantification developed in subpart 1 and by RNA sizing and quantification on a bioanalyzer, as well as by SEC.

In part B, the comparison of the self-developed techniques for exosome extraction, miRNA isolation and miRNA amplification with the currently leading, commercial kits was performed (Figure 24). For this purpose, 10 plasma and 10 serum samples from healthy volunteer donors were used. In each sample, exosomes and supernatants were separated by using the self-developed Mannuronate-Guluronate Polymer (MGP)–based method and the Total Exosome Isolation Reagent (TEI, a PEG-based kit from Invitrogen) which served as a reference assay. Subsequently, miRNAs were isolated from the exosomes and supernatants using the self-developed method with the non-chaotropic chemistry and the commercial acid phenol/chloroform-based kit (Total Exosome RNA & Protein Isolation Kit, Invitrogen). Then, the amplification data of the miRNA serial dilutions with my optimized method were compared with those of the commercial RT-qPCR and, based on the methods performance, my optimized technique was chosen for further analyses. Therefore, all miRNA samples isolated with both extraction methods were quantified by my optimized RT-qPCR method using a serial dilution of miRNAs for a miRNA copy number calibration.

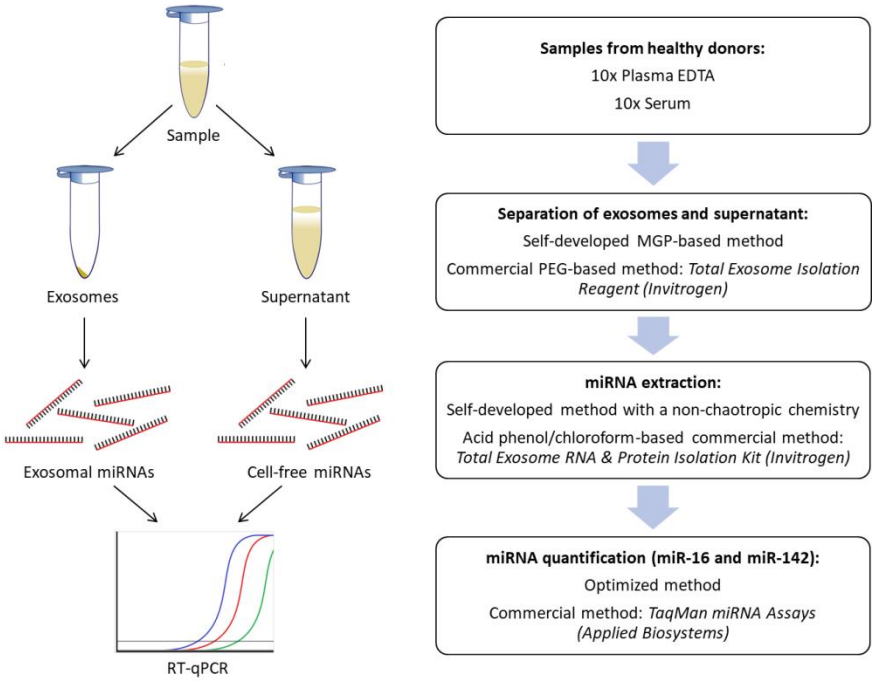

Figure 24: The workflow of part B - comparative study

2. Part A: Development of the methods

In these experiments, numerous variations of reagents and parameters as well as combinations thereof were examined and compared. Since the combinations of all variations would give an immense number of possibilities, the developmental approach relied on analyzing a set of reagents and parameters and choosing the most promising combination based on RT-qPCR results for miR-16 and miR-142. Subsequently, the chosen combination was applied to test and select further reagents and parameters (Table 5 and Table 6).

2.1. MiRNA quantification technique

The most common technique used for miRNA quantification is stem-loop-based RT-qPCR. Briefly, this method utilizes stem-loop primers for reverse transcription and is followed by TaqMan real-time PCR analysis. The stem-loop primer consists of a 3' sticky end complementary to the 3' end of miRNA sequence, two self-complementary regions forming the stem of the primer, and the non-complementary region forming the loop (Figure 25). The reverse transcription reaction includes 3 steps. The low temperature of the first step leads to the hybridization of the self-complementary regions of the loop, and formation of the sticky end, which anneals to the selected miRNA sequence. In the second step, the temperature increases, activating reverse transcriptase to elongate the stem-loop primer to produce cDNA. The last step consists of a temperature near the boiling point for a short time, which leads to a permanent inactivation of the reverse transcriptase. Afterward, the cDNA is ready for amplification by TaqMan real-time PCR. The difference in TaqMan real-time PCR of miRNAs is the specific localization of primers and probe. In the first cycle, the forward primer overlaps the cDNA strand at its 3' end to extend the target sequence and prevent the formation of primer-dimer structures between the forward primer and TaqMan probe. For the same reason, in the following cycle, the reverse primer binds for its most part to the sequence originating from the loop of the stem-loop primer, while the probe optimally binds for its most part to the sequence of miRNA origin and to a smaller extent to the stem-loop primer sequence (Figure 25).

2.1.1. Optimization of the technique: proceeding and final protocol

The development of the miRNA quantification procedure was based on the method developed by a former employee of Applied Biosystems, Dr. Caifu Chen and his colleagues (Chen et al., 2005) (Figure 18). I introduced some modifications to decrease time of the reaction and costs, but in particular to improve the quality. The procedure of the RT-qPCR with original primers (Applied Biosystems) and my elongated/modified primers is illustrated in Figure 25 and Figure 26. My optimized protocol and the comparison to the reference method are displayed in Table 3. The sequences of the primers and probes are listed in Table 4.

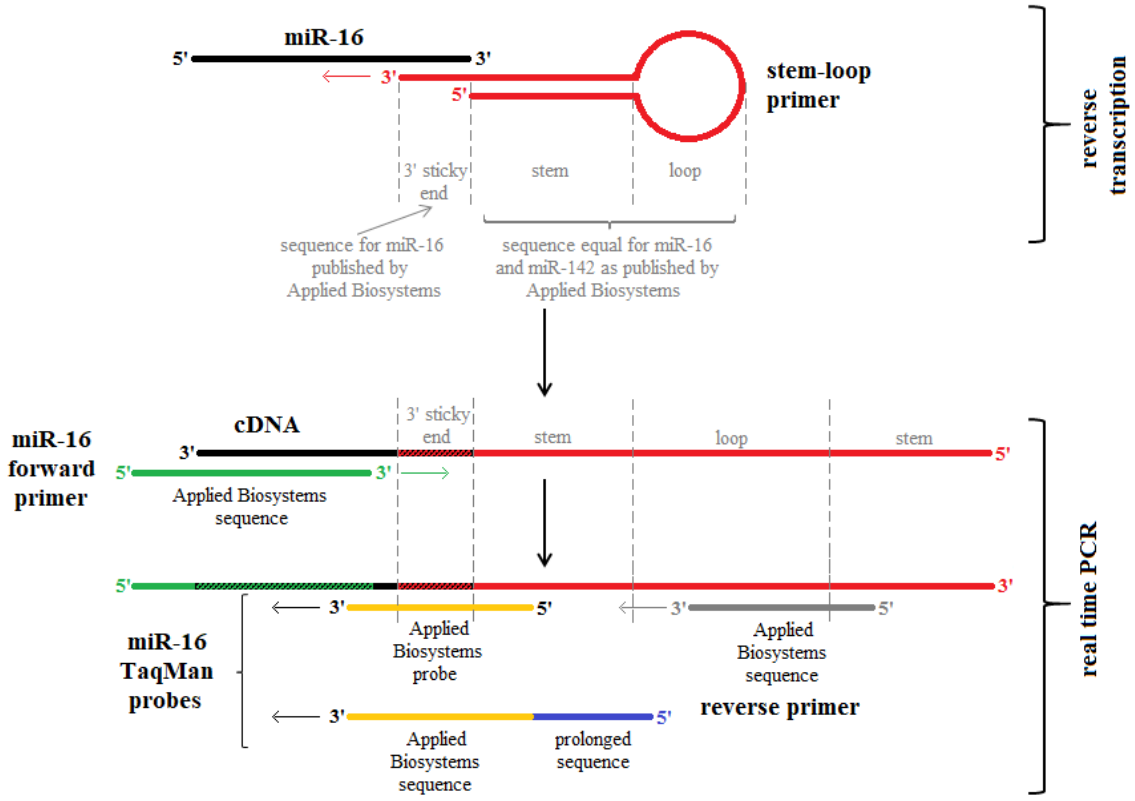

Figure 25: Schema of miR-16 reverse transcription followed by real-time PCR with the original and my elongated TaqMan probe

The core (stem and loop) sequences of the stem-loop primer are the same for miR-16 and miR-142, but the 3' sticky end sequence is specific for miR-16 as published by Applied Biosystems. The forward primer (green), probe (yellow) and reverse primer (grey) were published by Chen et al. The probe was extended at its 5' end by me (blue).

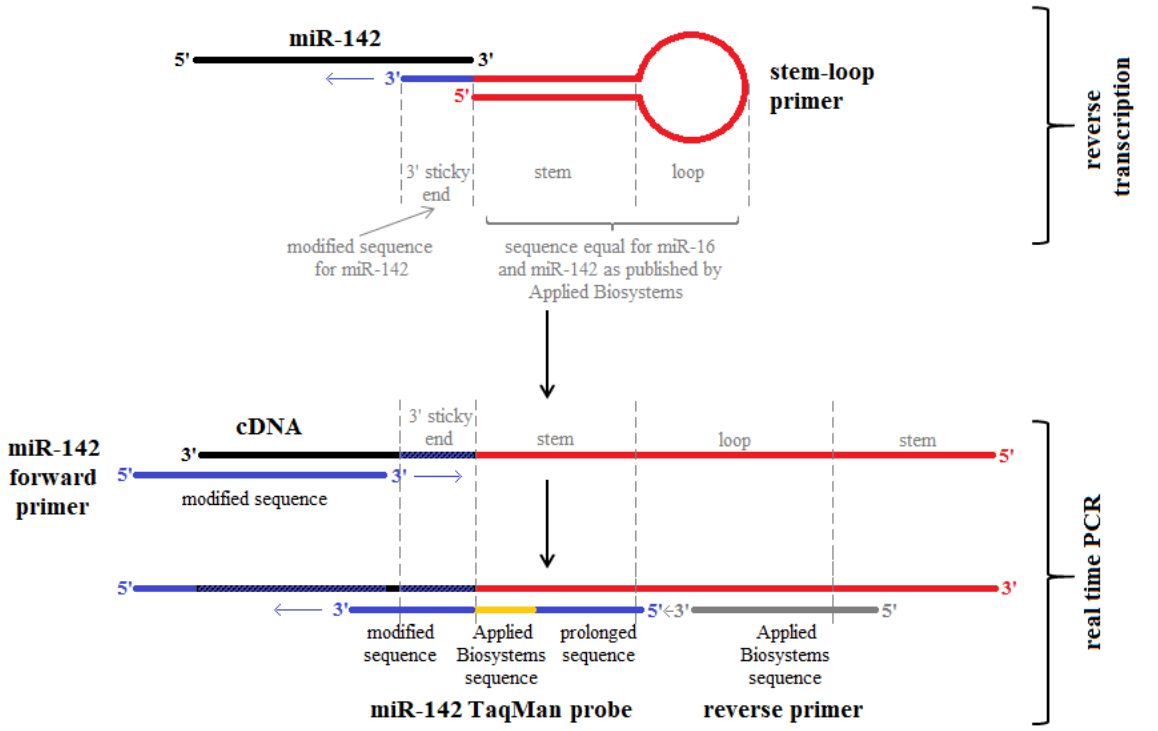

Figure 26: Schema of miR-142 reverse transcription followed by real-time PCR with my modified/ elongated TaqMan probe and primers

The core (stem and loop) sequences of the stem-loop primer are the same for miR-16 and miR-142, but the 3' sticky end sequence was modified to be complementary to miR-142. The forward primer sequence was modified to be specific to the miR-142 cDNA sequence. The reverse primer sequence (grey) was published by Applied Biosystems. The probe of miR-142 with the stem sequence (as published by Applied Biosystems, yellow) was extended at its 5' end and modified at its 3' end to create the complementarity to the miR-142 sequence. All my modifications are in blue.

Table 3: Comparison between the parameters of miRNA amplification method developed by Chen et al. (reference method) and my optimized miRNA amplification method (modified method)

	Parameter	Amount/concentration per reaction	
		Reference method (Chen et al., 2005)	**Modified method**
Reverse transcription (7.5 µl)	Template: miRNA	2.5 µl	2.5 µl
	Primer	50 nM stem-loop (Applied Biosystems)	250 nM stem-loop (Metabion)
	Buffer	1x RT buffer (Applied Biosystems)	1x RT-Buffer (Analytik Jena) + 9.35 mM DTT (Analytik Jena)
	dNTPs	0.25 mM each (Applied Biosystems)	0.25 mM each inNucleotide Mix (Analytik Jena)
	Reverse transcriptase	25 U MultiScribe reverse transcriptase (Applied Biosystems)	9.375 U RT-Enzyme (Analytik Jena)
	RNase inhibitor	1.9 U RNase inhibitor (Applied Biosystems)	excluded
	Procedure conditions	30 min – 16°C 30 min – 42°C 5 min – 85°C hold 4°C	30 min – 16°C 30 min – 42°C 5 min – 95°C hold 4°C

Real-time PCR (10 µl)	Template: cDNA	0.67 µl RT product	0.67 µl RT product
	Master mix	1x TaqMan Universal PCR Master Mix (Applied Biosystems)	1x SpeedAmp Optimization Buffer No. 5, pH 9 (Analytik Jena) 0.25 mM each inNucleotide Mix (Analytik Jena) 0.75 U innuTaq HOT-A DNA Polymerase (Analytik Jena)
	Probe	0.2 µM TaqMan FAM-BHQ-1-MGB probe (Applied Biosystems)	0.17 µM TagMan FAM-BHQ1 probe (Metabion)
	Forward primer	1.5 µM (Applied Biosystems)	0.33 µM (Metabion)
	Reverse primer	0.7 µM (Applied Biosystems)	0.17 µM (Metabion)
	Procedure conditions	10 min – 95°C 15 sec – 95°C | 40 cycles 1 min – 60°C	2 min – 95°C 5 sec – 95°C | 40 cycles 40 sec – 64°C

Table 4: Sequences of the primers and probes of my modified RT-qPCR method

Assay	Primer type	Sequence
miR-16	Reverse transcription stem-loop primer*	5'-GTC GTA TCC AGT GCA GGG TCC GAG GTA TTC GCA CTG GAT ACG ACC GCC AA-3'
	PCR forward primer*	5'-CGC GCT AGC AGC ACG TAA AT-3'
	PCR reverse primer*	5'-GTG CAG GGT CCG AGG T-3'
	PCR probe*	5'-FAM- TCG CAC TGG ATA CGA CCG CCA ATA T - BHQ1-3'
miR-142	Reverse transcription stem-loop primer*	5'-GTC GTA TCC AGT GCA GGG TCC GAG GTA TTC GCA CTG GAT ACG ACT CCA TA-3'
	PCR forward primer*	5'-GCC GCT GTA GTG TTT CCT ACT-3'
	PCR reverse primer*	5'-GTG CAG GGT CCG AGG T-3'
	PCR probe*	5'-FAM-CG CAC TGG ATA CGA CTC CAT AAA G - BHQ1-3'

*The sequences (black) were published by Chen et al. (Applied Biosystems). My modifications are in blue. The sequences of the stem and loop of the stem-loop primer are the same for miR-16 and miR-142 and were published by Chen et al. Only the sequences of 3' sticky ends differ for both miRNAs. The sequences of miR-16 and miR-142 probes were prolongated at their 5' ends (blue) while miR-142 probe sequence was also modified at its 3' end (blue) as shown in Figure 25 and Figure 26. The sequence of miR-16 forward primer was published by Chen et al. while the sequence of miR-142 forward primer was changed to create the complementarity to the miR-142 cDNA.

Several modifications were carried out. My first modification was to exclude the RNase inhibitor, which causes a rise in the signal of the negative control (master mix without template). This is caused by the contamination of the RNase inhibitor with nucleic acids originating from *Escherichia coli* used for the production of this enzyme. Since miRNAs, as compared to ribosomal RNAs or mRNAs and observed by Aryani et al. (Aryani and Denecke, 2015) and our lab, seem to be resistant to RNase activity, the exclusion of the RNase inhibitor is rather advantageous than disadvantageous. More importantly, I modified the TaqMan probe, which in my optimized method is longer than the probe

applied in the method published by Chen et al. (Figure 25). Instead of labeling with BHQ-1 and MGB, it only contains BHQ-1 at its 3' end, and therefore it requires a longer sequence. This length modification increases the probe melting temperature simultaneously maintaining the reaction specificity. A convenient side effect is that the probe with BHQ-1 alone is approximately 15-times cheaper than the probe with BHQ-1 plus MGB. The Hot-Start Taq polymerase (innuTaq HOT-A DNA Polymerase, Analytik Jena), used for the modified method, is very quickly activated, within 2 min, and extremely efficient (Figure 27). Together with the optimized chemistry of master mix and primer concentration, my method allowed reducing time of the real-time PCR reaction down to 64 min, while the protocol of Chen et al. (Chen et al., 2005) takes 93 min, thus, a time saving of nearly half an hour.

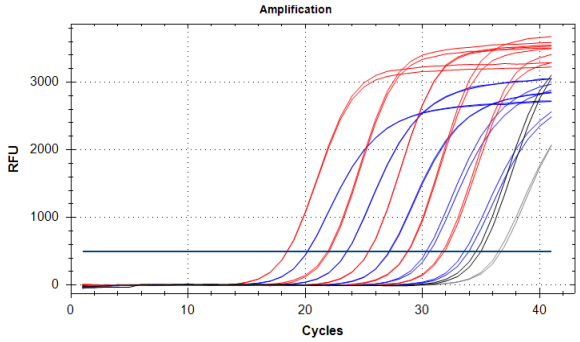

Figure 27: Influence of the Hot-Start Taq polymerase and chemistry on real-time PCR product formation

Amplification of miR-16 using my modified method (red) compared with the amplification using the reference method (blue). For both experiments, primers and procedure conditions of the reference method were used, whereas only the components of the master mix from Applied Biosystems (blue), including 1x RT buffer, 0.25 mM dNTPs, 25 U MultiScribe reverse transcriptase, 1.9 U RNase inhibitor, 1x TaqMan Universal PCR Master Mix differed from the components from Analytik Jena (red), including 1x RT-Buffer, 9.35 mM DTT, 0.25 mM each inNucleotide Mix, 9.375 U RT-Enzyme, 1x SpeedAmp Optimization Buffer No. 5, pH 9, 0.25 mM each in Nucleotide Mix, 0.75 U innuTaq HOT-A DNA Polymerase. A 10-fold serial dilution of synthetic miR-16 from $6.7x10^{-8}$ fM to $6.7x10^{-4}$ fM was used. The C_q values differ by 2, indicating that the performance of real-time PCR with the optimized master mix was 4-times higher. Black and grey curves correspond to the signal of the negative control from my modified method and the reference method, respectively.

2.1.2. Testing and verification

The (modified) primer set for miR-16 and miR-142 (Table **4**) was also checked *in silico* using the software BLAST (https://blast.ncbi.nlm.nih.gov/Blast.cgi), to avoid an unspecific alignment to other sequences. The specificity of my optimized method (Figure 28) for miR-16 (blue) and miR-142 (red) was also tested with $6.7x10^{-5}$ fM of synthetic sequences of miR-484 (black), miR-140-3p (orange), miR-483-5p (brown), let-7b (grey), cel-miR-39-3p (green) and 4 ng of human genomic DNA (yellow) isolated from whole blood (Figure 28A and B). The self-developed assays for both, miR-16 (Figure 28A) and miR-142 (Figure 28B) were highly specific and did not amplify other miRNAs (difference in C_q between target miRNA and another miRNA >14.53). To exclude a possible cross-reaction with genomic DNA, a real-time PCR without reverse transcription was performed. No signals were observed in this experiment, suggesting that the assay is highly RNA-specific (Figure 28A and B). Additionally, to ensure that no additional amplicons are generated, agarose gel electrophoresis of miR-16 and miR-142 PCR products was carried out (Figure 28C and D). The amplification products of miR-16 and miR-142 in concentrations of $6.7x10^{-8}$ fM as templates and water as negative control were used. A single amplicon of a size smaller than 100 bp, potentially corresponding to the size of 71 bp expected for the correct PCR products was observed on the gel (Figure 28C and D, lanes C). When RT-qPCRs without template (with water) were performed, only very weak bands smaller than the correct PCR product were observed, potentially referring to the primer-dimers size (Figure 28C and D, lanes B).

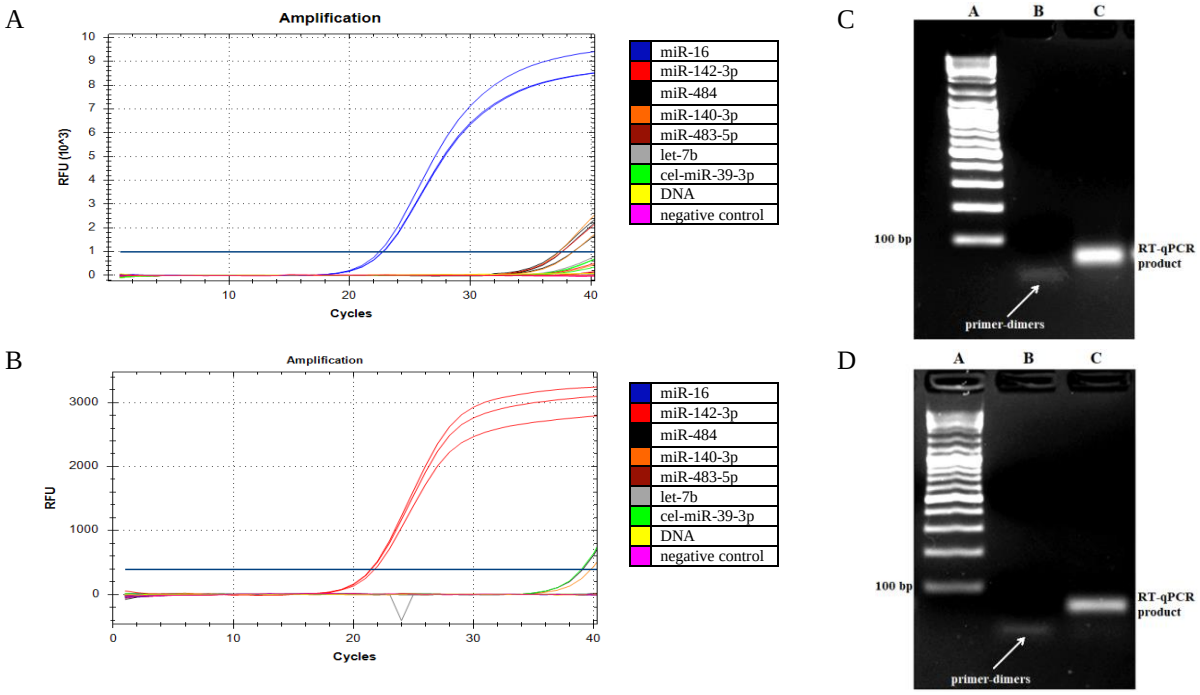

Figure 28: Verification of the specificity of my optimized RT-qPCR method

Seven different miRNA sequences of the same concentration ($6.7x10^{-5}$ fM) and genomic DNA (4 ng) were amplified with my modified RT-qPCR assay for A) miR-16 (blue) and B) miR-142 (red). While miR-16 and miR-142 exhibited strong signals with low C_q values of 22.61 for miR-16 and 21.55 for miR-142 (mean C_q values), the amplification of miR-484 (black), miR-140-3p (orange), miR-483-5p (brown), let-7b (grey), cel-miR-39-3p (green) or DNA (yellow) delivered no signal or very high C_q values. If the C_q values difference between the sample and the negative controls is smaller than 2 or the sample C_q values are over 37, then these signals are usually assumed to be negative results. Gel electrophoresis of C) miR-16 and D) miR-142 PCR products. The amplification of $6.7x10^{-8}$ fM synthetic miRNAs showed a single, prominent band lower than 100 bp (lanes C). There was no product in the negative control. However, a weak band at a smaller size potentially corresponding to primer-dimers was observed (lanes B). DNA ladder ranging from 10,000 to 100 bp (lanes A).

The sensitivity of my optimized method for miRNA quantification was tested by evaluation of the limit of quantification (LOQ). LOQ is defined as the lowest amount of the target in a sample that can be quantitatively determined (Forootan et al., 2017). The LOQ for both, miR-16 and miR-142 assay was $6.7x10^{-8}$ fM. Moreover, both assays expressed a dynamic range of over 7 orders of magnitude (Figure 29), being a standard for TaqMan gene expression assays (Chen et al., 2005). Finally, the modified assays showed an excellent real-time PCR linearity. The correlation coefficient of the standard curve (R^2) which should be higher than 0.98 (Broeders et al., 2014) was higher than 0.996 for all miRNA quantification experiments using my optimized method (0.999, Figure 29A; 0.999, Figure 29B; 0.997, Figure 44A; 0.999, 0.999, 0.997, 0.997, 0.999, 0.999, Figure 46B; 0.999, Figure 47A; 0.996, 0.997, 0.998, 0.997, 0.997, 0.998, Figure 48B).

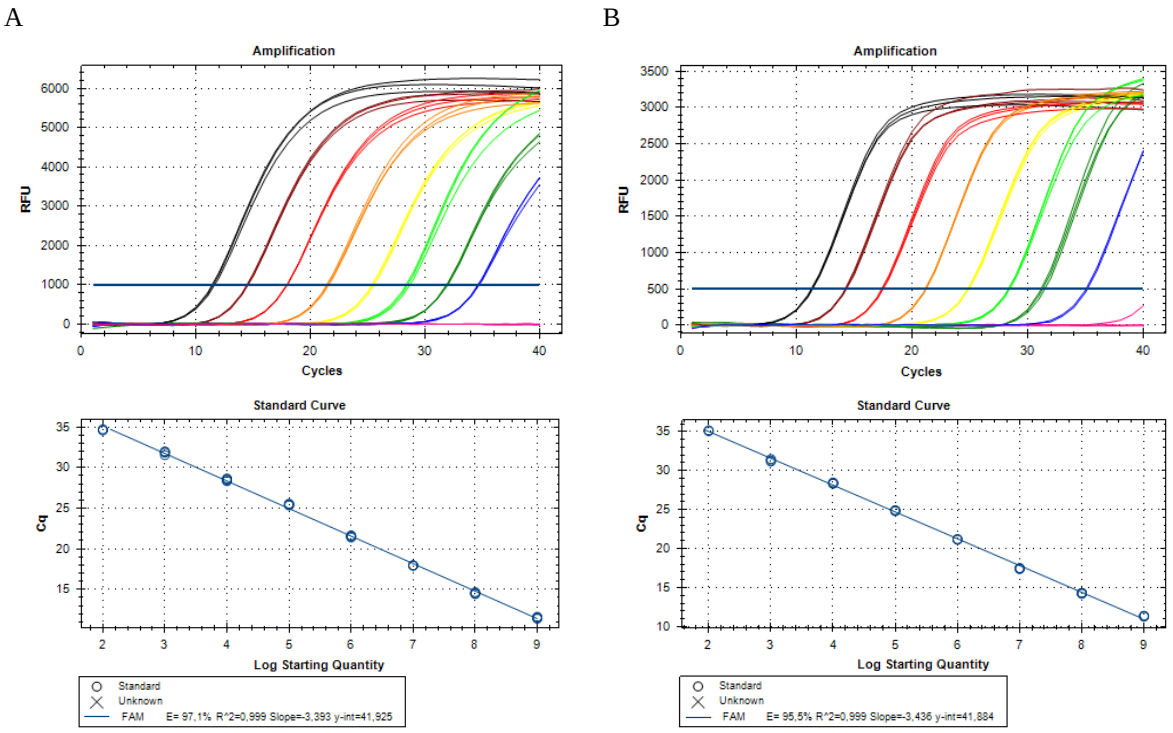

Figure 29: Representative amplification plots and standard curves using the optimized method

Amplification and standard curves of a 10-fold serial dilution of A) miR-16 and B) miR-142 which range from $6.7x10^{-8}$ fM to $6.7x10^{-1}$ fM (blue to black curves) using miR-16 and miR-142 primers and probes (Table **4**). Pink curves, negative control.

Ideally, the efficiency (E) of a real-time PCR should be 100%, which corresponds to a Cq difference between two dilution steps (slope) of -3.3 for a 10-fold target dilution. This means that in each replication cycle the amount of a target sequence should double. If the number of amplified molecules in a cycle is less than doubled, the efficiency is lower than

100%. Conversely, the efficiency higher than 100% indicates that unspecific products or primer-dimers are generated. The PCR efficiency can be calculated applying the formula E= 100*(10^-1/slope-1). Generally, for qPCR, the efficiency between 90 and 110 % is accepted (Broeders et al., 2014), corresponding to the slope range between -3.1 and -3.6. To calculate the efficiency of my optimized miRNA RT-qPCR, a 10-fold dilution series of miR-16 and miR-142 was prepared. The efficiency of the optimized RT-qPCR miR-16 assay was between 90 and 100% in all of experiments of this PhD thesis (97.1%, Figure 29A; 99.7%, Figure 44A; 99.3%, 90.7%, 99.1%, 96.6%, 93.0%, 94.8%, Figure 46B). The optimized RT-qPCR miR-142 assay exhibited lower efficiency of 80 to 96% (95.5%, Figure 29B; 95.4%, Figure 47A; 80.2%, 79.4%, 85.0%, 85.3%, 85.2%, 85.6%, Figure 48B). As compared in the later parts of this work (chapter 3.2.), the Applied Biosystems RT-qPCR miR-142 assay showed similar or even a lower efficiency of 77 to 88% (77.2%, 76.7%, 88.0%, 87.0%, 86.2%, 87.5%, Figure 48A). These findings suggest that miR-142 might be a difficult target for PCR amplification, possibly caused by its low GC (guanine/cytosine) content and stable secondary structures that might interfere the annealing of the stem-loop primer during the RT reaction.

2.2. Exosome isolation technique

MGP is composed of beta-D-Mannuronate and alfa-L-Guluronate, which can form homopolymers (MM- and GG-Blocks) and heteropolymers (MG- and GM-Blocks, Figure 30A). MGP has properties to form a hydrogel because GG-Blocks contain a special niche, in which calcium ions can be placed. In the presence of salt, salt ions zip poly-guluronate sequences and form an egg box-like conformation (Figure 30B) (Marburger, 2003).

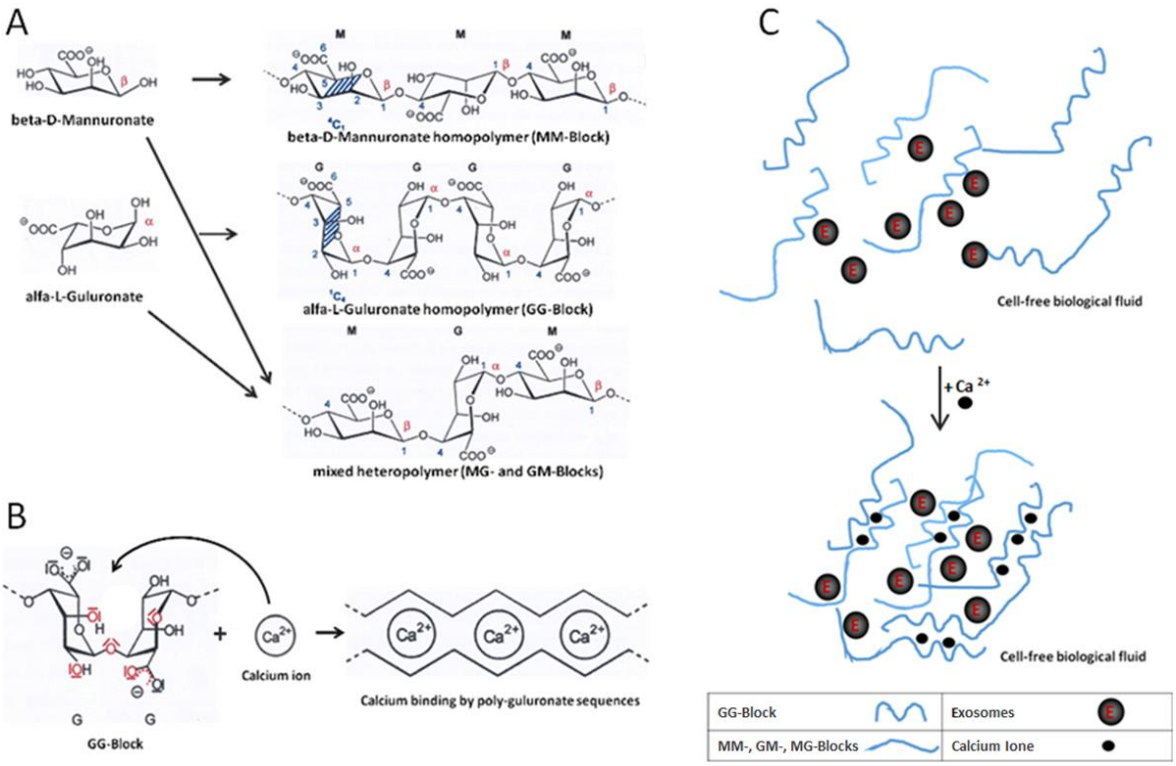

Figure 30: The theory of MGP action (taken from Marburger 2003; modified)
A) Composition and structure of MGP. B) Principle of hydrogel formation. C) Exosome capture in a MGP hydrogel.

I used this phenomenon to capture exosomes into the MGP structure. When the MGP solution is added to a biological fluid containing exosomes, followed by addition of calcium ions, MGP sequences in the area of GG-blocks are zipped by calcium ions, and the MG- and GM-Blocks entrap exosomes (Figure 30C). The MGP/exosome complex can then be centrifuged to separate exosomes and the supernatant.

2.2.1. Development proceeding

Reagents and parameters tested in this study to develop the method of exosome enrichment are listed in the following Table 5. The best reagents and parameters were chosen based on the C_q differences (CD) derived from the RT-qPCR results. For example, a comparison between 5 types of enrichment reagent 2 was carried out. Calcium chloride gave the highest concentration of miRNAs with a C_q of 28.49 for miR-16, and therefore it was selected as an enrichment reagent 2 and further tested in combination with other reagents and parameters (Figure 31).

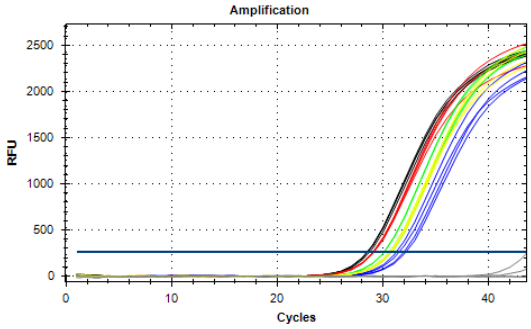

Figure 31: Comparison between exosome enrichment efficiency of different enrichment reagent 2 types
Different chemicals were tested as an enrichment reagent 2: calcium chloride (black), calcium acetate (red), ammonium chloride (green), zinc chloride (blue), manganese (II) chloride (yellow). Quantity and quality of isolated miR-16 were determined by my optimized RT-qPCR method. Negative control is in grey.

Table 5: Reagents and parameters tested for enrichment of exosomes

Tested reagents and parameters*	Variations	Mean RT-qPCR data as C_q difference (CD) between the variants**
Type of enrichment reagent 1	**MGP1 (Analytik Jena)*** **	**0**
	MGP2 (Analytik Jena)	1.48
	MGP3 (Analytik Jena)	1.48
	MGP4 (Analytik Jena)	1.60
	MGP5 (Analytik Jena)	0.56
Volume of enrichment reagent 1	20 µl	0.25
	30 µl* **	**0**
	40 µl	0.83
	50 µl	0.52
	60 µl	3.07
	90 µl	8.35
	100 µl	4.02
Incubation time using enrichment reagent 1	**None*** **	**0**
	1 min	-0.03****
	3 min	0.20
	30 min	0.10
	60 min	1.13
Temperature of incubation using enrichment reagent 1	4°C	0.23
	Room temperature* **	**0**
	50°C	7.94
Thermoshaker while incubation with enrichment reagent 1	**No shaking*** **	**0**
	400 rpm	0.69
Type of enrichment reagent 2	**Calcium chloride** **	**0**
	Calcium acetate	0.51
	Ammonium chloride	1.64
	Zink chloride	3.10
	Manganese (II) chloride	2.11
Volume of enrichment reagent 2	100 µl	0.11
	150 µl* **	**0**
	300 µl	0.89
	450 µl	1.19
Incubation time using enrichment reagent 2	1 min	0.80
	3 min	0.45
	10 min* **	**0**
	30 min	0.44
	60 min	0.62
Temperature of incubation using enrichment reagent 2	4°C	0.59
	Room temperature* **	**0**
	50°C	0.04****
Thermoshaker while incubation with enrichment reagent 2	**No shaking*** **	**0**
	400 rpm	0.74
Time and speed of centrifugation	1 min, 8,000 g	1.31
	1 min, 10,000 g	1.57
	1 min, 16,000 g	1.37
	2 min, 5,000 g	1.79
	3 min, 10,000 g	1.59
	3 min, 16,000 g	1.25

	10 min, 500 g	2.33
	15 min, 5,000 g	0.99
	15 min, 16,000 g	0.29
	30 min, 3,000 g	1.25
	30 min, 5,000 g	0.44
	30 min, 10,000 g	0.36
	30 min, 16,000 g* **	**0**
	60 min, 16,000 g	-0.13*****
Removal of residuals of supernatant	Washing with 1 ml RNase-free H_2O	3.50
	No washing	0.53
	Spin down for 10 s* **	**0**
Dissolving of the pellet for direct downstream applications	D1 (H_2O)	n.d.
	D2 (PBS)	n.d.
	D3 (RIPA)	n.d.
	D4 (50 mM tri-natriumcitrat)	n.d.
	D5 (100 mM tri-natriumcitrat)	n.d.
	D6 (150 mM tri-natriumcitrat)	n.d.
	D7 (200 mM tri-natriumcitrat)	n.d.
	D8 (50 mM EDTA)* **	n.d.
	D9 (100 mM EDTA)	n.d.
	D10 (500 mM EDTA)	n.d.
	D11 (1 M EDTA)	n.d.
	D12 (PBS + 50 mM EDTA)	n.d.

*For development of the exosome enrichment method, a plasma volume of 500 µl was used. Some data obtained with the best variations of reagents and parameters were verified with serum. **Calculated from the formula: $CD = C_{q(x)} - C_{q(y)}$, where x is any variant tested in a dark-grey box group and y is the best variant. The difference shows the magnitude of the aberrance of a variant from the best variant. The lower the CD value is the better is the quantity and quality of the PCR product. A CD value of 0 indicates the best variation within the group of single grey boxes. ***Chosen best variations of reagents and parameters are in bold. Variations of results similar to the best variation, that showed a minimal data improvement but **** were not confirmed by further intensification of the parameter, or ***** significantly increased the experiment duration/complexity, were not chosen for further testing. nd., not determinable.

2.2.2. Optimized protocol

First, 30 µl MGP is added to 500 µl of starting material (plasma, serum, urine or cell culture supernatant), and the mix is vortexed. Then, 150 µl 1 M calcium chloride solution is added, the sample is vortexed and incubated for 10 min at room temperature to allow creating the complex between exosomes and MGP. Subsequently, the sample is centrifuged for 30 min at 16,000 g, to pellet the complex of exosomes and MGP. The supernatant is transferred to a new tube, and the tube containing the pellet is centrifuged for 10 sec to remove the residues of the supernatant (Figure 32). The protocol takes around 45 min and can be successfully applied to sample volumes from 200 µl to 2 ml.

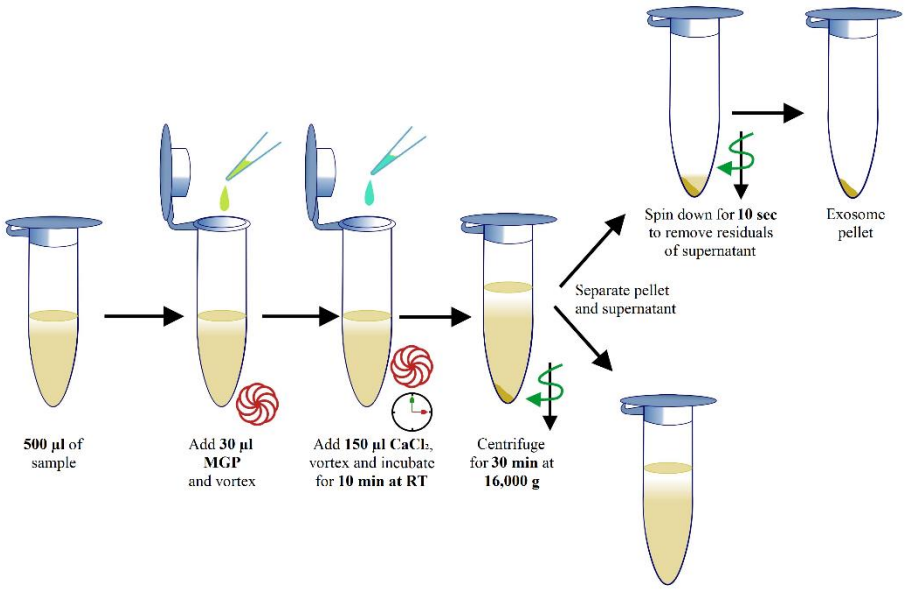

Figure 32: The workflow of the exosome enrichment protocol

2.2.3. Testing and verification

The MGP-based technique was tested on biological fluids, such as blood plasma, blood serum, urine, cell culture supernatant, and a dilution of commercial lyophilized exosome standards from plasma of healthy donors. Method efficiency, specificity and integrity of extracted exosomes were verified by NTA (Figure 35 and Figure 36), Western Blot (Figure 33A), confocal microscopy (Figure 33B and Figure 34) and SEC (Figure 37).

To test if the MGP-based method can isolate exosomes from different types of samples, a Western Blot using the anti-CD63 monoclonal antibody labelled with horseradish peroxidase (HRP) was performed under non-reducing conditions. As shown by the Western blot, the molecular weight of the bands containing the exosomal protein CD63 isolated from 500 µl plasma and 500 µl serum corresponds to the weight of the band of 4 µg exosome standards from plasma of healthy donors, used as a positive control, whereas the negative control (MGP enrichment using PBS) does not exhibit any band (Figure 33A). The molecular weight of these bands observed in both plasma and serum samples and even in the positive control is at 43 kDa which is not conform with the predicted weight of CD63 (63 kDa). However, the molecular weight of CD63 can vary between 25 and 65 kDa, caused by numerous post-translational modifications (e.g. glycosylation patterns) and cleavages, as well as relative charges and different experimental conditions. These findings demonstrate the successful extraction of exosomes from plasma and serum by my optimized method. In contrast, the band derived from urine is rather a smear, suggesting

the particular conditions in urine with its protease activity. Thus, urine seems to be not qualified for the extraction of exosomes.

To confirm the presence of exosomes, the dissolved pellet derived from 500 µl plasma was dyed with Exo-Red and visualized by confocal microscopy (Figure 33B). Exo-Red is based on acridine orange chemistry, and is qualified for the staining of nucleic acids. It is cell membrane permeable and intercalates non-covalently with exosomal RNA emitting a red fluorescence signal. In the experiment of Figure 33B, the exosome/MGP pellet was dissolved in PBS, which led to the formation of exosome agglomerates. In the following experiments, exosome/MGP pellets were always dissolved in 50 mM EDTA to avoid such an agglomeration.

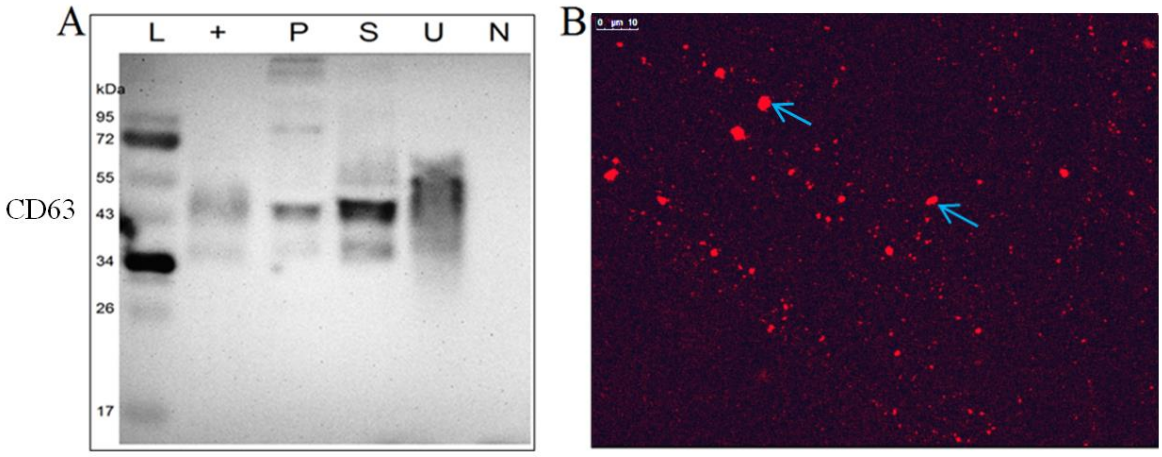

Figure 33: Verification of exosome isolation

A) Western Blot analysis of enriched exosomes. Molecular size protein ladder, L; positive control, +; plasma, P; serum, S; urine, U; negative control, N. B) Microscopic analysis of enriched exosomes. Blue arrows indicate exosome agglomerates.

To examine the integrity and biological activity of exosomes isolated with the self-developed MGP-based method, exosome pellets from 2 ml plasma and 2 ml serum were stained with PKH26 dye (red fluorescence). PKH26 is a fluorescent dye used for general cell membrane labelling. The breast cancer cell line MDA-MB-468 was stained with an antibody specific for the epithelial marker EpCAM (green fluorescence), and approximately 9,000,000 exosomes stained with PKH26 were added to 30.000 cells per well. After a 90-min incubation, cells were washed with PBS and fresh exosome-depleted cell medium was added. Cells in different phases of the cell cycle up-took the plasma- and serum-derived exosomes as detected by live cell confocal microscopy (Figure 34).

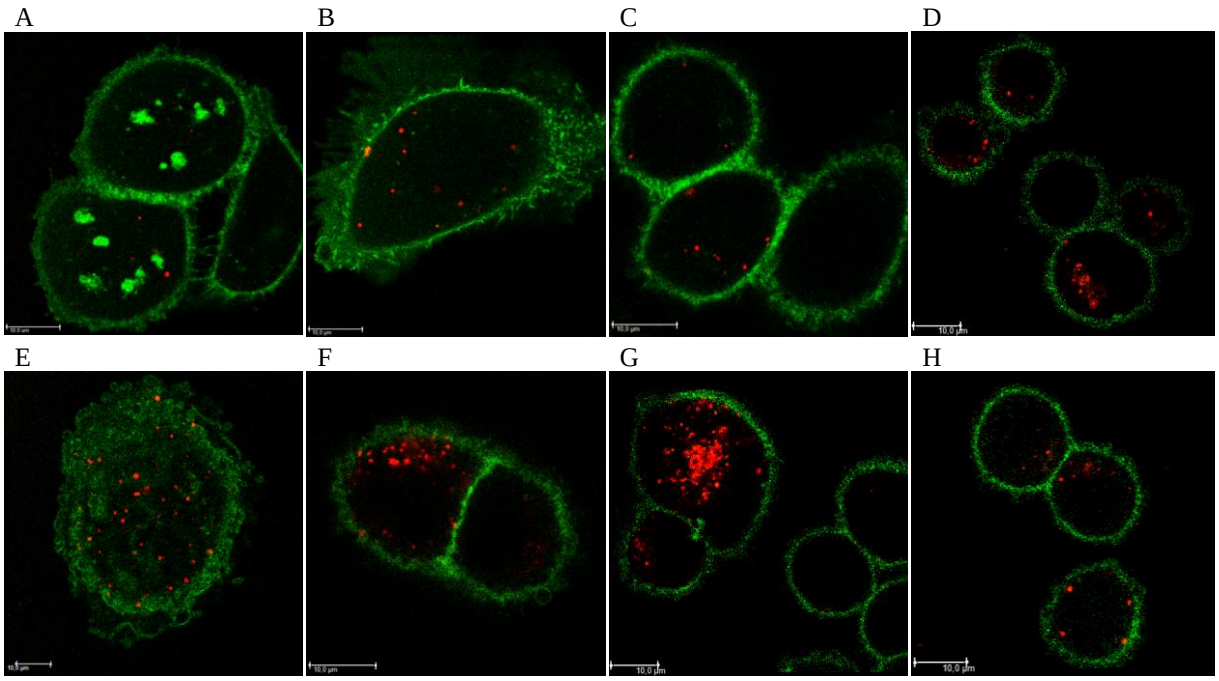

Figure 34: Confocal microscopy – Verification of the biological activity of exosomes isolated by the MGP method

Exosomes isolated from 2 ml plasma (A-D) and 2 ml serum (E-H). The cell membrane was stained in green, while exosomes were stained in red. The course of the pictures from A to D and from E to H reflects the varied accumulation of exosomes in different cells. The lower scale bar corresponds to 10 µm.

The size distribution of exosomes and their concentration were determined by NTA on a NanoSight device (Figure 35 and Figure 36). Exosomes isolated by the MGP-based technique were analyzed in different volumes of plasma, serum and cell culture supernatant. The size range of majority of the measured particles was between 20 and 300 nm demonstrating that the samples contained exosomes and bigger microvesicles or exosome aggregates. Nevertheless, the main size (mode) of isolated particles ranged between 94.2 and 125.9 nm, indicating that most of the isolated vesicles were exosomes. The concentration of particles was increasing along with the volume of starting material. To check the efficiency of the MGP-based method, the isolation of a known number of exosomes derived from the dilutions of lyophilized exosomal standards was performed by the MGP-based technique and ultracentrifugation. Then, the concentrations of exosomes isolated with both techniques were compared to those of exosomes in the starting dilution of lyophilized exosome standards. All three samples expressed a similar mode size and a number of vesicles (Figure 36B).

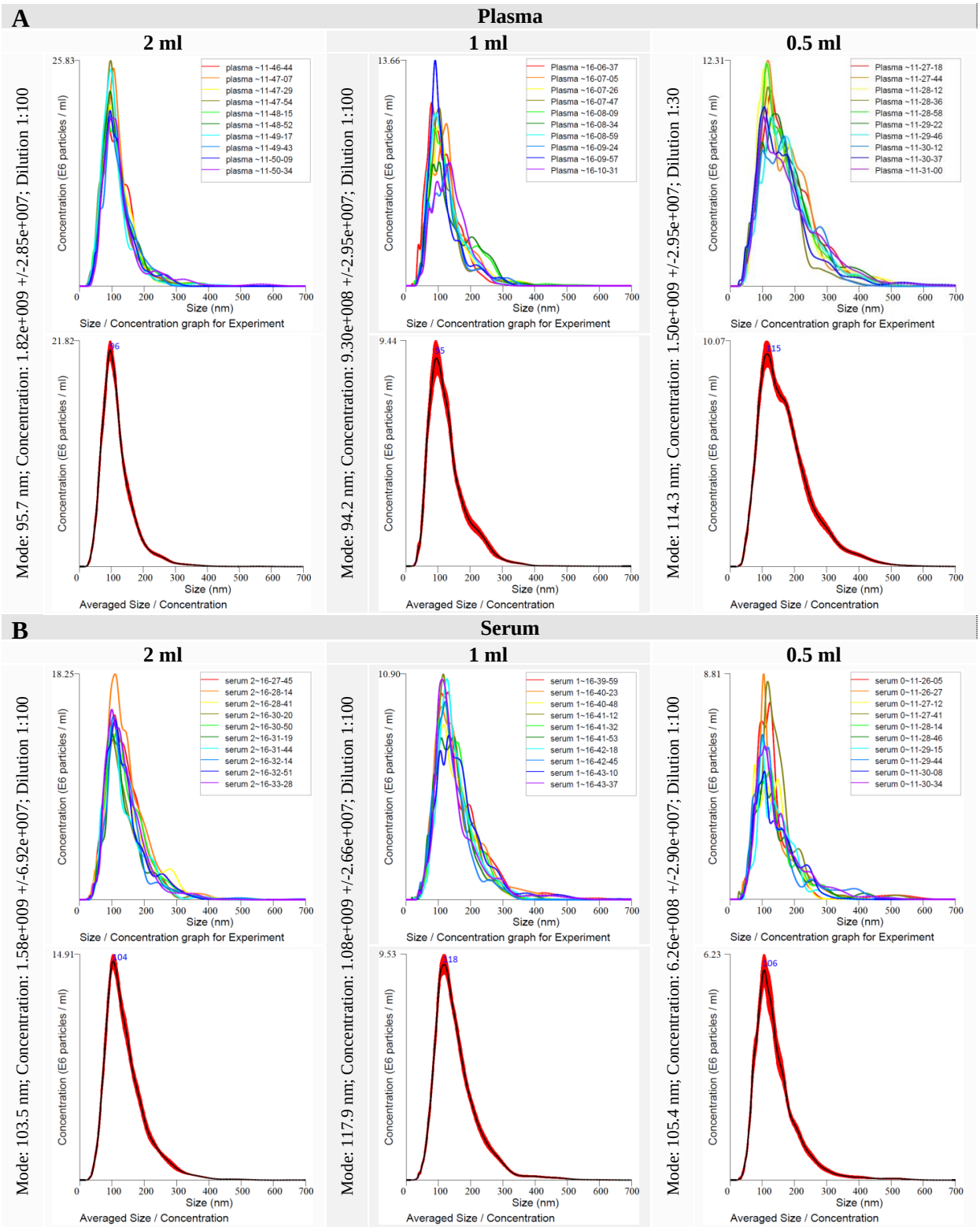

Figure 35: Size distribution and quantity of plasma- and serum-derived exosomes determined by NTA

The quantity and size of exosomes isolated by the MGP-based technique from different volumes of A) plasma and B) serum. Coloured plots (red to violet, upper graphs) represent 10 measurements (10 videos with a duration of 10 sec each) recorded for each sample. The 10 measurements were processed (lower graphs) to determine the mean (black plot), mode (values in blue) and standard deviation of results (thick red curve covering the black curve indicates +/- 1 standard error of the mean).

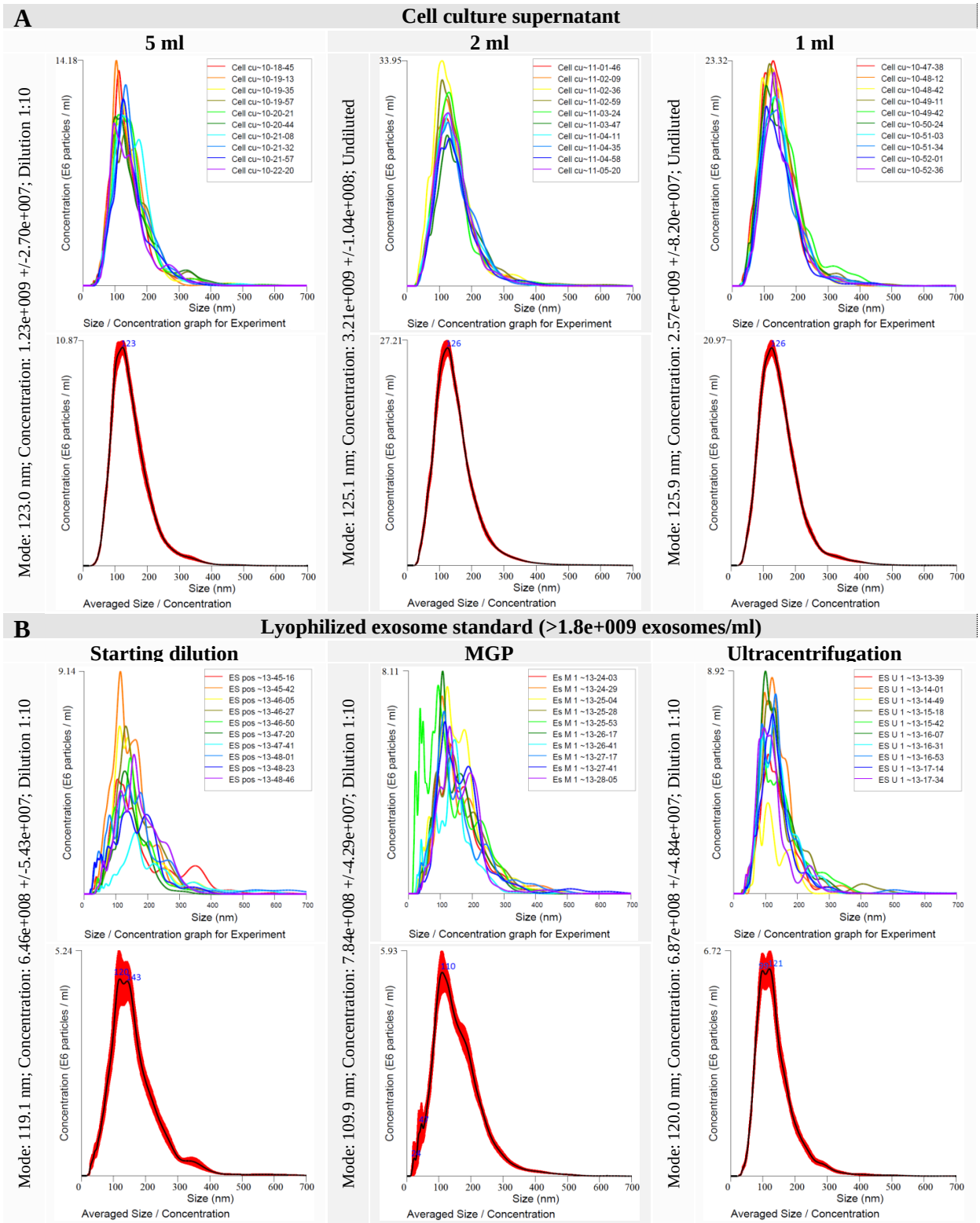

Figure 36: Size distribution and quantity of cell culture supernatant- and lyophilized exosome standard-derived exosomes determined by NTA

A) The quantity and size of exosomes isolated by the MGP-based technique from different volumes of cell culture supernatant. B) Efficiency of the MGP-based method was tested using known concentrations of lyophilized exosome standard. Coloured plots (red to violet, upper graphs) represent 10 measurements (10 videos with a duration of 10 sec each) recorded for each sample. The 10 measurements were processed (lower graphs) to determine the mean (black plot), mode (values in blue) and standard deviation of results (thick red curve covering the black curve indicates +/- 1 standard error of the mean).

SEC was performed to test if 1) MGP can also efficiently isolate exosomes from very diluted samples, and 2) MGP co-isolates plasma proteins. Plasma and serum samples (500 µl of each) were fractionated into 25 1-ml fractions by a SEC column. Then, exosomes were isolated from 500 µl of each fraction by the MGP-based method, followed by the isolation of miRNAs, and RT-qPCR for miR-16 and miR-142 performed with my self-developed and optimized methods. Moreover, the protein concentration in each fraction was measured with the Bradford protein assay. The portion of total miR-16 (blue), miR-142 (red), and protein (black) contained in each fraction are presented on the graphs below (Figure 37A and B). Additionally, SDS-PAGE of total protein was performed (Figure 37C and D). The majority of miRNAs were found in the early fractions from 7 to 14 for plasma and from 8 to 15 for serum, while most of the proteins were found in the late fractions from 14 to 20 and from 15 to 22 for plasma and serum, respectively. In conclusion, the MGP-based technique efficiently enriched exosomes from even very diluted samples, as shown by the SEC fractions. The quantity of miRNAs was elevated in the early fractions and decreased in the late fractions indicating that the self-developed technique allows isolating exosomes without the enrichment of proteins.

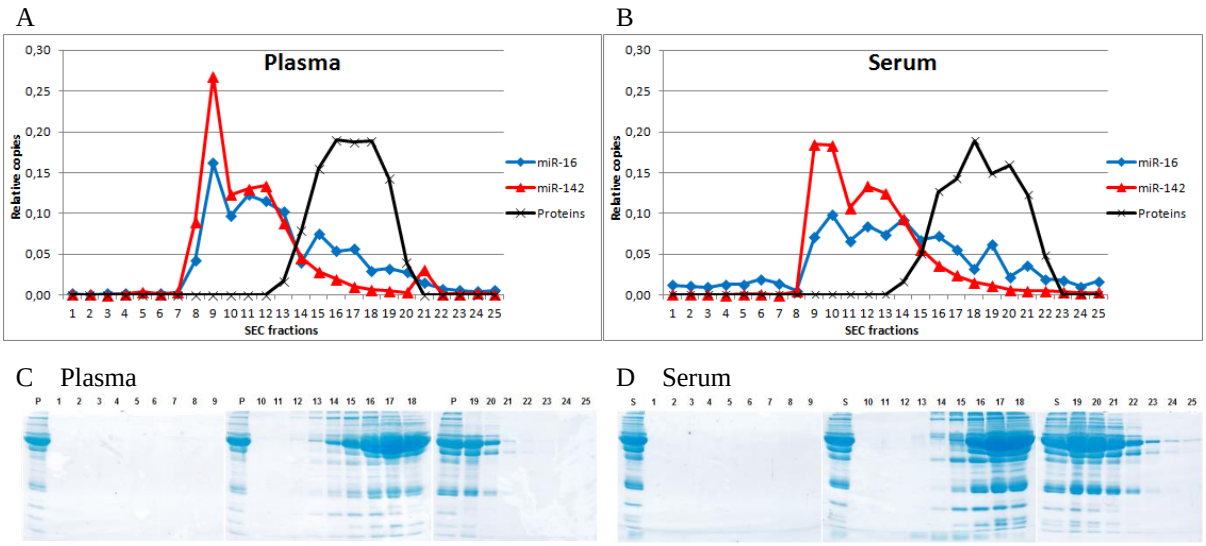

Figure 37: Isolation of exosome-derived miRNAs from SEC fractions by my self-developed techniques
For both, A) plasma and B) serum, miRNAs isolated and quantified by my optimized methods were found in the early fractions, and proteins measured by the Bradford assay were detected in the late fractions. SDS-PAGE of total protein in 25 SEC fractions confirmed the results of the Bradford assay for C) plasma and D) serum.

2.3. MiRNA isolation

2.3.1. Development of a miRNA isolation technique

For the development of the miRNA isolation method, different compositions of reagents and parameters were tested, and the yields of isolated miRNAs were compared by my optimized RT-qPCR. For example, first different lysis buffers of Analytik Jena were tested to select the best type and concentration of lysis agent for isolation of cell-free and exosome-derived miRNAs. Then, based on these results, the primary combination of lysis agents was chosen and further optimized (Figure 38).

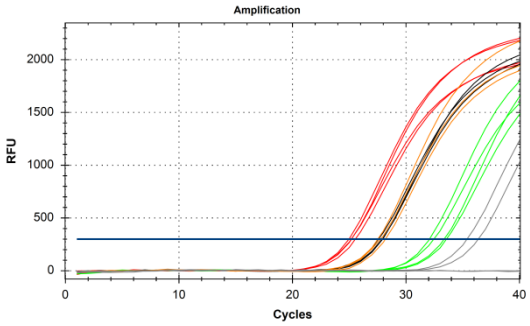

Figure 38: Comparison of the compositions of lysis solutions

The self-created lysis solutions tested in this experiment were: L6 (red), L7 (green), L8 (black), and L9 (orange). Grey curves indicate the negative control of this assay. The lysis solutions were used to isolate miRNAs from exosomes/MGP pellet prepared from 500 µl blood plasma. The performance of these solutions was determined by my optimized RT-qPCR method for miR-16, and the lysis buffer L6 displaying C_q of 25.23 in the PCR was used for further optimization of the protocol. For considerations of all experiments that I performed, please see the appendix at the end of the thesis.

Reagents and parameters tested in 500 µl of plasma to develop an easy and quick method of miRNA isolation are presented in Table 6. To test the extraction efficiency, miR-16 and miR-142 were amplified by my optimized RT-qPCR. The best variation was chosen based on the mean C_q differences (CD) between tested variations.

Table 6: Reagents and parameters tested for miRNA isolation

Tested reagents and parameters	Variations	Mean RT-qPCR results as C_q difference (CD) between variants*
Lysis solutions		
Solutions of Analytik Jena	SE (PME free-circulating DNA Extraction Kit, Analytik Jena)	6.80
	GS (PME free-circulating DNA Extraction Kit, Analytik Jena)	5.57
	SEP (innuCONVERT Bisulfite Body Fluids Kit, Analytik Jena)	4.70
	RLM (Analytik Jena)	5.43

	OPT (innuPREP Plant DNA Kit, Analytik Jena)	0.49
	QPT (innuPREP Tissue DNA Kit, Analytik Jena)	1.03
	QPS (innuPREP FFPE DNA Kit – IPC16, Analytik Jena)	0.44
	BLB (innuPREP Blood DNA MIDI Direct Kit, Analytik Jena)	12.33
	BC (innuCONVERT Bisulfite All-in-One Kit, Analytik Jena)	4.69
	CLS (Instant Virus RNA/DNA Kit, Analytik Jena)	6.86
	SLS (innuPREP Blood DNA Mini Kit, Analytik Jena)	8.12
	TLS (innuPREP Blood DNA Midi Kit, Analytik Jena)	0.83
	RL (innuPREP RNA mini Kit, Analytik Jena)	4.49
	Ery Lysis solution A (innuPREP Blood DNA Midi Kit, Analytik Jena)	6.95
	SLB (innuPREP Stool DNA Kit, Analytik Jena)	7.33
	ELS (innuSPEED Soil DNA Kit, Analytik Jena)	3.72
	WB (innuPREP Plant DNA/RNA Virus Kit – KFFLX, Analytik Jena)	1.48
	PL (innuPREP Plant RNA Kit, Analytik Jena)	5.52
	MA (innuPREP FFPE total RNA Kit, Analytik Jena)	2.56
	CBV (innuPREP Virus DNA/RNA Kit, Analytik Jena)	0.27
Solutions created	L1 (10 % SDS, 2.6 M Tris-HCl pH 8.0, 0.6M urea, 10mM EDTA, 1mM $CaCl_2$)	0.90
	L2 (5 % SDS, 1.3 M Tris-HCl pH 8.0, 0.3M urea, 10mM EDTA, 1mM $CaCl_2$)	0.13
	L3 (5 % SDS, 1.3 M Tris-HCl pH 8.0, 0.3M urea, 25mM EDTA, 1mM $CaCl_2$)	7.04
	L4 (5% SDS, 1.3 M Tris-HCl pH 8.0, 0.3M urea, 50mM EDTA, 1mM $CaCl_2$)	6.29
	L5 (5 % SDS, 1.3 M Tris-HCl pH 8.0, 0.3M urea, 100mM EDTA, 1mM $CaCl_2$)	5.99
	L6 (5 % SDS, 1.3 M Tris-HCl pH 8.0, 0.3M urea, 5mM Na-citrate, 1mM $CaCl_2$)**	**0**
	L7 (5 % SDS, 1.3 M Tris-HCl pH 8.0, 0.3M urea, 50mM Na-citrate, 1mM $CaCl_2$)	7.66
	L8 (5 % SDS, 1.3 M Tris-HCl pH 8.0, 0.3M urea, 5mM Na-acetate, 1mM $CaCl_2$)	2.51
	L9 (5 % SDS, 1.3 M Tris-HCl pH 8.0, 0.3M urea, 50mM Na-acetate, 1mM $CaCl_2$)	2.65
	L10 (5 % SDS, 1.3 M Tris-HCl pH 8.0, 0.3M urea)	2.86
	L11 (5 % SDS, 50 mM Tris-HCl pH 8.0, 0.3M urea, 10mM Na-citrate)	0.10
	L12 (5 % SDS, 50 mM Tris-HCl pH 8.0, 0.3M urea, 15mM Na-citrate)	0.31
	L13 (5 % SDS, 50 mM Tris-HCl pH 8.0, 0.3M urea, 20mM Na-citrate)	1.32
	L14 (5 % SDS, 50 mM Tris-HCl pH 8.0, 0.3M urea, 5mM Na-citrate, 1M GSCN)	4.86
	L15 (5 % SDS, 50 mM Tris-HCl pH 8.0, 0.3M urea, 5mM Na-citrate, 0.5% NLS)	0.71
	L16 (50 mM Tris-HCl pH 8.0, 95mM urea, 0.5% Tween 20, 1mM EDTA)	13.72
	L17 (1 % SDS, 50 mM Tris-HCl pH 8.0, 95mM urea, 0.5% Tween 20)	4.93
	L18 (1 % SDS, 95 mM urea, 0.5% Tween 20, 1mM EDTA)	6.45
	L19 (1 % SDS, 50 mM Tris-HCl pH 8.0, 0.5% Tween 20, 1mM EDTA)	5.08
	L20 (1 % SDS, 5 0mM Tris-HCl pH 8.0, 95mM urea, 1mM	4.96

	EDTA)	
	L21 (4 M GSCN)	5.41
	L22 (4 M GSCN, 100 mM Tris-HCl pH 8.0)	3.77
	L23 (5 M GSCN)	10.22
	L24 (5 M GSCN, 100 mM Tris-HCl pH 8.0)	7.61
Lysis solution volume	200 µl	1.56
	300 µl	1.21
	400 µl**	**0**
	500 µl	0.22
	600 µl	1.03
Proteinase K treatment		
Volume of proteinase K 20 mg/ml (innuPREP Proteinase K, Analytik Jena)	10 µl	0.25
	20 µl **	**0**
	30 µl	0.45
	40 µl	0.09***
	50 µl	0.32
Lysis conditions		
Lysis time and temperature	5 min, RT	1.22
	10 min, 70°C	0.22
	15 min 70°C	0.33
	20 min, 55°C**	**0**
	20 min, 70°C	0.34
	20 min, 85°C	0.46
	30 min, 70°C	0.49
Centrifugation		
Post-lysis centrifugation for removal of MGP residuals	none	1.72
	1 min, 16,000 g	1.48
	2 min, 16,000 g	0.24
	3 min, 16,000 g	0.26
	5 min, 16,000 g**	**0**
	10 min, 16,000 g	-0.08***
Binding buffer		
Type and volume of binding buffer	400 µl 100% EtOH	2.46
	600 µl 100% EtOH	0.79
	800 µl 100% EtOH**	**0**
	400 µl 100% isopropanol	3.44
	600 µl 100% isopropanol	1.53
	800 µl 100% isopropanol	1.06
	400 µl 55% tetrahydrofuran	10.46
	600 µl 100% tetrahydrofuran	5.62
	600 µl 55% tetrahydrofuran	9.25
	400 µl RBF (innuPREP DNA Sizing Kit, Analytik Jena)	13.23
	200 µl VL (Analytik Jena)	11.75
	400 µl SBS (innuPREP Plant DNA Kit, Analytik Jena)	12.44
Spin columns		
Type of filter material	**SC1 (innuPREP Virus RNA Kit, Analytik Jena)****	**0**
	SC2 (innuPREP Blood DNA Midi Kit, Analytik Jena)	0.31
	SC3 (innuPREP TCM DNA Extraction Kit, Analytik Jena)	0.27
	SC4 (innuPREP Plasmid Mini Kit 2.0, Analytik Jena)	0.22

	SC5 (innuPREP RNA mini Kit, Analytik Jena)	0.35
	SC6 (innuCONVERT Bisulfite Body Fluids Kit, Analytik Jena)	0.23
	SC7 (innuPREP Gel Extraction Kit, Analytik Jena)	0.30
	SC8 (Analytik Jena)	1.45
	SC9 (Analytik Jena)	0.83
	SC10 (Analytik Jena)	2.12
	SC11 (Analytik Jena)	1.50
Washing solutions		
Washing solutions, combinations and volumes	500 µl C (blackPREP FFPE DNA Kit, Analytik Jena) + 650 µl BS (blackPREP FFPE DNA Kit, Analytik Jena) + 2x 650 µl 100% EtOH	0.80
	650 µl BS + 2x 650 µl 100% EtOH	0.18
	500 µl C + 2x 650 µl 100% EtOH	0.48
	650 µl BS + 650 µl 100% EtOH	0.50
	200 µl BS + 650 µl 100% EtOH + 200 µl 100% EtOH (in combination with columns SC8-SC11)	0.33
	100 µl BS + 500 µl 100% EtOH + 200 µl 100% EtOH (in combination with columns SC8-SC11)	0.41
	200 µl HS (innuPREP DNA Mini Kit, Analytik Jena) + 650 µl LS (innuPREP Blood RNA Kit, Analytik Jena) + 200 µl LS (in combination with columns SC8-SC11)	0.08***
	500 µl HS + 650 µl LS**	**0**
	300 µl HS + 500 µl LS	0.24
	500 µl HS + 2x 650 µl LS	0.08***
	500 µl HS + 650 µl LS + 650 µl 100% EtOH	0.01***
	500 µl GS (innuCONVERT Bisulfite Body Fluids Kit, Analytik Jena) + 650 µl LS	1.63
Elution		
Combination of elution volume, time and temperature	50 µl Elution Buffer (innuPREP Blood DNA Mini Kit, Analytik Jena), 2 min at RT	0.89
	50 µl H_2O, 2 min at RT	0.25
	100 µl H_2O, 1 min at RT	0.61
	100 µl H_2O, 10 min at RT	0.22
	100 µl H_2O, 1 min at RT + 1x re-elution (1 min, RT) with flow-through	0.53
	100 µl H_2O, 1 min at RT + 2x re-elution (1 min, RT) with flow-through	0.72
	100 µl H_2O**, 10 min at RT + 1x re-elution (10 min, RT) with flow-through****	**0**
	100 µl H_2O, 20 min at RT + 1x re-elution (20 min, RT) with flow-through	0.17
	100 µl H_2O at 70°C, 20 min at 40°C + 1x re-elution (20 min, 40°C) with flow-through	0.57

*Calculated from the formula: CD= $C_{q(x)}$-$C_{q(y)}$, in which x is any variant tested and y is the best variant. The difference shows the magnitude of the aberrance of a variant from the best variant.**Chosen best variations of reagents and parameters are in bold. ***Variations of results similar to the best variation, that showed a minimal data improvement but significantly increased the experiment duration, complexity or quantity of buffers used, were not chosen for further testing. A CD value of 0 indicates the best variation within the group of single grey boxes. GSCN, guanidinium thiocyanate; NLS, N-Lauroylsarcosine sodium salt; RT, room temperature; H_2O, RNase-free water.

2.3.2. Final protocols

After numerous experiments, the best reagents and parameters were defined, allowing creating the final protocols for miRNAs isolation from exosome pellets and cell-free supernatants derived from plasma or serum samples. To isolate exosomal miRNAs, first, the exosome pellet is dissolved in 400 µl lysis buffer L6, and 20 µl proteinase K is added to the lysis. The mixture is incubated for 20 min on a thermoshaker at 55°C and 1,000 rpm to lyse the MGP-trapped exosomes. After lysis, the sample is centrifuged for 5 min at 16,000 g to remove the residues of the polymer. The supernatant is then transferred into a new tube and mixed with 800 µl absolute ethanol to create binding conditions. The mixture is loaded twice on the spin column to bind miRNAs to the filter material. The spin column is washed to remove the impurities with 500 µl Washing Solution HS followed by 650 µl of Washing Solution LS. After each binding and washing step, the spin column is centrifuged for 1 min at 11,000 g, and the flow-through is each time discarded. Afterwards, the spin column is centrifuged for 3 min at 16,000 g to remove the residuals of ethanol. One hundred µl of RNase-free water is added onto the top of the filter material. Then, the spin column is incubated for 10 min at room temperature, and centrifuged for 1 min at 11,000 g. The flow-through (eluate) is re-loaded onto the same filter material, and incubation and centrifugation are repeated. The final eluate contains the exosomal miRNAs (Figure 39).

The protocol for isolation of cell-free miRNAs from the supernatant or plasma and serum directly is similar Figure 40). The differences are that for 200 µl of supernatant, plasma or serum used as starting material, 1.2 ml of absolute ethanol is used, and therefore, the sample is loaded three times onto the spin column. The step of centrifugation for 5 min at 16,000 g is also excluded, since there are no residuals of MGP to remove. Moreover, it is possible to increase the starting material volume, if volumes of lysis buffer L6, proteinase K, and absolute ethanol are kept proportionate.

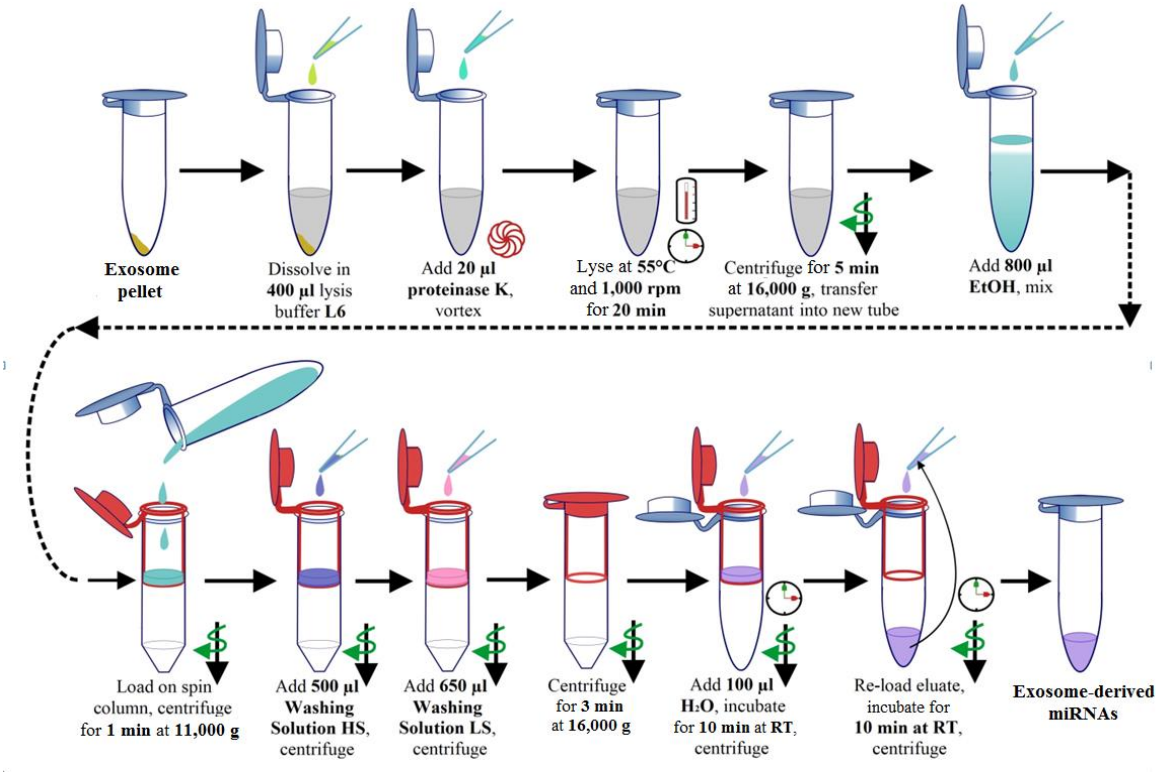

Figure 39: The workflow of the miRNA isolation from an exosome pellet

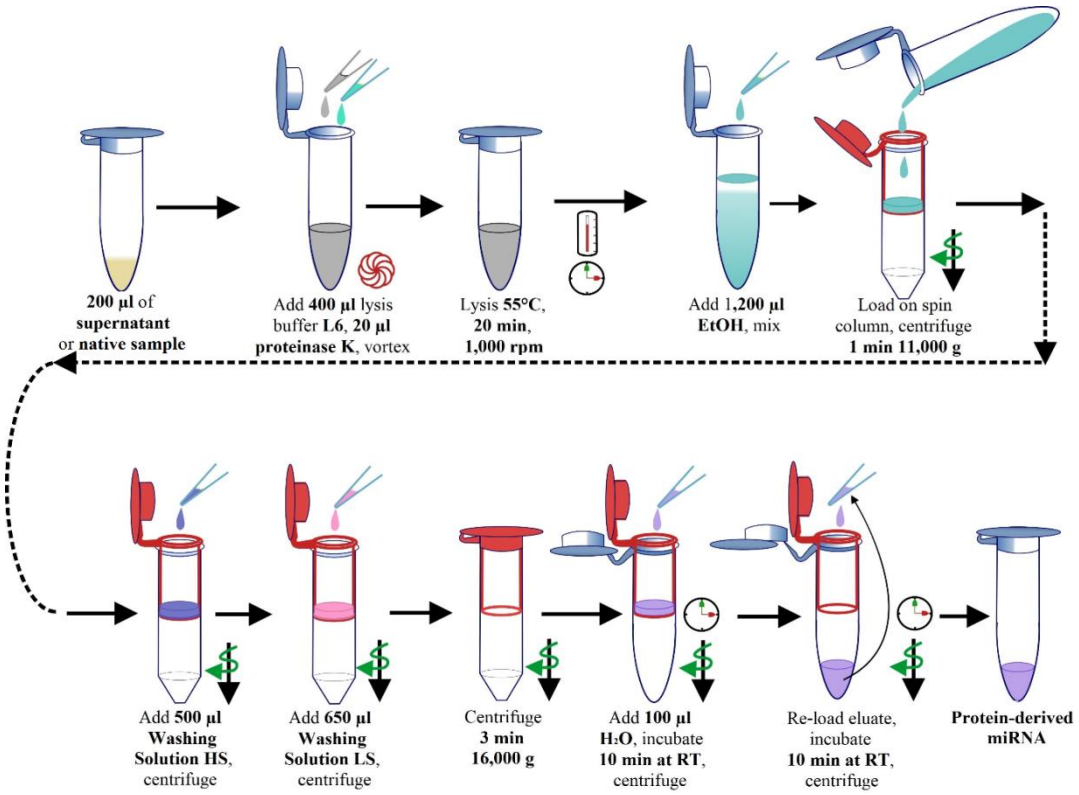

Figure 40: The workflow of cell-free miRNA isolation from supernatant or plasma and serum samples

2.3.3. Testing and verification

The applicability of the isolation method of exosomal and cell-free miRNAs was verified in 0.5 ml of different types of samples by my optimized RT-qPCR (Figure 41). Supernatants from all plasma EDTA (C_q 26.98), plasma CPD (C_q 26.47) and serum (C_q 26.57) samples contained similar yields of cell-free miR-16 that were higher than the miR-16 levels in pellets (C_q 27.92 for plasma EDTA, C_q 27.67 for plasma CPD and C_q 28.10 for serum). In contrary, the yields of miR-142 were C_q 4.77 to 5.31 higher in the pellets than in the supernatants for all types of samples (plasma EDTA: C_q 28.21 vs. C_q 32.98; plasma CPD: C_q 27.30 vs. C_q 31.93; serum: C_q 27.94 vs. C_q 33.25 for pellet vs. supernatant, respectively).

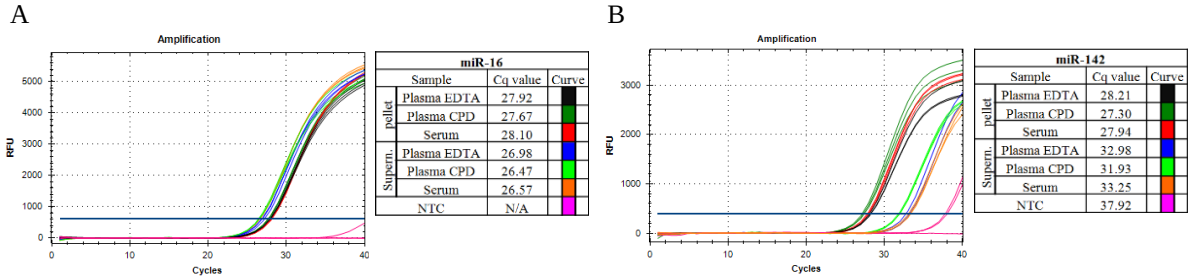

Figure 41: Isolation of miRNAs from exosome pellets and exosome-depleted supernatants derived from different sample types

Exosomal and cell-free miRNAs were isolated from exosome pellets and exosome-depleted supernatants, respectively, extracted from 500 µl plasma EDTA, plasma CPD and serum by my MGP-based method. RT-qPCRs with my optimized method were performed for A) miR-16 and B) miR-142. The mean C_q values are shown for both sources of each sample type in tables next to the diagrams. NTC, no template control; N/A, not applicable.

To check if the self-developed methods are scalable to different volumes of starting material, exosome-derived miRNAs were isolated from four different volumes of plasma EDTA and serum. Increases in miRNA quantity were observed which positively correlated with the increase in the sample volume (Figure 42).

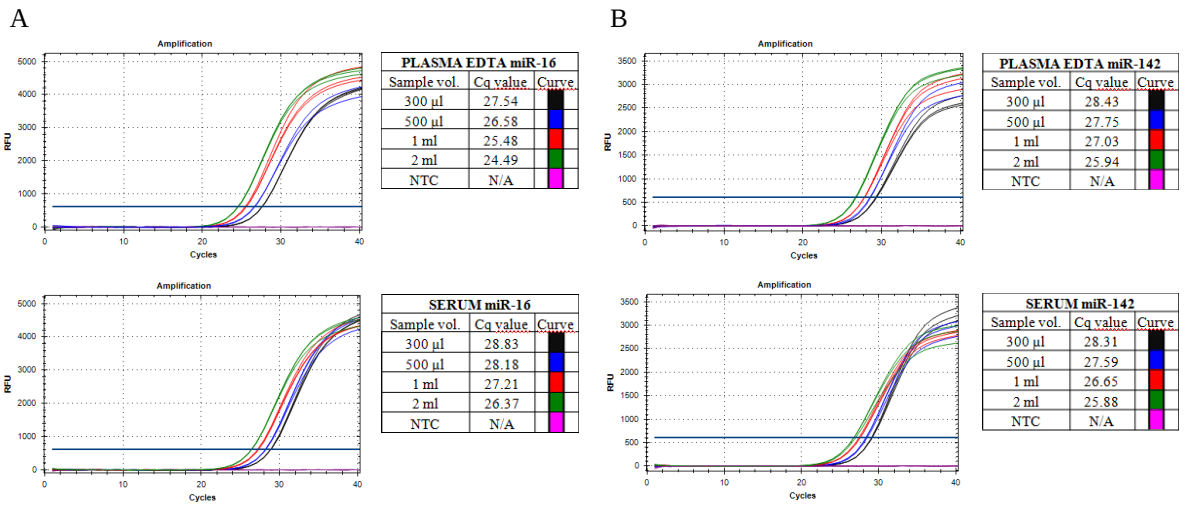

Figure 42: Exosome-derived miRNA isolation from increasing sample volumes

The C_q values derived from my optimized RT-qPCRs are shown for A) miR-16 and B) miR-142 using plasma and serum samples. NTC, no template control; N/A, not applicable.

The quantity and size distribution of exosome-derived RNA isolated from plasma EDTA and serum were verified on the Agilent Bioanalyzer (Figure 43). The concentrations of small RNA, as well as of miRNAs were higher in serum than plasma. It is well accepted that the extraction from serum provides higher RNA amounts than the extraction from plasma. This is caused by the different blood collection system used for serum, leading to the release of cellular content during the process of blood cells clotting (Witwer et al., 2013). However, almost 50 % of isolated plasma and serum RNA were composed of miRNAs.

Plasma EDTA

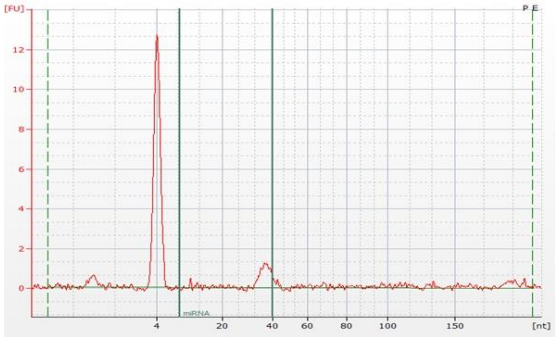

Name	From [nt]	To [nt]	Average Size [nt]	Size distribution in CV [%]	Conc. [pg/µl]	% of Total
miRNA	10	40	33	24,9	92,0	46
Small RNA	0	208	28	100,0	201,7	100

Serum

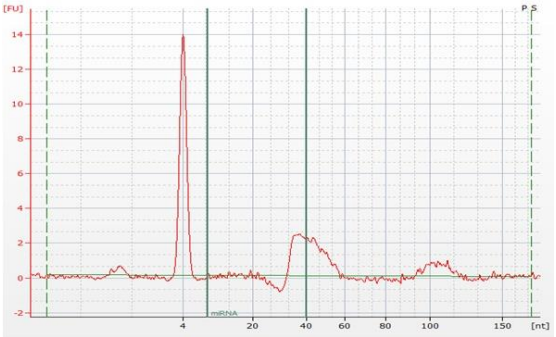

Name	From [nt]	To [nt]	Average Size [nt]	Size distribution in CV [%]	Conc. [pg/µl]	% of Total
miRNA	10	40	36	13,2	164,1	47
Small RNA	0	170	29	100,0	352,3	100

Figure 43: Determination of the RNA content in exosome preparations

Representative electropherograms of exosomes obtained from 500 µl plasma EDTA and serum. Electropherograms were generated on the Agilent 2100 Bioanalyzer using the Small RNA kit (Agilent). The peak at 4 nt indicates the RNA marker. The two vertical green boarder lines (from 10 to 40 nt) represent the area of miRNA detection in each diagram. The tables below the diagrams display values calculated by the Agilent 2100 expert software: regions of miRNA (from 10 to 40 nt) and small RNA (from 0 to 208 and 170 nt for plasma and serum, respectively), average size in each region (in plasma 33 nt for miRNA and 28 nt for small RNA, in serum 36 nt for miRNA and 29 nt for small RNA), size distribution in CV (coefficient of variance) in each region (100% for small RNA in both, serum and plasma and 24.9% and 13.2% for miRNA in plasma and serum, respectively), concentration in each region (92 pg/µl for miRNA and 201.7 pg/µl for small RNA in plasma, 164.1 pg/µl for miRNA and 352.3 pg/µl for small RNA in serum), percentage of total RNA detected (100% for small RNA in both, serum and plasma and 46% and 47% for miRNA in plasma and serum, respectively).

3. Part B: Comparative study

3.1. MiRNA quantification (miR-16 and miR-142)

To check the performance of the optimized RT-qPCR method, 10-fold serial dilutions of miR-16 and miR-142 were prepared and amplified with this method and compared with the data of the commercial TaqMan MicroRNA Reverse Transcription Kit and TaqMan miRNA assay (Applied Biosystems). Both methods were checked for their efficiency and slope, linearity, sensitivity, as well as repeatability (short-term precision or intra-assay variance) and reproducibility (long-term precision or inter-assay variance).

A serial dilution from $4x10^2$ to $4x10^9$ copies of synthetic miR-16 was used in each reaction to compare the performance of both methods (Figure 44). The highest concentration of miR-16 used as starting material for the Applied Biosystems assay led to an over-amplification - a PCR artifact which is caused by an exhaustion of some essential PCR components, i.e. primers, and a self-amplification of the target. In this regard, the RT-qPCR efficiency, slope, and linearity were calculated from the serial dilutions from $4x10^2$ to $4x10^8$ copies per reaction. The amplification of miR-16 with my optimized method exhibited a very good efficiency of 99.7% and slope of -3.33, while the TaqMan miRNA assay (Applied Biosystems) efficiency and slope were 119.1% and -2.936, respectively. The TaqMan miRNA assay efficiency was much higher than expected, which could be caused by the presence of unspecific products or the formation of primer-dimers. Both assays presented equal linearity of R^2=0.997 and sensitivity of LOD=$4x10^2$. Besides, the Applied Biosystems assay led to early signals in the negative control, being possibly induced by the cross-reaction between primer-dimers and probe or the presence of foreign nucleic acids derived from the RNase inhibitor extraction source.

A

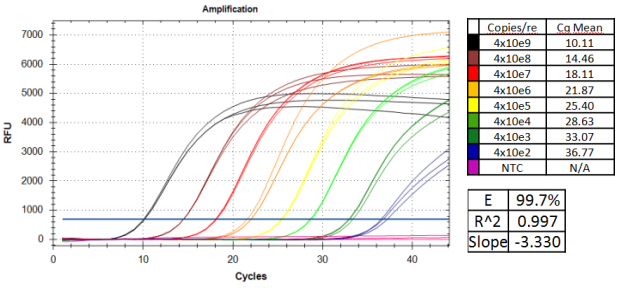

B

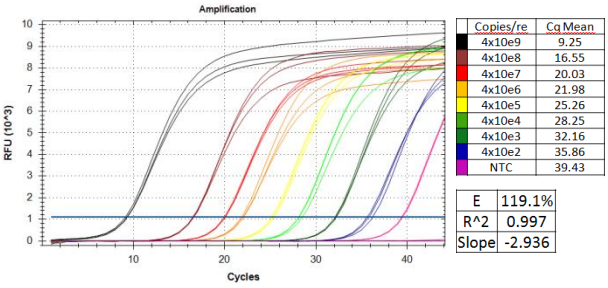

Figure 44: Comparison of miR-16 quantification methods

RT-qPCR of serial dilutions from $4x10^9$ to $4x10^2$ copies of miR-16 per PCR reaction performed by my optimized method (A) and the Applied Biosystems TaqMan miRNA assay (B). E, efficiency; R^2, linearity; NTC, no template control; N/A, not applicable.

In addition, a gel electrophoresis of PCR products was performed (Figure 45). There were no additional bands observed in the PCR products of miR-16 dilutions using both methods (lanes 3-5 and 8-10). However, a weak band of a size similar to the size of the miR-16 amplicon appeared in the negative control (lane 7) using the commercial kit, while a band corresponding to the primer-dimers (lane 2) was present in the negative control using the optimized method.

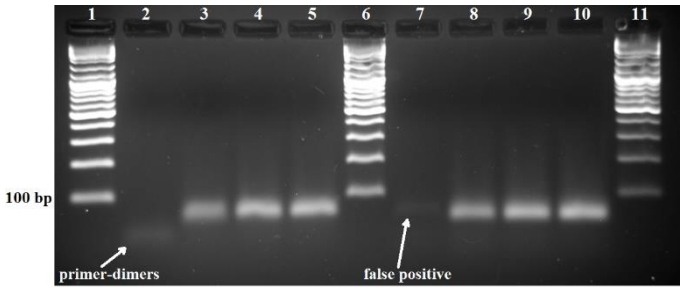

Figure 45: Comparison of PCR products derived from the optimized and commercial method by agarose gel electrophoresis

Samples amplified by my self-developed method (lanes 2-5) and the Applied Biosystems TaqMan miRNA assay (lanes 7-10). Lanes 1, 6 and 11 represent the DNA ladder with the lowest band of 100 bp. Negative controls (lanes 2 and 7) and PCR products obtained from the amplification of $6.7x10^{-8}$, $6.7x10^{-7}$ and $6.7x10^{-6}$ fM of synthetic miR-16 (lanes 3-5 and 8-10).

Subsequently, the intra-assay variance was measured for both methods by performing 3 replicates for each serial dilution of $4x10^7$, $4x10^6$, $4x10^5$ and $4x10^4$ copies of miR-16 per reaction in the single RT-qPCR assays. To show the reproducibility defined as inter-assay variance and measured by mean slope and slope SD, the experiment was repeated 6 times on 3 different days (2 assays per day), each day using new serial dilutions. The 6-time repetition should also confirm the repeatability as measured by the C_q standard deviation (SD) and mean C_q SD. The data included determination of the efficiency and linearity of the amplification and appearance of false positive signals. For the commercial assay (Figure 46A), C_q SD varied between the replicates of all 6 RT-qPCRs from 0.02 to 0.72, while the mean C_q SD of each assay oscillated from 0.09 to 0.38. In the 6 assays performed with my optimized method (Figure 46B), these measurements varied from 0.01 to 0.44 (C_q SD) and from 0.09 to 0.27 (mean C_q SD). The mean slope of the Applied Biosystems TaqMan miRNA assay ranged from -3.785 to -2.831, exceeding the commonly accepted slope range of -3.6 to -3.1, while my optimized method exhibited mean slopes from -3.556 to -3.334, thus, being within the accepted range. However, the calculated mean slope does

not reveal the regularity of slopes between the consecutive target dilutions. Therefore, I calculated the SD of singular slopes (slope SD). Slope SDs oscillating from 0.26 to 1.50 exposed an irregularity of slope distribution using the commercial kit. Slope SDs of my optimized method varied from 0.09 to 0.37. The efficiency, which is calculated from the mean slope of the standard curve using the formula $E=(10^{-(1/\text{mean slope})}-1)*100\%$, also varied for the data derived from the Applied Biosystems assay and ranged from 83.7% to 125.6%, while my optimized method ranged from 90.7% to 99.1% which is in the accepted range of 90% to 110%. Moreover, the moment of an arising signal in the negative control was early for the Applied Biosystems TaqMan miRNA assay, as detected at $C_q<35$ for some RT-qPCR runs, while it was later at $C_q>38$ for my optimized method.

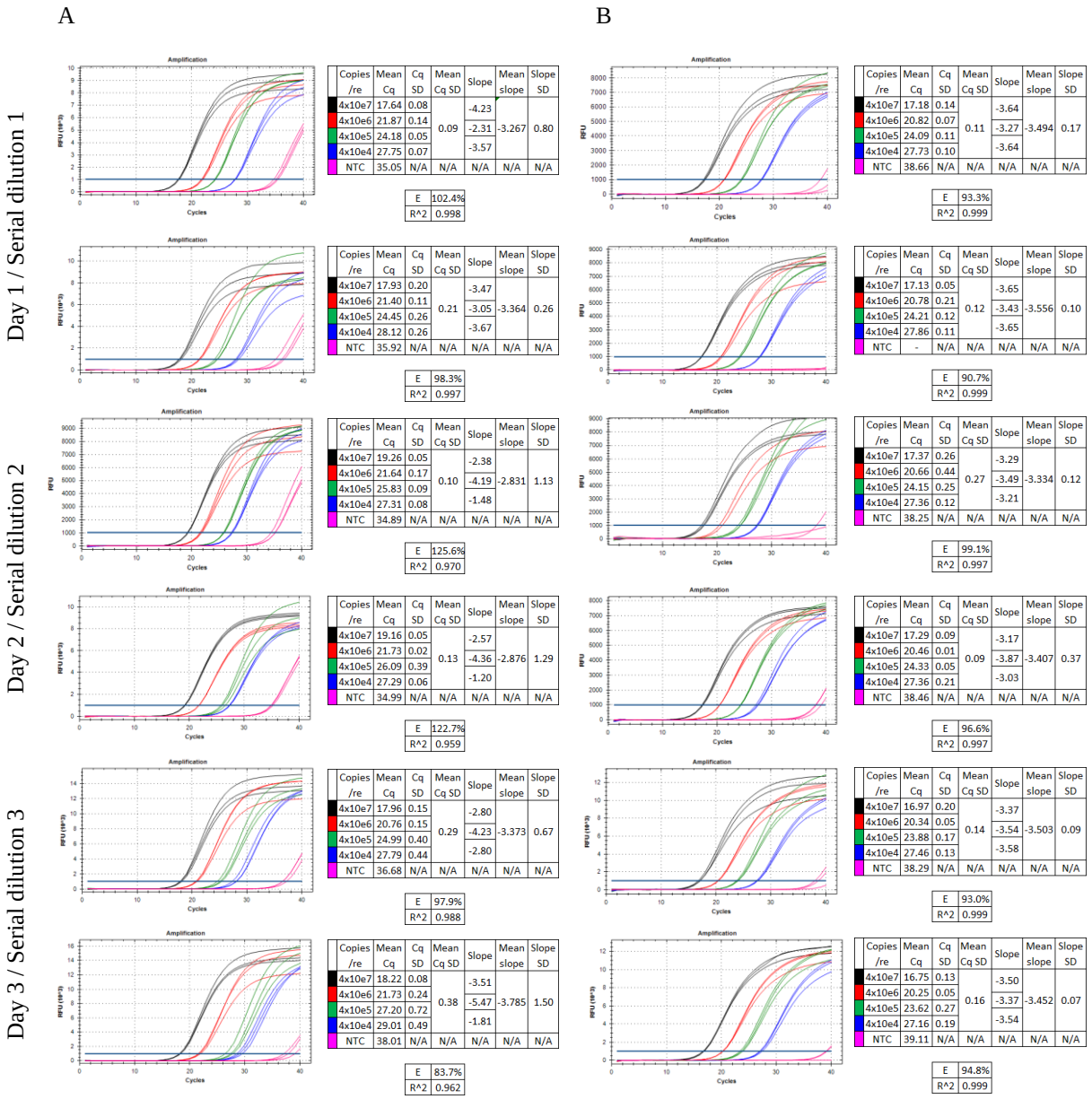

A	Copies /re	Mean Cq	Cq SD	Mean Cq SD	Slope	Mean slope	Slope SD
Day 1 / Serial dilution 1	4x10e7	17.64	0.08	0.09	-4.23	-3.267	0.80
	4x10e6	21.87	0.14		-2.31		
	4x10e5	24.18	0.05		-3.57		
	4x10e4	27.75	0.07				
	NTC	35.05	N/A	N/A	N/A	N/A	N/A
	E	102.4%					
	R^2	0.998					
Day 1 / Serial dilution 2	4x10e7	17.93	0.20	0.21	-3.47	-3.364	0.26
	4x10e6	21.40	0.11		-3.05		
	4x10e5	24.45	0.26		-3.67		
	4x10e4	28.12	0.26				
	NTC	35.92	N/A	N/A	N/A	N/A	N/A
	E	98.3%					
	R^2	0.997					
Day 2 / Serial dilution 2	4x10e7	19.26	0.05	0.10	-2.38	-2.831	1.13
	4x10e6	21.64	0.17		-4.19		
	4x10e5	25.83	0.09		-1.48		
	4x10e4	27.31	0.08				
	NTC	34.89	N/A	N/A	N/A	N/A	N/A
	E	125.6%					
	R^2	0.970					
Day 2 / Serial dilution 3	4x10e7	19.16	0.05	0.13	-2.57	-2.876	1.29
	4x10e6	21.73	0.02		-4.36		
	4x10e5	26.09	0.39		-1.20		
	4x10e4	27.29	0.06				
	NTC	34.99	N/A	N/A	N/A	N/A	N/A
	E	122.7%					
	R^2	0.959					
Day 3 / Serial dilution 3	4x10e7	17.96	0.15	0.29	-2.80	-3.373	0.67
	4x10e6	20.76	0.15		-4.23		
	4x10e5	24.99	0.40		-2.80		
	4x10e4	27.79	0.44				
	NTC	36.68	N/A	N/A	N/A	N/A	N/A
	E	97.9%					
	R^2	0.988					
	4x10e7	18.22	0.08	0.38	-3.51	-3.785	1.50
	4x10e6	21.73	0.24		-5.47		
	4x10e5	27.20	0.72		-1.81		
	4x10e4	29.01	0.49				
	NTC	38.01	N/A	N/A	N/A	N/A	N/A
	E	83.7%					
	R^2	0.962					

B	Copies /re	Mean Cq	Cq SD	Mean Cq SD	Slope	Mean slope	Slope SD
Day 1 / Serial dilution 1	4x10e7	17.18	0.14	0.11	-3.64	-3.494	0.17
	4x10e6	20.82	0.07		-3.27		
	4x10e5	24.09	0.11		-3.64		
	4x10e4	27.73	0.10				
	NTC	38.66	N/A	N/A	N/A	N/A	N/A
	E	93.3%					
	R^2	0.999					
Day 1 / Serial dilution 2	4x10e7	17.13	0.05	0.12	-3.65	-3.556	0.10
	4x10e6	20.78	0.21		-3.43		
	4x10e5	24.21	0.12		-3.65		
	4x10e4	27.86	0.11				
	NTC	-	N/A	N/A	N/A	N/A	N/A
	E	90.7%					
	R^2	0.999					
Day 2 / Serial dilution 2	4x10e7	17.37	0.26	0.27	-3.29	-3.334	0.12
	4x10e6	20.66	0.44		-3.49		
	4x10e5	24.15	0.25		-3.21		
	4x10e4	27.36	0.12				
	NTC	38.25	N/A	N/A	N/A	N/A	N/A
	E	99.1%					
	R^2	0.997					
Day 2 / Serial dilution 3	4x10e7	17.29	0.09	0.09	-3.17	-3.407	0.37
	4x10e6	20.46	0.01		-3.87		
	4x10e5	24.33	0.05		-3.03		
	4x10e4	27.36	0.21				
	NTC	38.46	N/A	N/A	N/A	N/A	N/A
	E	96.6%					
	R^2	0.997					
Day 3 / Serial dilution 3	4x10e7	16.97	0.20	0.14	-3.37	-3.503	0.09
	4x10e6	20.34	0.05		-3.54		
	4x10e5	23.88	0.17		-3.58		
	4x10e4	27.46	0.13				
	NTC	38.29	N/A	N/A	N/A	N/A	N/A
	E	93.0%					
	R^2	0.999					
	4x10e7	16.75	0.13	0.16	-3.50	-3.452	0.07
	4x10e6	20.25	0.05		-3.37		
	4x10e5	23.62	0.27		-3.54		
	4x10e4	27.16	0.19				
	NTC	39.11	N/A	N/A	N/A	N/A	N/A
	E	94.8%					
	R^2	0.999					

Figure 46: Comparison of the reproducibility of miR-16 amplification methods

RT-qPCRs performed with the Applied Biosystems TaqMan miRNA assay (A) and my optimized method (B). Each of 3 days, a new serial dilution of miR-16 ($4x10^4$-$4x10^7$ copies per reaction) was prepared and amplified twice with each assay to give 6 repetitions performed on 3 days. Mean C_q and C_q SD were calculated for each miR-16 dilution, and mean C_q SD was calculated for each RT-qPCR run. The slope was calculated as a difference between mean C_qs of consecutive miR-16 dilutions. The mean slope was calculated from the standard curve of serial dilutions by the BioRad CFX Manager 3.1 software, and the slope SD was calculated to exhibit deviations of slopes from the mean slope. All SDs were calculated from the formula $\sqrt{\frac{\sum(x-\bar{x})^2}{n}}$. Re, reaction; SD, standard deviation; NTC, no template control; N/A, not applicable.

My optimized method was also tested under the same parameters and conditions for the amplification of miR-142 in comparison with the Applied Biosystems TaqMan miRNA assay. Similar to miR-16, the highest miR-142 concentration used as starting material in the RT-qPCR led to an over-amplification with the commercial kit. Therefore, this concentration was excluded from the calculation of the efficiency, slope and linearity. Using my optimized method, the efficiency was 95.4%, the slope -3.483 and the linearity 0.999. For the Applied Biosystems TaqMan miRNA assay, the efficiency, slope and linearity were 107.6%, -3.153 and 0.997, respectively. For both methods, the efficiency, linearity and sensitivity were in the commonly accepted ranges (Figure 47).

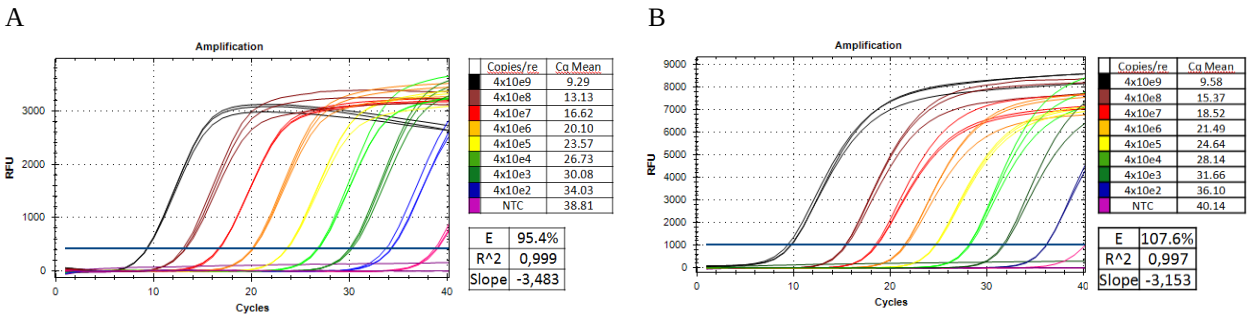

Figure 47: Comparison of miR-142 quantification methods

A 10-fold serial dilution of miR-142 ($4x10^9$-$4x10^2$ copies per reaction) was amplified by my optimized RT-qPCR method (A) and the TaqMan miRNA assay (Applied Biosciences) (B). E, efficiency; R^2, linearity; NTC, no template control; N/A, not applicable.

Similar to miR-16, the repeatability of the amplification of miR-142 was also tested using both assays. For the Applied Biosystems TaqMan miRNA assay, the C_q SD of all replicates in 6 RT-qPCR runs ranged from 0.03 to 0.29, and the mean C_q SD of assays varied from 0.08 to 0.22 (Figure 48A). My optimized method exhibited slightly better repeatability data with C_q SD from 0.01 to 0.21 and mean C_q SD from 0.09 to 0.15 (Figure 48B). The mean slope varied from -4.044 to -3.647 with slope SD from 0.20 to 0.66 for the Applied Biosystems kit, and from -3.939 to -3.724 with slope SD from 0.24 to 0.53 for my optimized assay. All these data of slopes and hence, efficiencies of both RT-qPCR methods are lower than the commonly accepted range (slope between -3.6 and -3.1). This may be caused by the low GC content in the miR-142 sequence and its susceptibility to form stable secondary structures, inhibiting the cDNA synthesis by disturbing the hybridization of the stem-loop primer to the miRNA sequence. Nevertheless, the signals in the negative control did not arise within 40 PCR cycles for both methods (Figure 48).

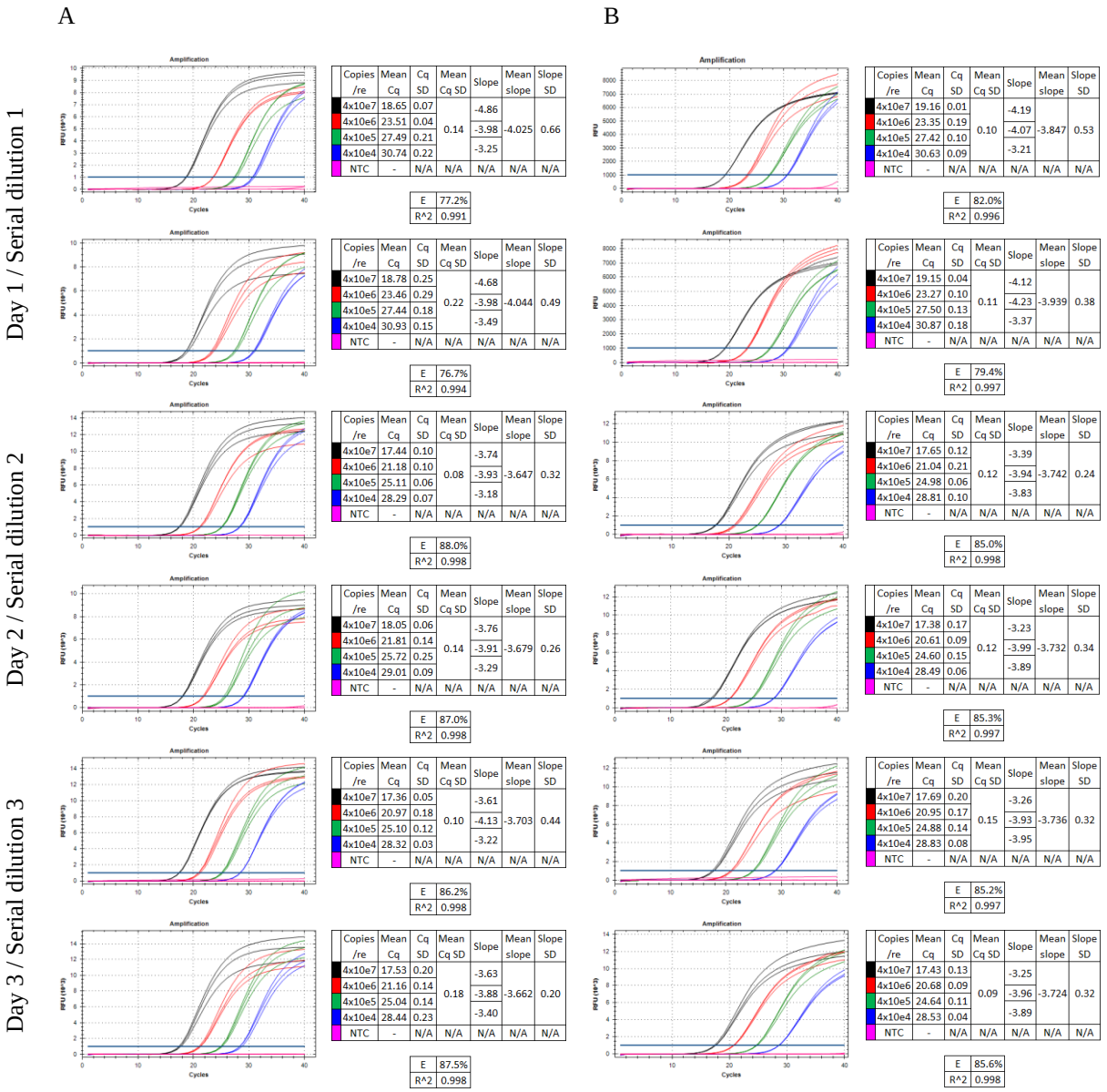

A	Copies /re	Mean Cq	Cq SD	Mean Cq SD	Slope	Mean slope	Slope SD
Day 1 / Serial dilution 1	4x10e7	18.65	0.07	0.14	-4.86	-4.025	0.66
	4x10e6	23.51	0.04		-3.98		
	4x10e5	27.49	0.21		-3.25		
	4x10e4	30.74	0.22				
	NTC	-	N/A	N/A	N/A	N/A	N/A
	E	77.2%					
	R^2	0.991					
	4x10e7	18.78	0.25	0.22	-4.68	-4.044	0.49
	4x10e6	23.46	0.29		-3.98		
	4x10e5	27.44	0.18		-3.49		
	4x10e4	30.93	0.15				
	NTC	-	N/A	N/A	N/A	N/A	N/A
	E	76.7%					
	R^2	0.994					
Day 2 / Serial dilution 2	4x10e7	17.44	0.10	0.08	-3.74	-3.647	0.32
	4x10e6	21.18	0.10		-3.93		
	4x10e5	25.11	0.06		-3.18		
	4x10e4	28.29	0.07				
	NTC	-	N/A	N/A	N/A	N/A	N/A
	E	88.0%					
	R^2	0.998					
	4x10e7	18.05	0.06	0.14	-3.76	-3.679	0.26
	4x10e6	21.81	0.14		-3.91		
	4x10e5	25.72	0.25		-3.29		
	4x10e4	29.01	0.09				
	NTC	-	N/A	N/A	N/A	N/A	N/A
	E	87.0%					
	R^2	0.998					
Day 3 / Serial dilution 3	4x10e7	17.36	0.05	0.10	-3.61	-3.703	0.44
	4x10e6	20.97	0.18		-4.13		
	4x10e5	25.10	0.12		-3.22		
	4x10e4	28.32	0.03				
	NTC	-	N/A	N/A	N/A	N/A	N/A
	E	86.2%					
	R^2	0.998					
	4x10e7	17.53	0.20	0.18	-3.63	-3.662	0.20
	4x10e6	21.16	0.14		-3.88		
	4x10e5	25.04	0.14		-3.40		
	4x10e4	28.44	0.23				
	NTC	-	N/A	N/A	N/A	N/A	N/A
	E	87.5%					
	R^2	0.998					

B	Copies /re	Mean Cq	Cq SD	Mean Cq SD	Slope	Mean slope	Slope SD
Day 1 / Serial dilution 1	4x10e7	19.16	0.01	0.10	-4.19	-3.847	0.53
	4x10e6	23.35	0.19		-4.07		
	4x10e5	27.42	0.10		-3.21		
	4x10e4	30.63	0.09				
	NTC	-	N/A	N/A	N/A	N/A	N/A
	E	82.0%					
	R^2	0.996					
	4x10e7	19.15	0.04	0.11	-4.12	-3.939	0.38
	4x10e6	23.27	0.10		-4.23		
	4x10e5	27.50	0.13		-3.37		
	4x10e4	30.87	0.18				
	NTC	-	N/A	N/A	N/A	N/A	N/A
	E	79.4%					
	R^2	0.997					
Day 2 / Serial dilution 2	4x10e7	17.65	0.12	0.12	-3.39	-3.742	0.24
	4x10e6	21.04	0.21		-3.94		
	4x10e5	24.98	0.06		-3.83		
	4x10e4	28.81	0.10				
	NTC	-	N/A	N/A	N/A	N/A	N/A
	E	85.0%					
	R^2	0.998					
	4x10e7	17.38	0.17	0.12	-3.23	-3.732	0.34
	4x10e6	20.61	0.09		-3.99		
	4x10e5	24.60	0.15		-3.89		
	4x10e4	28.49	0.06				
	NTC	-	N/A	N/A	N/A	N/A	N/A
	E	85.3%					
	R^2	0.997					
Day 3 / Serial dilution 3	4x10e7	17.69	0.20	0.15	-3.26	-3.736	0.32
	4x10e6	20.95	0.17		-3.93		
	4x10e5	24.88	0.14		-3.95		
	4x10e4	28.83	0.08				
	NTC	-	N/A	N/A	N/A	N/A	N/A
	E	85.2%					
	R^2	0.997					
	4x10e7	17.43	0.13	0.09	-3.25	-3.724	0.32
	4x10e6	20.68	0.09		-3.96		
	4x10e5	24.64	0.11		-3.89		
	4x10e4	28.53	0.04				
	NTC	-	N/A	N/A	N/A	N/A	N/A
	E	85.6%					
	R^2	0.998					

Figure 48: Comparison of the reproducibility of miR-142 amplification methods

RT-qPCRs performed with the Applied Biosystems TaqMan miRNA assay (A) and my optimized method (B). Three serial dilutions of miR-142 ($4x10^4$-$4x10^7$ copies per reaction) were prepared and amplified twice with each assay to give 6 repetitions performed on 3 days. The mean C_q and C_q SD were calculated for each miR-142 dilution, and mean C_q SD was calculated for each RT-qPCR run. The slope was calculated as a difference between mean C_qs of consecutive miR-142 dilutions. The mean slope was calculated from the standard curve of serial dilutions by the BioRad CFX Manager 3.1 software, and the slope SD was calculated to exhibit deviations of slopes from the mean slope. All SDs were calculated from the formula $\sqrt{\frac{\sum(x-\bar{x})^2}{n}}$. Re, reaction; SD, standard deviation; NTC, no template control; N/A, not applicable; E, efficiency; R^2, linearity.

3.2. Extraction of exosomes

3.2.1. Enrichment of polystyrene beads

First, to examine the ability of the self-developed method (MGP) as well as the Invitrogen Total Exosome Isolation Reagent (TEI) to enrich pure exosomes of size from 60 to 120 nm in diameter (Zijlstra and Di Vizio, 2018), an experiment was carried out using polystyrene beads. A 0.124% (w/v) dilution of blue-dyed Uniform Dyed Microspheres of a mean diameter of 53 nm was prepared in RNase-free water and aliquoted into 3 samples of 500 µl each. The first sample served as a control for incubation time and centrifugation speed and time, i.e. it was incubated for 30 min at room temperature and centrifuged for 30 min at 16,000 g to check if polystyrene beads tend to self-sediment under these conditions. The second and third samples were processed according to the MGP-based and TEI (for serum) exosome enrichment protocols, respectively. No self-sedimentation of polystyrene beads was observed (sample 1 after incubation, Figure 49B and after centrifugation, Figure 49C). However, only after the incubation with MGP components, the separation of the sample into 2 phases was observed: an upper clear phase and a lower blue-coloured phase of cloudy appearance (sample 2, Figure 49B). After the centrifugation step, a polystyrene beads/MGP pellet was crated, leaving the supernatant of the second sample clear (sample 2, Figure 49C). The third sample treated with TEI did neither show any differences after the incubation (sample3, Figure 49B) nor after the centrifugation (sample 3, Figure 49C). The lack of pelletizing in TEI sample might be caused by the absence of proteins in the dilution of blue-dyed Uniform Dyed Microspheres, however, their presence seems to be necessary for PEG-based precipitation methods. A similar observation was reported by Lane at al. (Lane et al., 2015) when they used TEI to isolate fluorescin-labelled liposomes of ~100 nm in diameter from serum-free cell media with and without supplementary proteins.

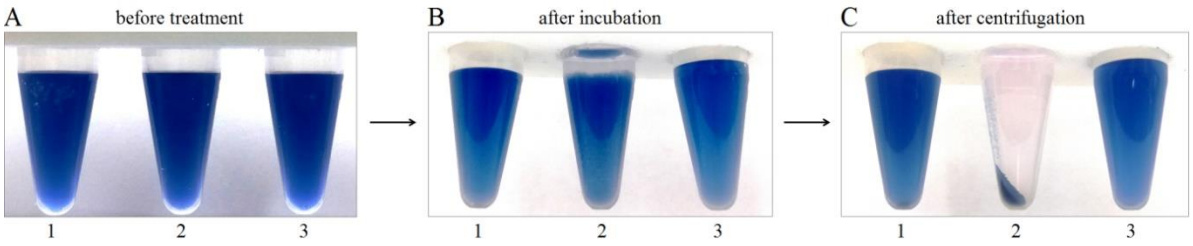

Figure 49: The competence of MGP and TEI to capture polystyrene beads

A) Blue-dyed polystyrene beads of a mean diameter of 53 nm and a concentration of 0.124% were aliquoted into 3 samples (1-3) of 500 µl. B) Following the protocols, 30 µl of MGP and 150 µl of $CaCl_2$ were added to the sample 2 and mixed, while 100 µl of TEI solution was added to the sample 3. As expected, sample 1 remained unchanged (negative control). After the incubation 2 phases were created in sample 2, while sample 3 remained unchanged. C) After centrifugation, a pellet was only visible in sample 2.

3.2.2. Enrichment of exosomes from lyophilized exosome standards

Because of the suspicion that the polystyrene beads were not precipitated by the TEI method due to the lack of protein in the sample, since the adsorption of protein on the surface of the beads is probably the key reason to PEG-induced sedimentation (Lane et al., 2015), an experiment was performed to test the ability of both techniques (TEI and MGP) to recover pure exosomes with their surface proteins from protein-free samples. MGP and TEI for plasma and serum were used to isolate exosomes from 3 µg of commercial lyophilized exosome standards from plasma of healthy donors supplemented with 500 µl of RNase-free water. Then, miRNAs were isolated from MGP- and TEI-derived pellets and supernatants according to the self-developed miRNA isolation method and Total Exosome RNA & Protein Isolation Kit (Invitrogen), respectively. Finally, RT-qPCRs for miR-16 and miR-142 were performed with my optimized method for all samples (Figure 50). The use of TEI for serum provided more miR-16 and miR-142 in the exosome pellet than TEI for plasma (C_q differences of 0.39 and 1.47, respectively). These findings suggest that TEI for plasma may be less efficient to recover lyophilized exosome standards than TEI for serum. These hardly measurable levels of miRNAs in lyophilized exosomes using the TEI for plasma (C_q 35.03 for miR-16 and C_q 34.46 for miR-142) also effectuated the higher levels of miRNAs in the corresponding supernatant (C_q 34.12 for miR-16 and C_q 33.33 for miR-142). In contrary, TEI for serum could enrich more exosomes as indicated by slightly lower C_q values for miRNAs isolated from the pellet (C_q 34.64 for miR-16 and 32.99 for miR-142) than from the supernatant (C_q 35.18 for miR-16 and 33.11 for miR-142). Nevertheless, the exosome recovery of both TEI kits (for plasma and serum) was pretty

low, further suggesting that TEI requires more protein in the samples to perform the exosome precipitation. In contrary to the low specificity of TEI, the real-time PCR of miR-16 and miR-142 derived from the exosome/MGP pellet showed a higher C_q of 4.01 and 2.69, respectively, than that of TEI for serum. No miRNAs were detected in the MGP supernatant as measured for miR-16 [not applicable (N/A)] and miR-142 (C_q 38.79). These data indicate that the MGP-based method was around 10-times more efficient to recover exosomes than TEI, and is independent from the presence of protein in the sample.

A

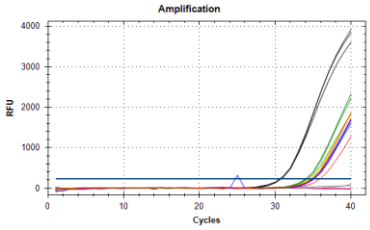

miR-16		
	Sample	Cq Mean
	MGP pellet	30.63
	MGP sup.	N/A
	TEI (p) pellet	35.03
	TEI (s) pellet	34.64
	TEI (p) sup.	34.12
	TEI (s) sup.	35.18
	NTC	N/A

B

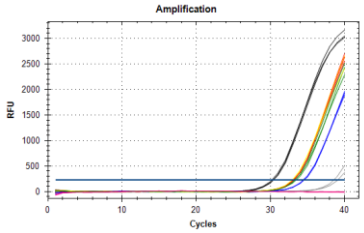

miR-142		
	Sample	Cq Mean
	MGP pellet	30.30
	MGP sup.	38.79
	TEI (p) pellet	34.46
	TEI (s) pellet	32.99
	TEI (p) sup.	33.33
	TEI (s) sup.	33.11
	NTC	N/A

Figure 50: Comparison of exosomes enrichment by MGP and TEI methods

MGP and TEI (for plasma and serum) were used to recover exosomes from 3 µg of lyophilized exosome standards from plasma of healthy donors in 500 µl water. The self-developed miRNA isolation method and Total Exosome RNA & Protein Isolation Kit were applied to extract miRNAs from pellets and supernatants. Isolated miRNAs were amplified by my optimized RT-qPCR for A) miR-16 and B) miR-142. Sup., supernatant; p, plasma; s, serum; NTC, no template control; N/A, not applicable.

3.2.3. Co-isolation of plasma proteins

Finally, to compare the amount of plasma proteins co-isolated by MGP and TEI, an exosome extraction from 10 plasma and 10 serum samples of healthy donors was performed by both methods. There were visual differences between the exosome pellets obtained by the two methods. The pellets derived from TEI were bigger and more yellow for both, plasma and serum samples than the pellets derived from MGP, suggesting an excess of plasma proteins in the exosome pellets derived from TEI (Figure 51A and B). To confirm this hypothesis, an SDS-PAGE of exosome pellets prepared with both techniques, as well as of (unprocessed) plasma and serum samples was performed (Figure 51C and D). As shown on the SDS-PAGEs, lane “MGP” displayed a weaker protein ladder than lane “TEI”. With the exception of the smaller sized proteins, almost all proteins contained in the plasma sample were also well visible in the TEI pellets. Thus, TEI pellets contained much more proteins than MGP pellets and somewhat less protein than the plasma sample.

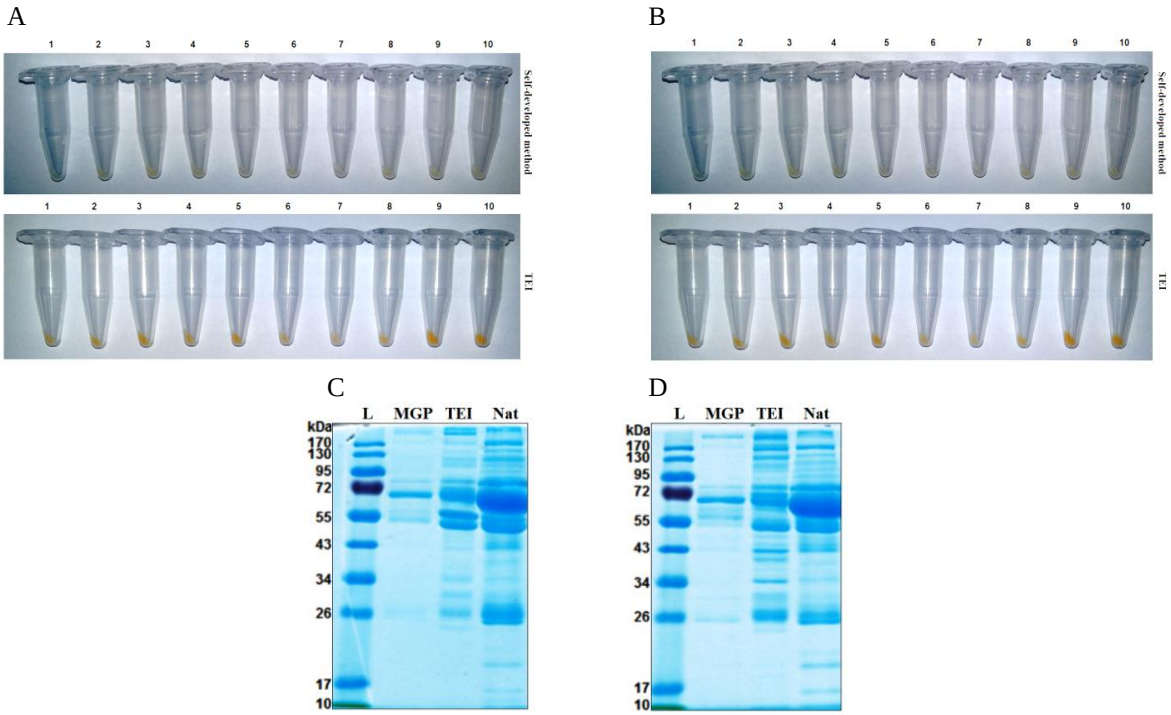

Figure 51: Protein content in exosome pellets derived from MGP and TEI

Pellets obtained from 10 samples (1-10) of 500 µl plasma EDTA (A) and serum (B) using MGP (upper row) and TEI (lower row). SDS-PAGE of exosome pellets isolated from 500 µl plasma EDTA (C) and serum (D) by both methods (MGP and TEI) and of plasma and serum samples (C, D, Nat). Equal volumes of each sample were loaded on the gel (MGP and TEI pellets were dissolved up to equal final volume). Protein ladder is marked as L.

To further confirm these findings, the protein concentration in the pellets and corresponding supernatants derived from 500 µl plasma EDTA and serum, as well as in unprocessed plasma and serum were measured by the Bradford technique. The protein content was 5.1 and 2.3 times higher in TEI than in MGP pellets isolated from plasma and serum, respectively. In contrary, MGP supernatants contained more proteins than TEI supernatants (Figure 52). These results confirm that exosome pellets prepared from TEI method are enriched in proteins.

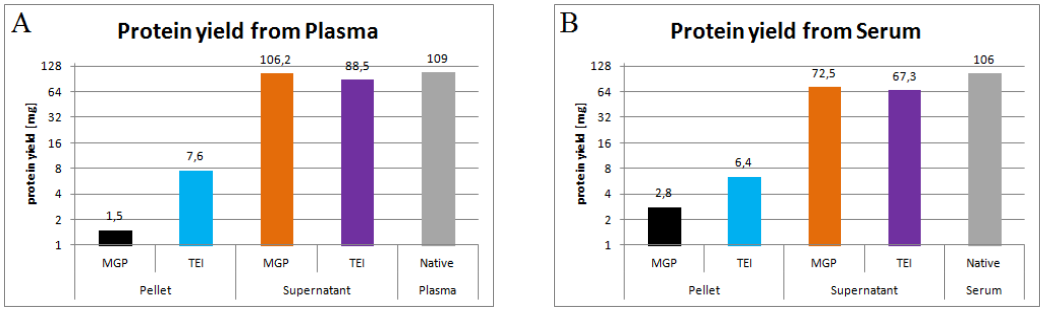

Figure 52: Protein yield in pellets and supernatants prepared from the TEI and MGP-based methods

Protein concentrations of exosome pellets and supernatants prepared from 500 µl A) plasma and B) serum measured by the Bradford assay. Protein content in unprocessed plasma and serum are in grey.

3.3. MiRNA extraction

To compare the yield of miRNAs in exosome pellets and supernatants prepared with MGP and TEI, each of 10 plasma EDTA and 10 serum samples were divided into 2 aliquots of 500 µl. In each of 20 samples, exosomes were separated from supernatants by both methods, MGP and TEI. Subsequently, miRNAs were isolated from exosome pellets and corresponding supernatants by the self-developed miRNA isolation method and Invitrogen Total Exosome RNA & Protein Isolation kit (Figure 53).

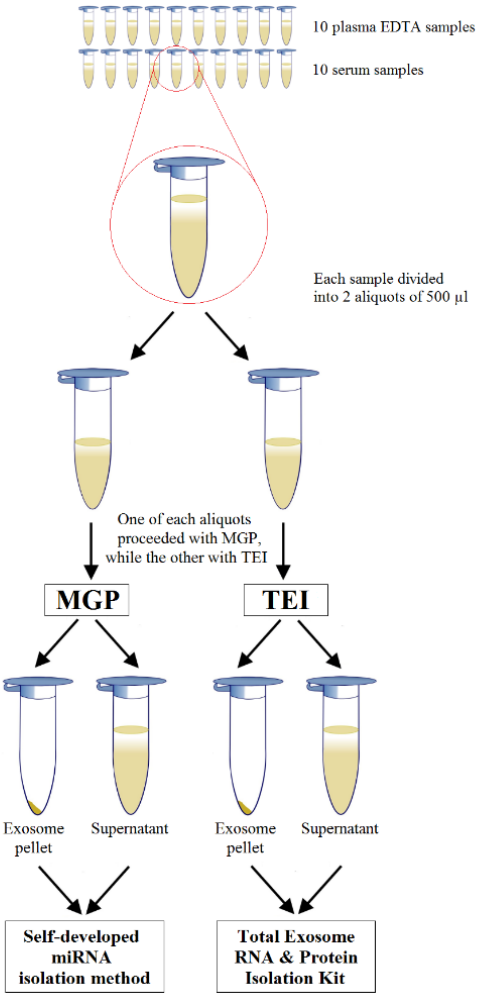

Figure 53: Workflow of the comparative study on exosomal (pellet) and cell-free (supernatant) miRNA extraction

Finally, RT-qPCRs with my optimized method were performed to quantify miR-16 and miR-142 in both fractions (Figure 56). The 10-fold serial dilutions ($4x10^4$-$4x10^7$ copies per reaction) of miR-16 and miR-142 were used for the preparation of standard curves and direct miRNA quantification. MiRNAs were quantified in exosomes (Figure 54A, C, E, and G) and supernatants (Figure 54B, D, F, and H) of each donor to check the efficiency of

exosome isolation by both methods, and the correlation between miRNA and its source. TEI pellets derived from plasma contained more miR-16 (Figure 54A) and less miR-142 (Figure 54C) than MGP pellets. MGP supernatants derived from plasma comprised more miR-16 than TEI supernatants (Figure 54B). The quantity of miR-142 isolated from MGP and TEI supernatants varied between the plasma samples (Figure 54D). Surprisingly, in most of the serum samples, MGP pellets, as well as MGP supernatants, contained more miR-16 and miR-142 than TEI pellets and supernatants (Figure 54E-H).

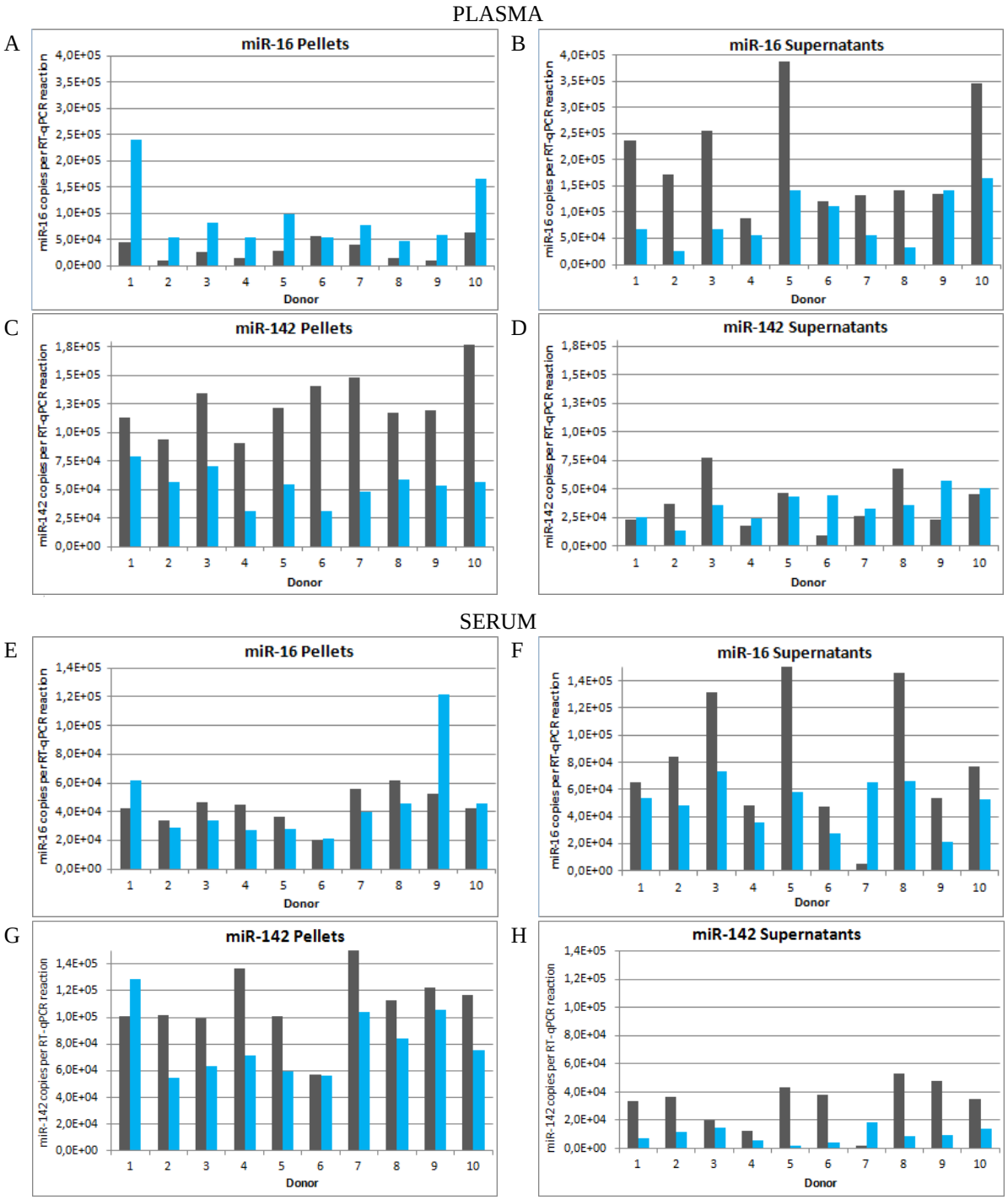

Figure 54: MiRNA content in plasma- and serum-derived exosome pellets and supernatants prepared by MGP and TEI methods

The levels of miRNAs in exosome pellets and supernatants obtained by the MGP-based method are depicted as grey columns, and by the TEI method as blue columns. MiR-16 concentrations in exosome pellets (A) and supernatants (B) derived from plasma of 10 healthy donors (1-10). MiR-142 concentrations in exosome pellets (C) and supernatants (D) derived from plasma of 10 healthy donors. MiR-16 concentration in exosome pellets (E) and supernatants (F) derived from serum of 10 healthy donors (1-10). MiR-142 concentrations in exosome pellets (G) and supernatants (H) derived from serum of 10 healthy donors. All miRNAs concentrations were measured by my optimized RT-qPCR method.

The miRNA quantities differed between miRNA species (miR-16 and miR-142), sources (pellet and supernatant) and preparation methods (TEI and MGP). Therefore, the miRNAs amounts in the pellet and supernatant for plasma and serum from each donor were summed to obtain the total miR-16 and total miR-142 quantities isolated by both methods:

$$\text{miRNA quantity in pellet} + \text{miRNA quantity in supernatant} = \text{total miRNAs}$$

As shown in Figure 55, my self-developed techniques isolated more total miRNAs than the Invitrogen kit independently from the miRNA species and type of sample.

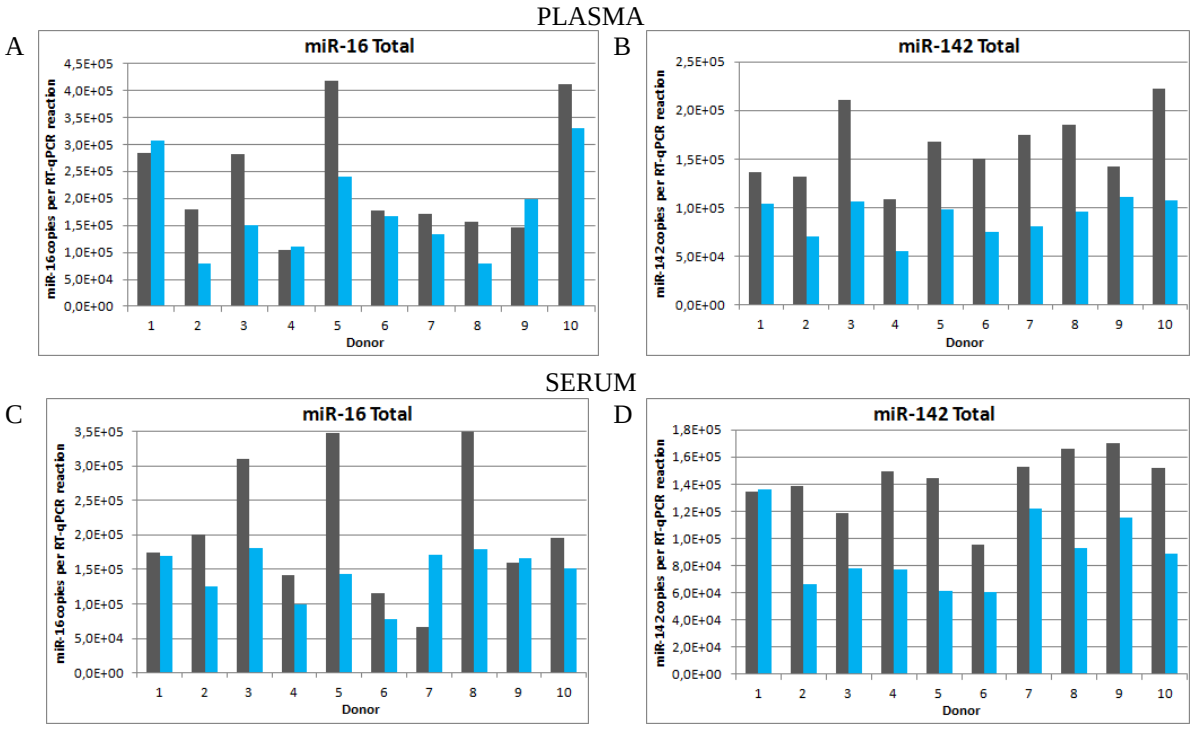

Figure 55: Amounts of total miR-16 and total miR-142 isolated by two techniques

The levels of miRNAs isolated by the MGP-based method are depicted as grey columns and by the TEI kit as blue columns. Plasma total miR-16 (A) and miR-142 (B). Serum total miR-16 (C) and miR-142 (D).

Additionally, box blots and the statistical method ANOVA with Tukey´s HSD test for the occurrence of miRNAs in exosomes and supernatants derived from 10 plasma and 10 serum samples and isolated by both methods was applied for miR-16 and miR-142 to exhibit the differences between both isolation techniques and between the occurrence of a particular miRNA in the two (exosomal and cell-free) fractions (Figure 56). My self-developed techniques indicated that the majority of miR-16 can be found in the supernatants of both plasma (Figure 56A, $p=0.0001$) and serum samples (Figure 56B, $p=0.004$), thus they are rather cell-free. In contrary, most of miR-142 occurred in exosomes derived from plasma (Figure 56C, $p=0.0001$) and serum (Figure 56D,

p=0.0001), thus they are rather of exosomal origin. The results obtained by the Invitrogen kit were congruent to those of my self-developed technique, with an exception of miR-16 occurrence in plasma. Here, the Invitrogen kit indicated a similar distribution of miR-16 between exosomes and cell-free supernatants (Figure 56A, p=0.758). This might be caused by the co-isolation of miRNA/protein complexes by this kit. There were also significant differences between both methods in the amount of miR-16 in plasma exosomes (Figure 56A, p=0.005) and supernatants (Figure 56A, p=0.002) and in the amount of miR-142 in serum exosomes (Figure 56D, p=0.007) and supernatants (Figure 56D, p=0.005). However, the differences of miR-16 in serum in both, exosomes (Figure 56B, p=0.853) and supernatants (Figure 56Figure 56B, p=0.05), as well as of miR-142 in plasma supernatants (Figure 56C, p=0.872) were not significant.

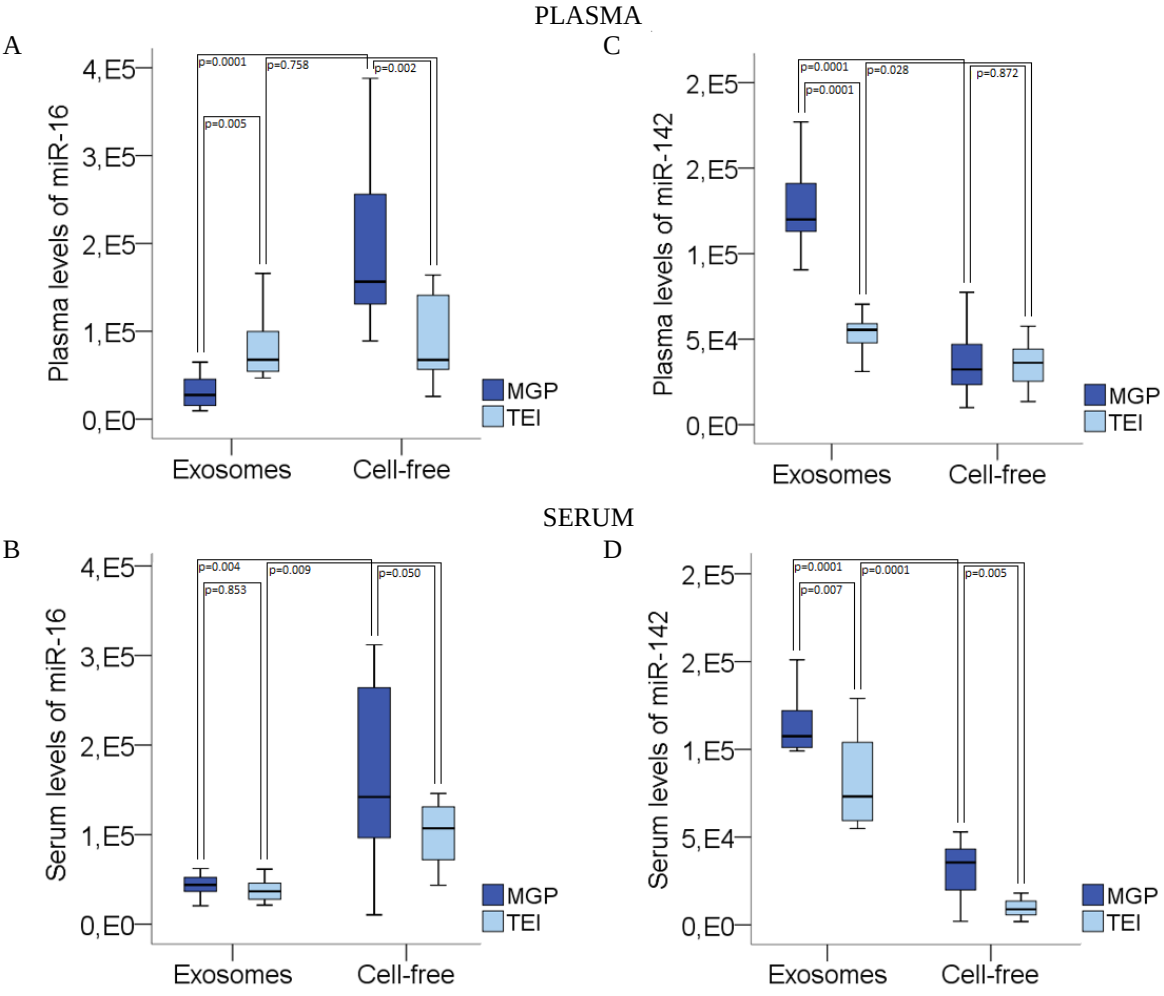

Figure 56: Occurrence of miR-16 and miR-142 in exosomes and as cell-free molecules

Distribution of miRNAs between exosomes and supernatants as derived from the data of MGP are depicted as dark blue boxes and of TEI are depicted as light blue boxes. Occurrence of miR-16 in exosomes and supernatants derived from plasma (A) and serum (B). Occurrence of miR-142 in exosomes and supernatants derived from plasma (C) and serum (D).

VI. DISCUSSION

The deregulation of miRNA expression has been linked with the pathogenesis of benign and malignant diseases (Schwarzenbach, 2015; Schwarzenbach et al., 2014). To better understand the association between miRNAs and human disease and their potential as non-invasive disease biomarkers, a variety of techniques have been used to quantify miRNAs in body tissues and fluids (Kalogianni et al., 2018; Schwarzenbach, 2017b). In particular, methods for quantification of circulating, cell-free and exosomal miRNAs frequently disclose technical problems, resulting in an inconsistency of the reported results (Hruštincová et al., 2015), and complicating the establishment of a non-invasive consensus biomarker that may be implicated in clinical use.

In the current study, I developed a new workflow for measurement of cell-free and exosomal miRNA in cell-free body fluids. It covers three main steps: a method for exosome extraction based on MGP capturing, a new miRNA extraction technique using the non-chaotropic chemistry of Analytik Jena and a modified miRNA quantification by real-time PCR based on the excellent assay by Chen et al. (Applied Biosystems) (Chen et al., 2005). In my experiments, I examined numerous reagents and varied parameters as well as combinations thereof. I chose the most promising combinations, and verified them by real-time PCR using my modified miR-16 and miR-142 RT-qPCR assays.

1. MiRNA quantification technique

There are three common strategies for the amplification of miRNAs by PCR. Two of them involve direct reverse transcription, with the difference that one uses linear, and the other stem-loop primers, which are both miRNA-specific. The third strategy applies the polyadenylation of all miRNAs in the sample, followed by reverse transcription with universal oligo (dT) primers. However, the stem-loop primer provides a better specificity and efficiency of reverse transcription than the other methods. The stem-loop at 5’ end of the reverse transcription primer allows reducing the amplification of pre- and pri-miRNAs (Dong et al., 2013). Moreover, the stem-loop approach discriminates among iso-miRNAs, which differ by only one nucleotide, and is also not influenced by the presence of genomic DNA (Chen et al., 2005).

My advanced miRNA quantification procedure comprising reverse transcription and TaqMan real-time PCR is based on the Applied Biosystems assay that uses such stem-loop

primers and was first published by Chen et al. (Chen et al., 2005) However, several modifications were carried out, e.g., the exclusion of the RNase inhibitor, the modification of the TaqMan probe by labeling it with only BHQ-1 at its 3' end and elongating it by additional nucleotides, optimization of primer concentration, the use of another Taq polymerase which is more quickly activated and a different master mix composition. In respect to the optimized chemistry of master mix, and Hot-Start Taq polymerase, my optimized method allowed reducing time of the real-time PCR reaction for nearly half an hour and increasing 4-times the real-time PCR efficiency. Additionally, modification of the TaqMan probe significantly reduced the cost of real-time PCR. Besides, my optimized method for miR-16 and miR-142 exhibited excellent specificity when using different miRNA as templates (miR-484, miR-140-3p, miR-483-5p, let-7b, cel-miR-39-3p) for amplification with a hardly detectable non-specific signal. Moreover, my optimized real-time PCR is also highly RNA specific, as shown by its insensitivity to genomic DNA used as a target. As checked by gel electrophoresis, there was only a single, prominent band for the PCR product of miR-16 and miR-142, demonstrating that no additional amplicons were formed. Furthermore, there were no products in the negative control (no template), but only a band that much lower migrated and corresponded to the size of primer-dimers. In addition, as compared with the Applied Biosystems TaqMan miRNA assay, my optimized method demonstrated a higher performance. For both miRNAs, miR-16 and miR-142, my optimized RT-qPCR showed a dynamic range of 7 orders of magnitude. Because of an over-amplification of the highest miRNAs concentration and early C_q values of the negative controls, the Applied Biosystems TaqMan miRNA assay showed a dynamic range of only 6 orders of magnitude within the acceptable efficiency levels. However, both assays showed a LOD of 400 copies per PCR for both, miR-16 and miR-142. Chen et al. from Applied Biosystems (Chen et al., 2005) described that the sensitivity of their method is 7 copies per PCR, but such a detection of so few copies cannot be reliable, since the signals from the negative controls, especially using the Applied Biosystems TaqMan miRNA assay for miR-16, were too early, arising often just three C_q values after the dilution of 400 copies. Therefore, it was not possible to discriminate between the signal from 7 copies per reaction and the signal from a negative control. Furthermore, gel electrophoresis revealed some unspecific products in the negative control using the Applied Biosystems TaqMan miRNA assay for miR-16, while only primer dimers were observed with my optimized method. Although the amplification of miR-16 with both

assays exhibited a similar sensitivity, my optimized quantification method exhibited a better efficiency and slope than the Applied Biosystems TaqMan miRNA assay. When performing six repetitions of RT-qPCR with both methods, the commercial assay displayed low linearity and high slope SDs that reveal slope distribution irregularities. Such an irregular pattern of slopes derived from the 10-fold diluted concentrations of miRNAs of a known number of copies does not allow a reliable quantification of miRNAs in plasma and serum. Moreover, the dispersed data of mean slopes and slope SDs showed a low reproducibility of the data using the Applied Biosystems TaqMan miRNA assay. Performing six repetitions of RT-qPCR for miR-142, I observed that both methods, the Applied Biosystems TaqMan miRNA assay and my optimized assay, provided proper linearity, C_q SDs and mean C_q SDs that reflected a good repeatability. Moreover, they were highly reproducible as shown by low values of slope SDs in all 6 repetitions. However, both assays presented data of the mean slopes out of the accepted range. This might be due to the GC content and secondary structure of miR-142 sequence which impede the amplification, especially that at the same time the linearity of both assays was high. These findings show that there is a high probability of big differences in mean slopes when quantifying different miRNAs. Therefore, it is highly recommended to prepare a standard curve for each assay separately.

2. Exosome isolation technique

Commonly used exosome isolation techniques include ultracentrifugation, polymer precipitation, density gradient ultracentrifugation, filtration, SEC and immunoaffinity assays (Konoshenko et al., 2018; Schwarzenbach, 2017b; Szatanek et al., 2017). Despite some advantages of each technique, all of them struggle with serious issues, e.g. ultracentrifugation and density gradient ultracentrifugation require expensive equipment and are time-consuming, filtration cause significant loss of exosomes or their damage and deformation, exosomes obtained by SEC are highly diluted, immunoaffinity assays relies on a specific binding of antibodies to exosomes which may be disturbed by the quality of the antibodies and the antibody-binding solid phase, and precipitation-based techniques co-precipitate plasma proteins. Of interest is a method that purifies a high number of exosomes, without co-purification of material of non-exosomal origin, and at the same time retains the biological activity of isolated vesicles, is cheap, easy, fast and non-laborious.

In this regard, I developed a polymer-based method which bypassed the precipitation, but entrapped exosomes into a polymeric net. The MGP-based technique is easy, fast and non-laborious, involving only 3 main steps: mixing the polymer with the sample, a short incubation step at room temperature and low speed centrifugation in a desktop microcentrifuge (thus no ultracentrifugation). Besides, the MGP-based isolation of exosomes is inexpensive, because it does not require specialized equipment or reagents, such as ultracentrifuge or antibodies.

To test this MGP-based method for its efficiency and quality of exosome extraction, I carried out a Western Blot using an antibody specific for CD63, a known exosomal marker. MGP pellets from both plasma and serum presented prominent bands at the size of 43 kDa corresponding to the size of the band containing the lyophilized exosome standard which served as positive control on the gel. The protein band derived from urine was rather a smear, caused probably by the high protease activity present in the urine. The 43-kDa band detected in plasma and serum is also in line with the size of CD63 which varies from 25 to 65 kDa mainly because of its glycosylation patterns (Ageberg and Lindmark, 2003; Sampey et al., 2016). These findings show that plasma and serum, but not urine, are ideal sources for the extraction of exosomes. Therefore, in the following experiments I only investigated plasma and serum, and excluded urine. The presence of exosomes in the MGP pellet was additionally confirmed by confocal microscopy. First, the MGP pellets derived from serum and plasma were stained with Exo-Red and directly visualized. Then, exosomes from MGP pellets were dyed with PKH26 and added to the EpCAM-stained MDA-MB-468 cells to observe the exosome uptake. Both experiments indicated that exosomes are available in the MGP pellet, and that these exosomes are intact and biologically active. Interestingly, various quantities of exosomes were uptaken by the cells, supporting the theory of a preferential exosome shuttle.

In a recent publication, the authors divided exosomes into 2 groups: Exo-S (S for small) of a diameter from 60-80 nm and Exo-L (L for large) from 90-120 nm. They identified also smaller (~35 nm) non-membranous particles and called them exomeres. All 3 subpopulations of vesicles differed in their protein and nucleic acid cargo (Zhang et al., 2018). In this context, I carried out NTA and showed that vesicles extracted by my MGP-based method have a diameter from 20 to 400 nm. This finding demonstrates that MGP captures both, Exo-S and Exo-L subpopulations of exosomes, as well as exomeres. However, MGP pellets also contained vesicles bigger than 120 nm, suggesting that MGP

isolates either bigger microvesicles (≤1000 nm) or exosome agglomerates. Since it is well known that exosomes tend to agglomerate during the exosome extraction (Cheng et al., 2019; Yassin et al., 2016), these larger vesicles are probably exosome agglomerates. Moreover, to eliminate bigger microvesicles, all samples were filtrated through a 0.22-µm Whatman filter prior to the MGP isolation and NTA analysis. As revealed by the number of exosomes measured by NTA in the MGP pellets prepared from different sample volumes, the amount of starting material used for the exosome preparation positively correlated with the quantity of isolated vesicles. Therefore, the MGP-based exosome extraction can be successfully scaled up to the desired sample volume. Moreover, NTA indicated that MGP does not only isolate vesicles at size range of exosomes with a scaling ability, but also isolates similar quantities of exosomes to those obtained by ultracentrifugation, as tested on samples of lyophilized exosome standards. However, the measurements of lyophilized exosome standards showed a high variance in the repetitions, potentially caused by the sample treatment prior to exosome separation, like freeze drying or freezing of the lyophilized exosome standards that can cause morphological changes in exosomes and their clumping (Malenovská, 2014; Pérez-Bermúdez et al., 2017). Besides, I also demonstrated that my technique can harvest exosomes from different types of samples, such as plasma EDTA, plasma CPD, serum, cell culture supernatant. Furthermore, as shown by the performance of SEC, the MGP-based method is highly efficient to isolate exosomes even from extremely diluted samples. Moreover, the co-isolation of plasma proteins by MGP is narrow, as demonstrated by the relatively very low miRNA concentrations in fractions enriched with proteins. Additionally, I demonstrated that the properly operating SEC column can be self-constructed for low costs. My self-constructed column could separate exosomes in early fractions and proteins in late fractions, what is consistent with the experiments performed by other groups (Arroyo et al., 2011; Benedikter et al., 2017; Takov et al., 2019).

Among the extraction methods, ultracentrifugation is the most commonly used technology for exosome concentration (Konoshenko et al., 2018). To get a relatively pure exosome pellet, ultracentrifugation requires differential centrifugation steps with ultrahigh speeds up to 200,000 g. (Greening et al., 2015). The precipitation with polyethylene glycol (PEG), a water-soluble polymer, is the second method of choice to isolate exosomes (Konoshenko et al., 2018). Nath Neerukonda et al. (Nath Neerukonda et al., 2019) compared the exosome purification between these both methods: ultracentrifugation and the PEG-based

TEI reagent from Invitrogen. Using NTA and transmission electron microscopy, they found that both procedures successfully isolated exosomes with an acceptable size range and morphology, but the use of TEI to purify exosomes from serum was more efficient, quick and isolated a slightly higher exosome number. The authors confirmed this finding by the higher total miRNA content in TEI-precipitated exosomes in comparison to that in ultracentrifugation-purified exosomes as determined by RT-qPCR. For these reasons, I compared my newly established MGP-based exosome extraction method with the TEI method that is apparently better than ultracentrifugation. First, I exposed that TEI is not capable of isolating polystyrene beads dissolved in water, while MGP performed this separation with very high efficiency, leaving no visible beads in the supernatant. Then, I used both methods to re-isolate the lyophilized exosome standard dissolved in water. Here, TEI isolated very small amounts of exosomes, around 10-times less than MGP. To further check if both methods co-isolate proteins, I performed SDS-PAGE and the Bradford assay of the exosome pellets derived from different sources. The protein content was much higher in TEI than in MGP exosome pellets, but somewhat less than the proteins detected in a plasma sample. Performing gel electrophoresis, the coomassie blue protein staining showed that almost all proteins contained in the plasma samples, with the exception of the smaller proteins, were also present in the TEI pellets while the protein content of MGP pellets was narrow. It is well known that the exosome precipitation methods also co-purify protein complexes along with exosomes that can influence downstream RNA profiling. In this regard, Van Deun et al. found that TEI isolated 8 times more protein than ultracentrifugation by calculating the concentration of proteins per number of exosomes isolated by each method (Van Deun et al., 2014). Interestingly, another study disclosed that the presence of proteins in the sample is necessary for TEI to perform the precipitation and that TEI along with the concentration of exosomes co-isolates a material of similar physical properties (Lane et al., 2015).

3. MiRNA isolation technique

Traditionally, isolation of RNA as well as miRNAs from different samples starts with the lysis of the starting material, often in the presence of proteolytic enzymes or chaotropic buffers. Subsequently, RNA is purified by acid phenol/chloroform extraction and isolated by alcohol precipitation. Alternatively, RNA can be bound to mineral supports, e.g. glass powders or silica gels, in presence of highly concentrated solutions of different chaotropic salts, such as guanidine hydrochloride, guanidine thiocyanate or potassium iodide. These salts are responsible for the lysis of the starting material, inactivation of nucleases and subsequent binding of the RNA to the solid surface after addition of alcohol. However, because of its protein-denaturing action, the high ion strength of chaotropic salts does not allow the parallel use of proteolytic enzymes necessary for lysing the complexes. Moreover, these salts act inhibitory on numerous downstream applications. Therefore, extensive washing steps are required to remove the high salts concentrations from the mineral supports.

High concentrations of anti-chaotropic salts in combination with proteolytic enzymes have also been reported as components of buffers for efficient lysis. While chaotropic and anti-chaotropic salts destroy or enhance regular hydrogen bonds in water, respectively, non-chaotropic salts do not harbor any of these activities. Non-chaotropic salts, e.g., magnesium chloride or aluminium chloride that are located in the middle of the Hofmeister series (a classification of ions in order of their ability to salt out or salt in proteins) are protein-stabilizing salts (Hillebrand, 2009). Based on these features, I also tested non-chaotropic salts for the establishing of a new miRNA extraction. Alike to the development of a new exosome extraction method and RT-qPCR, I examined numerous different compositions of reagents, however, mainly based on the Analytik Jena non-chaotropic chemistry, to efficiently extract miRNAs from diverse sources.

The final protocol covers a composition of agents which efficiently lyse exosomes, as well as digest proteins and MGP, leading to the release of nucleic acids which then easily bind to the filter material. The composition allows reducing the salt concentration in the lysis buffer, and therefore, reducing the number of washing steps. The composition comprises: chaotropic salt like urea, non-chaotropic salt like calcium chloride, Tris-HCl as a buffer, SDS as a detergent, trisodium citrate (Na_3-citrate) as a chelating agent forming the lysis solution, proteinase K and absolute ethanol. Urea, as a chaotropic agent, reduces the hydrophobic behaviour of proteins by disrupting the hydrogen binding among amino acids

in hydrophobic regions (Boom et al., 1990; Hatefi and Hanstein, 1969). Moreover, urea acts as a deactivator of RNases. Typically, a concentration of 3.5-8 M is used (Almarza et al., 2006) while in my experiments, the concentration of urea was reduced down to 300 mM. Calcium chloride reinforces the lysis of the sample, and therefore, allows reducing the urea concentration and using proteinase K. Tris-HCl keeps constantly the pH and the physiological ionic strength of the solution. It protects the proteins from precipitation or destabilization, and therefore, prevents the formation of insoluble precipitates (Deutscher, 1990; Taha and Lee, 2010). SDS, an ionic surfactant with an amphiphilic structure, promotes the solubilisation of proteins through binding its hydrophobic part to the hydrophobic portion of a protein and its hydrophilic part to water molecules (Bhuyan, 2010). Natrium citrate chelates calcium ions and disrupts the plasma membrane of cells (Nagaoka et al., 2010). Proteinase K is a serine endopeptidase known to digest proteins in their native structures. It is among others responsible for the hydrolysis of RNase A and DNase I, and therefore, protects released cell-free and exosomal nucleic acids from degradation (Ghéczy et al., 2016). Ethanol is a nucleic acids precipitation agent (Zeugin and Hartley, 1985), and is used to enhance binding of nucleic acids on solid surfaces, such as silica or nylon membranes and beads (Lienau and Hurley, 2002). By applying the combination of non-chaotropic and chaotropic chemistry in reduced concentration, the miRNA purification by acid phenol/chloroform extraction, as well as the extensive washing steps are not necessary any more. These modifications deliver a shorter protocol without using substances that are hazardous to the health and the environment.

For the development of the miRNA isolation method, we also examined numerous different procedure parameters, such as volume of the used reagents, and time and temperature of incubation steps. Ultimately, the final protocols for miRNA isolation from exosome pellet and supernatant were examined by my optimized RT-qPCR assays for miR-16 and miR-142. Both protocols could efficiently isolate miRNAs from different types of samples, like plasma EDTA, plasma CPD or serum. Moreover, there was a positive correlation between sample volume used for miRNA isolation and yield of isolated miRNAs. Finally, higher levels of miR-16 were quantified from plasma-derived supernatants than in the exosomes. These findings were confirmed when serum was used. Inversely, higher amounts of miR-142 were detected in exosomes derived from plasma than in supernatant, which were also found in serum. The detections that miR-16 rather circulates in a cell-/exosome-free form than in exosomes, whereas miR-142 rather

circulates in exosome than cell-freely are in line with the observations by several previous studies (Arroyo et al., 2011; Cheng et al., 2014a; Enderle et al., 2015; Karttunen et al., 2019). However, a somewhat smaller portion of miR-16 seems to be associated with the exosomal fraction, since in my experiments the increase in sample volume led to the increase in miR-16 quantity in the exosome pellet. Interestingly, the most significant increase in the levels of exosomal miR-142 compared with the levels of cell-free miR-142 was found in serum. In addition, the examination of quantity and size distribution of exosomal RNAs isolated from plasma and serum on an Agilent Bioanalyzer showed that the concentrations of small RNAs, as well as of miRNAs were higher in serum than plasma. It is well accepted that the extraction from serum provides higher amounts of nucleic acids than the extraction from plasma. This is caused by the different blood collection systems (D.-J. Kim et al., 2012; Lee et al., 2001). These elevated miRNA levels in serum may be influenced by the process of clot formation which releases vesicles (Kirschner et al., 2013; Witwer et al., 2013). However, plasma as well as serum contained almost 50 % miRNAs of the total isolated RNAs.

4. The workflow for miRNA analysis

The full workflow of my methods for miRNA analysis (exosome extraction, miRNA isolation, reverse transcription and qPCR) was also tested on 10 plasma and 10 serum samples and compared with the Invitrogen TEI method, followed by the Invitrogen Total Exosome RNA & Protein Isolation kit and my modified qPCR. Here, the application of the whole package of my newly established assays confirmed my data above that the levels of miR-16 are significantly higher in the plasma and serum supernatant than in the exosomes. However, the TEI method showed similar levels of miR-16 in both fractions of plasma, but significant higher levels in the serum supernatant than in the exosomes. These findings demonstrate that the TEI assay delivers different data for plasma and serum, whereas our method provides congruent data. The discrepant results derived from the TEI method might be due to the fact that plasma contains more proteins than serum (Smith et al., 2013) and that TEI co-isolates much more plasma proteins than the MGB-based assay which influence the downstream quantification of miR-16.

There are numerous assays for exosome extraction and miRNA isolation and quantification on the market. In particular, the stem-loop RT-qPCR assay from Applied Biosystems is qualified for the quantification of miRNAs from plasma and serum. However, each technique may demand for optimization. In my PhD study, I developed an improved procedure beginning from the MGP-based exosome extraction, over the miRNA isolation and ending with RT-qPCR. My assay system is a promising sensitive and specific technical approach for different cell-free body fluids. It is faster in the performance than commonly used procedures and is not influenced by the source (plasma or serum) used for the analysis.

VII. FUTURE PERSPECTIVES

Further investigations are planned to check if the package of developed methods (exosome enrichment, miRNAs isolation and miRNAs quantification) can be used as a state of art for exosomal and cell-free miRNAs detection and quantification. Plasma and serum samples, as well as other body fluids from a large cohort of donors, including patients with different diseases and healthy individuals, will be tested. The provided data will be examined for their conformity, repeatability and reproducibility.

So far, my assays work perfectly for the quantification of miR-16 and miR-142. Now, it is planned to design primer sets and probes for other miRNAs, e.g. commonly used miRNAs, among others miR-21, miR-20a, miR-200. These miRNAs will then be further quantified with my assays. The analyses will allow properly examining whether these miRNAs are preferentially present in exosomes or circulate as cell-free (exosome-free) molecules in the blood. These investigations are of interest since the packaging of particular miRNAs into exosomes is the first step in cell-to-cell communication resulting in the spread of disease.

In summary, exosomal miRNAs may be the fundament for developing a new class of agents that specifically target miRNA pathways, and be attractive candidates for therapeutic target molecules and disease markers for clinical application in malignant as well as benign diseases. Blood-based quantification of exosomal miRNAs may be eligible for companion diagnostics, because blood constitutes a pool of exosomes derived from different sources. A further important feature is the possibility of taking repeated blood samples to keep disease course under surveillance. Since multiple markers rather than a single marker will give the best diagnosis and prognosis, minimally invasive blood analyses of exosomal miRNAs could have potential to complement the existing biomarkers. To approach miRNAs to the clinics, the identification and assembly of clinically relevant exosomal miRNAs are of great interest, as well as standardized analysis methods are urgently needed. Therefore, it was necessary to develop assays that support an efficient, rapid and easy miRNA quantification.

VIII. REFERENCES

Adams, L., 2017. Non-coding RNA: Pri-miRNA processing: structure is key. Nat. Rev. Genet. 18, 145. https://doi.org/10.1038/nrg.2017.6

Ageberg, M., Lindmark, A., 2003. Characterisation of the biosynthesis and processing of the neutrophil granule membrane protein CD63 in myeloid cells. Clin. Lab. Haematol. 25, 297–306.

Alexander, R.P., Laurent, L.C., Alexander, R.P., 2015. Isolation of extracellular vesicles and RNA using the miRcury Biofluids Kit. Protoc. Exch. https://doi.org/10.1038/protex.2015.114

Almarza, J., Morales, S., Rincon, L., Brito, F., 2006. Urea as the only inactivator of RNase for extraction of total RNA from plant and animal tissues. Anal. Biochem. 358, 143–145. https://doi.org/10.1016/j.ab.2006.03.040

Andreu, Z., Rivas, E., Sanguino-Pascual, A., Lamana, A., Marazuela, M., González-Alvaro, I., Sánchez-Madrid, F., de la Fuente, H., Yáñez-Mó, M., 2016. Comparative analysis of EV isolation procedures for miRNAs detection in serum samples. J. Extracell. Vesicles 5, 31655. https://doi.org/10.3402/jev.v5.31655

Ardekani, A.M., Naeini, M.M., 2010. The Role of MicroRNAs in Human Diseases. Avicenna J. Med. Biotechnol. 2, 161–179.

Arroyo, J.D., Chevillet, J.R., Kroh, E.M., Ruf, I.K., Pritchard, C.C., Gibson, D.F., Mitchell, P.S., Bennett, C.F., Pogosova-Agadjanyan, E.L., Stirewalt, D.L., Tait, J.F., Tewari, M., 2011. Argonaute2 complexes carry a population of circulating microRNAs independent of vesicles in human plasma. Proc. Natl. Acad. Sci. U. S. A. 108, 5003–5008. https://doi.org/10.1073/pnas.1019055108

Aryani, A., Denecke, B., 2015. In vitro application of ribonucleases: comparison of the effects on mRNA and miRNA stability. BMC Res. Notes 8. https://doi.org/10.1186/s13104-015-1114-z

Bartel, D.P., 2009. MicroRNA Target Recognition and Regulatory Functions. Cell 136, 215–233. https://doi.org/10.1016/j.cell.2009.01.002

Batrakova, E.V., Kim, M.S., 2015. Using exosomes, naturally-equipped nanocarriers, for drug delivery. J. Control. Release Off. J. Control. Release Soc. 219, 396–405. https://doi.org/10.1016/j.jconrel.2015.07.030

Bayraktar, R., Roosbroeck, K.V., Calin, G.A., 2017. Cell-to-cell communication: microRNAs as hormones. Mol. Oncol. 11, 1673–1686. https://doi.org/10.1002/1878-0261.12144

Bebelman, M.P., Smit, M.J., Pegtel, D.M., Baglio, S.R., 2018. Biogenesis and function of extracellular vesicles in cancer. Pharmacol. Ther. 188, 1–11. https://doi.org/10.1016/j.pharmthera.2018.02.013

Bellingham, S.A., Guo, B.B., Coleman, B.M., Hill, A.F., 2012. Exosomes: Vehicles for the Transfer of Toxic Proteins Associated with Neurodegenerative Diseases? Front. Physiol. 3. https://doi.org/10.3389/fphys.2012.00124

Benedikter, B.J., Bouwman, F.G., Vajen, T., Heinzmann, A.C.A., Grauls, G., Mariman, E.C., Wouters, E.F.M., Savelkoul, P.H., Lopez-Iglesias, C., Koenen, R.R., Rohde, G.G.U., Stassen, F.R.M., 2017. Ultrafiltration combined with size exclusion chromatography efficiently isolates extracellular vesicles from cell culture media for compositional and functional studies. Sci. Rep. 7, 15297. https://doi.org/10.1038/s41598-017-15717-7

Bhuyan, A.K., 2010. On the mechanism of SDS-induced protein denaturation. Biopolymers 93, 186–199. https://doi.org/10.1002/bip.21318

Binderup, H.G., Madsen, J.S., Heegaard, N.H.H., Houlind, K., Andersen, R.F., Brasen, C.L., 2018. Quantification of microRNA levels in plasma – Impact of preanalytical and analytical conditions. PLoS ONE 13. https://doi.org/10.1371/journal.pone.0201069

Boom, R., Sol, C.J., Salimans, M.M., Jansen, C.L., Wertheim-van Dillen, P.M., van der Noordaa, J., 1990. Rapid and simple method for purification of nucleic acids. J. Clin. Microbiol. 28, 495–503.

Boon, R.A., Vickers, K.C., 2013. Intercellular Transport of MicroRNAs. Arterioscler. Thromb. Vasc. Biol. 33, 186–192. https://doi.org/10.1161/ATVBAHA.112.300139

Boulanger Chantal M., Amabile Nicolas, Tedgui Alain, 2006. Circulating Microparticles. Hypertension 48, 180–186. https://doi.org/10.1161/01.HYP.0000231507.00962.b5

Bradford, M.M., 1976. A rapid and sensitive method for the quantitation of microgram quantities of protein utilizing the principle of protein-dye binding. Anal. Biochem. 72, 248–254. https://doi.org/10.1016/0003-2697(76)90527-3

Broeders, S., Huber, I., Grohmann, L., Berben, G., Taverniers, I., Mazzara, M., Roosens, N., Morisset, D., 2014. Guidelines for validation of qualitative real-time PCR methods. Trends Food Sci. Technol. 37, 115–126. https://doi.org/10.1016/j.tifs.2014.03.008

Campomenosi, P., Gini, E., Noonan, D.M., Poli, A., D'Antona, P., Rotolo, N., Dominioni, L., Imperatori, A., 2016. A comparison between quantitative PCR and droplet digital PCR technologies for circulating microRNA quantification in human lung cancer. BMC Biotechnol. 16. https://doi.org/10.1186/s12896-016-0292-7

Cesselli, D., Parisse, P., Aleksova, A., Veneziano, C., Cervellin, C., Zanello, A., Beltrami, A.P., 2018. Extracellular Vesicles: How Drug and Pathology Interfere With Their Biogenesis and Function. Front. Physiol. 9. https://doi.org/10.3389/fphys.2018.01394

Chen, C., Ridzon, D.A., Broomer, A.J., Zhou, Z., Lee, D.H., Nguyen, J.T., Barbisin, M., Xu, N.L., Mahuvakar, V.R., Andersen, M.R., Lao, K.Q., Livak, K.J., Guegler, K.J., 2005. Real-time quantification of microRNAs by stem-loop RT-PCR. Nucleic Acids Res. 33, e179. https://doi.org/10.1093/nar/gni178

Chen, C., Skog, J., Hsu, C.-H., Lessard, R.T., Balaj, L., Wurdinger, T., Carter, B.S., Breakefield, X.O., Toner, M., Irimia, D., 2010. Microfluidic isolation and transcriptome analysis of serum microvesicles. Lab. Chip 10, 505–511. https://doi.org/10.1039/b916199f

Cheng, J., Nonaka, T., Wong, D.T.W., 2019. Salivary Exosomes as Nanocarriers for Cancer Biomarker Delivery. Mater. Basel Switz. 12. https://doi.org/10.3390/ma12040654

Cheng, L., Sharples, R.A., Scicluna, B.J., Hill, A.F., 2014a. Exosomes provide a protective and enriched source of miRNA for biomarker profiling compared to intracellular and cell-free blood. J. Extracell. Vesicles 3. https://doi.org/10.3402/jev.v3.23743

Cheng, L., Sun, X., Scicluna, B.J., Coleman, B.M., Hill, A.F., 2014b. Characterization and deep sequencing analysis of exosomal and non-exosomal miRNA in human urine. Kidney Int. 86, 433–444. https://doi.org/10.1038/ki.2013.502

Cheng, L., Sun, X., Scicluna, B.J., Coleman, B.M., Hill, A.F., 2014c. Characterization and deep sequencing analysis of exosomal and non-exosomal miRNA in human urine. Kidney Int. 86, 433–444. https://doi.org/10.1038/ki.2013.502

Chevillet, J.R., Lee, I., Briggs, H.A., He, Y., Wang, K., 2014. Issues and Prospects of microRNA-Based Biomarkers in Blood and Other Body Fluids. Molecules 19, 6080–6105. https://doi.org/10.3390/molecules19056080

Chomczynski, P., Sacchi, N., 1987. Single-step method of RNA isolation by acid guanidinium thiocyanate-phenol-chloroform extraction. Anal. Biochem. 162, 156–159. https://doi.org/10.1016/0003-2697(87)90021-2

Corcoran, C., Friel, A.M., Duffy, M.J., Crown, J., O'Driscoll, L., 2011. Intracellular and Extracellular MicroRNAs in Breast Cancer. Clin. Chem. 57, 18–32. https://doi.org/10.1373/clinchem.2010.150730

Cortez, M.A., Bueso-Ramos, C., Ferdin, J., Lopez-Berestein, G., Sood, A.K., Calin, G.A., 2011. MicroRNAs in body fluids—the mix of hormones and biomarkers. Nat. Rev. Clin. Oncol. 8, 467–477. https://doi.org/10.1038/nrclinonc.2011.76

Davies, R.T., Kim, J., Jang, S.C., Choi, E.-J., Gho, Y.S., Park, J., 2012. Microfluidic filtration system to isolate extracellular vesicles from blood. Lab. Chip 12, 5202–5210. https://doi.org/10.1039/C2LC41006K

Deutscher, M.P., 1990. Guide to Protein Purification. Gulf Professional Publishing.

Dong, H., Lei, J., Ding, L., Wen, Y., Ju, H., Zhang, X., 2013. MicroRNA: Function, Detection, and Bioanalysis. Chem. Rev. 113, 6207–6233. https://doi.org/10.1021/cr300362f

Enderle, D., Spiel, A., Coticchia, C.M., Berghoff, E., Mueller, R., Schlumpberger, M., Sprenger-Haussels, M., Shaffer, J.M., Lader, E., Skog, J., Noerholm, M., 2015. Characterization of RNA from Exosomes and Other Extracellular Vesicles Isolated by a Novel Spin Column-Based Method. PLOS ONE 10, e0136133. https://doi.org/10.1371/journal.pone.0136133

Endzeliņš, E., Berger, A., Melne, V., Bajo-Santos, C., Soboļevska, K., Ābols, A., Rodriguez, M., Šantare, D., Rudņickiha, A., Lietuvietis, V., Llorente, A., Linē, A., 2017. Detection of circulating miRNAs: comparative analysis of extracellular vesicle-incorporated miRNAs and cell-free miRNAs in whole plasma of prostate cancer patients. BMC Cancer 17. https://doi.org/10.1186/s12885-017-3737-z

Escrevente, C., Keller, S., Altevogt, P., Costa, J., 2011. Interaction and uptake of exosomes by ovarian cancer cells. BMC Cancer 11, 108. https://doi.org/10.1186/1471-2407-11-108

Evander, M., Gidlöf, O., Olde, B., Erlinge, D., Laurell, T., 2015. Non-contact acoustic capture of microparticles from small plasma volumes. Lab. Chip 15, 2588–2596. https://doi.org/10.1039/C5LC00290G

Forootan, A., Sjöback, R., Björkman, J., Sjögreen, B., Linz, L., Kubista, M., 2017. Methods to determine limit of detection and limit of quantification in quantitative real-time PCR (qPCR). Biomol. Detect. Quantif. 12, 1–6. https://doi.org/10.1016/j.bdq.2017.04.001

Gallart-Palau, X., Serra, A., Wong, A.S.W., Sandin, S., Lai, M.K.P., Chen, C.P., Kon, O.L., Sze, S.K., 2015. Extracellular vesicles are rapidly purified from human plasma by PRotein Organic Solvent PRecipitation (PROSPR). Sci. Rep. 5. https://doi.org/10.1038/srep14664

Gámez-Valero, A., Monguió-Tortajada, M., Carreras-Planella, L., Franquesa, M., Beyer, K., Borràs, F.E., 2016. Size-Exclusion Chromatography-based isolation minimally alters Extracellular Vesicles' characteristics compared to precipitating agents. Sci. Rep. 6, 33641. https://doi.org/10.1038/srep33641

Garcia-Elias, A., Alloza, L., Puigdecanet, E., Nonell, L., Tajes, M., Curado, J., Enjuanes, C., Díaz, O., Bruguera, J., Martí-Almor, J., Comín-Colet, J., Benito, B., 2017. Defining quantification methods and optimizing protocols for microarray hybridization of circulating microRNAs. Sci. Rep. 7, 7725. https://doi.org/10.1038/s41598-017-08134-3

Ghéczy, N., Küchler, A., Walde, P., 2016. Proteinase K activity determination with β-galactosidase as sensitive macromolecular substrate. Anal. Biochem. 513, 54–60. https://doi.org/10.1016/j.ab.2016.08.030

Golstein, P., Kroemer, G., 2007. Cell death by necrosis: towards a molecular definition. Trends Biochem. Sci. 32, 37–43. https://doi.org/10.1016/j.tibs.2006.11.001

Green, D.R., Llambi, F., 2015. Cell Death Signaling. Cold Spring Harb. Perspect. Biol. 7. https://doi.org/10.1101/cshperspect.a006080

Greening, D.W., Xu, R., Ji, H., Tauro, B.J., Simpson, R.J., 2015. A protocol for exosome isolation and characterization: evaluation of ultracentrifugation, density-gradient separation, and immunoaffinity capture methods. Methods Mol. Biol. Clifton NJ 1295, 179–209. https://doi.org/10.1007/978-1-4939-2550-6_15

Hackett, N.R., El Sawy, T., Lee, L.Y., Silva, I., O'Leary, J., Rosengart, T.K., Crystal, R.G., 2000. Use of Quantitative TaqMan Real-Time PCR to Track the Time-Dependent Distribution of Gene Transfer Vectors in Vivo. Mol. Ther. 2, 649–656. https://doi.org/10.1006/mthe.2000.0203

Hatefi, Y., Hanstein, W.G., 1969. SOLUBILIZATION OF PARTICULATE PROTEINS AND NONELECTROLYTES BY CHAOTROPIC AGENTS*. Proc. Natl. Acad. Sci. U. S. A. 62, 1129–1136.

He, M., Zeng, Y., 2016. Microfluidic Exosome Analysis toward Liquid Biopsy for Cancer. J. Lab. Autom. 21, 599–608. https://doi.org/10.1177/2211068216651035

Heinemann, M.L., Ilmer, M., Silva, L.P., Hawke, D.H., Recio, A., Vorontsova, M.A., Alt, E., Vykoukal, J., 2014. Benchtop isolation and characterization of functional exosomes by sequential filtration. J. Chromatogr. A 1371, 125–135. https://doi.org/10.1016/j.chroma.2014.10.026

Helwa, I., Cai, J., Drewry, M.D., Zimmerman, A., Dinkins, M.B., Khaled, M.L., Seremwe, M., Dismuke, W.M., Bieberich, E., Stamer, W.D., Hamrick, M.W., Liu, Y., 2017. A Comparative Study of Serum Exosome Isolation Using Differential Ultracentrifugation and Three Commercial Reagents. PloS One 12, e0170628. https://doi.org/10.1371/journal.pone.0170628

Henne, W.M., Buchkovich, N.J., Emr, S.D., 2011. The ESCRT Pathway. Dev. Cell 21, 77–91. https://doi.org/10.1016/j.devcel.2011.05.015

Hikita, T., Kuwahara, A., Watanabe, R., Miyata, M., Oneyama, C., 2019. Src in endosomal membranes promotes exosome secretion and tumor progression. Sci. Rep. 9, 3265. https://doi.org/10.1038/s41598-019-39882-z

Hillebrand, T., 2009. Method for the isolation of nucleic acids from any starting material. US20090047724A1.

Hruštincová, A., Votavová, H., Dostálová Merkerová, M., 2015. Circulating MicroRNAs: Methodological Aspects in Detection of These Biomarkers. Folia Biol. (Praha) 61, 203–218.

Huang, E., Liu, R., Chu, Y., 2015. miRNA-15a/16: as tumor suppressors and more. Future Oncol. Lond. Engl. 11, 2351–2363. https://doi.org/10.2217/fon.15.101

Huang, X., Yuan, T., Tschannen, M., Sun, Z., Jacob, H., Du, M., Liang, Meihua, Dittmar, R.L., Liu, Y., Liang, Mingyu, Kohli, M., Thibodeau, S.N., Boardman, L., Wang, L., 2013. Characterization of human plasma-derived exosomal RNAs by deep sequencing. BMC Genomics 14, 319. https://doi.org/10.1186/1471-2164-14-319

Jeppesen, D.K., Fenix, A.M., Franklin, J.L., Higginbotham, J.N., Zhang, Q., Zimmerman, L.J., Liebler, D.C., Ping, J., Liu, Q., Evans, R., Fissell, W.H., Patton, J.G., Rome, L.H., Burnette, D.T., Coffey, R.J., 2019. Reassessment of Exosome Composition. Cell 177, 428-445.e18. https://doi.org/10.1016/j.cell.2019.02.029

Jing, Q., Huang, S., Guth, S., Zarubin, T., Motoyama, A., Chen, J., Di Padova, F., Lin, S.-C., Gram, H., Han, J., 2005. Involvement of microRNA in AU-rich element-mediated mRNA instability. Cell 120, 623–634. https://doi.org/10.1016/j.cell.2004.12.038

Kalogianni, D.P., Kalligosfyri, P.M., Kyriakou, I.K., Christopoulos, T.K., 2018. Advances in microRNA analysis. Anal. Bioanal. Chem. 410, 695–713. https://doi.org/10.1007/s00216-017-0632-z

Kamm, R.C., Smith, A.G., 1972. Nucleic acid concentrations in normal human plasma. Clin. Chem. 18, 519–522.

Karttunen, J., Heiskanen, M., Navarro-Ferrandis, V., Gupta, S.D., Lipponen, A., Puhakka, N., Rilla, K., Koistinen, A., Pitkänen, A., 2019. Precipitation-based extracellular vesicle isolation from rat plasma co-precipitate vesicle-free microRNAs. J. Extracell. Vesicles 8, 1555410. https://doi.org/10.1080/20013078.2018.1555410

Kehl, T., Backes, C., Kern, F., Fehlmann, T., Ludwig, N., Meese, E., Lenhof, H.-P., Keller, A., 2017. About miRNAs, miRNA seeds, target genes and target pathways. Oncotarget 8, 107167–107175. https://doi.org/10.18632/oncotarget.22363

Kim, D.-J., Linnstaedt, S., Palma, J., Park, J.C., Ntrivalas, E., Kwak-Kim, J.Y.H., Gilman-Sachs, A., Beaman, K., Hastings, M.L., Martin, J.N., Duelli, D.M., 2012. Plasma Components Affect Accuracy of Circulating Cancer-Related MicroRNA Quantitation. J. Mol. Diagn. JMD 14, 71–80. https://doi.org/10.1016/j.jmoldx.2011.09.002

Kim, Y.-K., Yeo, J., Kim, B., Ha, M., Kim, V.N., 2012. Short Structured RNAs with Low GC Content Are Selectively Lost during Extraction from a Small Number of Cells. Mol. Cell 46, 893–895. https://doi.org/10.1016/j.molcel.2012.05.036

Kirschner, M.B., Kao, S.C., Edelman, J.J., Armstrong, N.J., Vallely, M.P., Zandwijk, N. van, Reid, G., 2011. Haemolysis during Sample Preparation Alters microRNA Content of Plasma. PLOS ONE 6, e24145. https://doi.org/10.1371/journal.pone.0024145

Koczera, P., Martin, L., Marx, G., Schuerholz, T., 2016. The Ribonuclease A Superfamily in Humans: Canonical RNases as the Buttress of Innate Immunity. Int. J. Mol. Sci. 17. https://doi.org/10.3390/ijms17081278

Konoshenko, M.Y., Lekchnov, E.A., Vlassov, A.V., Laktionov, P.P., 2018. Isolation of Extracellular Vesicles: General Methodologies and Latest Trends [WWW Document]. BioMed Res. Int. https://doi.org/10.1155/2018/8545347

Kordelas, L., Rebmann, V., Ludwig, A.-K., Radtke, S., Ruesing, J., Doeppner, T.R., Epple, M., Horn, P.A., Beelen, D.W., Giebel, B., 2014. MSC-derived exosomes: a novel tool to treat therapy-refractory graft-versus-host disease. Leukemia 28, 970–973. https://doi.org/10.1038/leu.2014.41

Kumar, P., Dezso, Z., MacKenzie, C., Oestreicher, J., Agoulnik, S., Byrne, M., Bernier, F., Yanagimachi, M., Aoshima, K., Oda, Y., 2013. Circulating miRNA biomarkers for Alzheimer's disease. PloS One 8, e69807. https://doi.org/10.1371/journal.pone.0069807

Kutyavin, I.V., Afonina, I.A., Mills, A., Gorn, V.V., Lukhtanov, E.A., Belousov, E.S., Singer, M.J., Walburger, D.K., Lokhov, S.G., Gall, A.A., Dempcy, R., Reed, M.W., Meyer, R.B., Hedgpeth, J., 2000. 3′-Minor groove binder-DNA probes increase sequence specificity at PCR extension temperatures. Nucleic Acids Res. 28, 655–661.

Lane, R.E., Korbie, D., Anderson, W., Vaidyanathan, R., Trau, M., 2015. Analysis of exosome purification methods using a model liposome system and tunable-resistive pulse sensing. Sci. Rep. 5. https://doi.org/10.1038/srep07639

Lawrie, C.H., Gal, S., Dunlop, H.M., Pushkaran, B., Liggins, A.P., Pulford, K., Banham, A.H., Pezzella, F., Boultwood, J., Wainscoat, J.S., Hatton, C.S.R., Harris, A.L., 2008. Detection of elevated levels of tumour-associated microRNAs in serum of patients with diffuse large B-cell lymphoma. Br. J. Haematol. 141, 672–675. https://doi.org/10.1111/j.1365-2141.2008.07077.x

Lee, C.-T., Risom, T., Strauss, W.M., 2007. Evolutionary conservation of microRNA regulatory circuits: an examination of microRNA gene complexity and conserved microRNA-target interactions through metazoan phylogeny. DNA Cell Biol. 26, 209–218. https://doi.org/10.1089/dna.2006.0545

Lee, K., Shao, H., Weissleder, R., Lee, H., 2015. Acoustic Purification of Extracellular Microvesicles. ACS Nano 9, 2321–2327. https://doi.org/10.1021/nn506538f

Lee, R.C., Feinbaum, R.L., Ambros, V., 1993. The C. elegans heterochronic gene lin-4 encodes small RNAs with antisense complementarity to lin-14. Cell 75, 843–854.

Lee, T.H., Montalvo, L., Chrebtow, V., Busch, M.P., 2001. Quantitation of genomic DNA in plasma and serum samples: higher concentrations of genomic DNA found in serum than in plasma. Transfusion (Paris) 41, 276–282.

Lekchnov, E.A., Zaporozhchenko, I.A., Morozkin, E.S., Bryzgunova, O.E., Vlassov, V.V., Laktionov, P.P., 2016. Protocol for miRNA isolation from biofluids. Anal. Biochem. 499, 78–84. https://doi.org/10.1016/j.ab.2016.01.025

Li, P., Kaslan, M., Lee, S.H., Yao, J., Gao, Z., 2017. Progress in Exosome Isolation Techniques. Theranostics 7, 789–804. https://doi.org/10.7150/thno.18133

Lienau, E., Hurley, J., 2002. DNA isolation method and kit. US20020072110A1.

Liga, A., Vliegenthart, A.D.B., Oosthuyzen, W., Dear, J.W., Kersaudy-Kerhoas, M., 2015. Exosome isolation: a microfluidic road-map. Lab. Chip 15, 2388–2394. https://doi.org/10.1039/C5LC00240K

Linares, R., Tan, S., Gounou, C., Arraud, N., Brisson, A.R., 2015. High-speed centrifugation induces aggregation of extracellular vesicles. J. Extracell. Vesicles 4, 29509. https://doi.org/10.3402/jev.v4.29509

Lis, J.T., 1980. Fractionation of DNA fragments by polyethylene glycol induced precipitation. Methods Enzymol. 65, 347–353.

Livshits, M.A., Khomyakova, E., Evtushenko, E.G., Lazarev, V.N., Kulemin, N.A., Semina, S.E., Generozov, E.V., Govorun, V.M., 2015. Isolation of exosomes by differential centrifugation: Theoretical analysis of a commonly used protocol. Sci. Rep. 5, 17319. https://doi.org/10.1038/srep17319

Lo Russo, G., Tessari, A., Capece, M., Galli, G., de Braud, F., Garassino, M.C., Palmieri, D., 2018. MicroRNAs for the Diagnosis and Management of Malignant Pleural Mesothelioma: A Literature Review. Front. Oncol. 8, 650. https://doi.org/10.3389/fonc.2018.00650

Malenovská, H., 2014. The influence of stabilizers and rates of freezing on preserving of structurally different animal viruses during lyophilization and subsequent storage. J. Appl. Microbiol. 117, 1810–1819. https://doi.org/10.1111/jam.12654

Mandel, P., Metais, P., 1948. Les acides nucléiques du plasma sanguin chez l'homme. C. R. Seances Soc. Biol. Fil. 142, 241–243.

Marburger, A., 2003. Alginate und Carrageenane – Eigenschaften, Gewinnung and Anwendungen in Schule und Hochschule (Doctoral dissertation) 437.

Margis, Regina, Margis, Rogério, Rieder, C.R.M., 2011. Identification of blood microRNAs associated to Parkinsońs disease. J. Biotechnol. 152, 96–101. https://doi.org/10.1016/j.jbiotec.2011.01.023

McAlexander, M.A., Phillips, M.J., Witwer, K.W., 2013. Comparison of Methods for miRNA Extraction from Plasma and Quantitative Recovery of RNA from Cerebrospinal Fluid. Front. Genet. 4. https://doi.org/10.3389/fgene.2013.00083

McDonald, J.S., Milosevic, D., Reddi, H.V., Grebe, S.K., Algeciras-Schimnich, A., 2011. Analysis of Circulating MicroRNA: Preanalytical and Analytical Challenges. Clin. Chem. 57, 833–840. https://doi.org/10.1373/clinchem.2010.157198

Mehal, W., Imaeda, A., 2010. Cell Death and Fibrogenesis. Semin. Liver Dis. 30, 226–231. https://doi.org/10.1055/s-0030-1255352

Meliopoulos, V.A., Schultz-Cherry, S., 2018. Although it's painful: The importance of stringent antibody validation. PLOS Pathog. 14, e1006701. https://doi.org/10.1371/journal.ppat.1006701

miRBase: Homo sapiens miRNAs (1917 sequences) [GRCh38] [WWW Document], n.d. URL http://www.mirbase.org/cgi-bin/mirna_summary.pl?org=hsa (accessed 2.8.19).

Mitchell, P.S., Parkin, R.K., Kroh, E.M., Fritz, B.R., Wyman, S.K., Pogosova-Agadjanyan, E.L., Peterson, A., Noteboom, J., O'Briant, K.C., Allen, A., Lin, D.W., Urban, N., Drescher, C.W., Knudsen, B.S., Stirewalt, D.L., Gentleman, R., Vessella, R.L., Nelson, P.S., Martin, D.B., Tewari, M., 2008. Circulating microRNAs as stable blood-based markers for cancer detection. Proc. Natl. Acad. Sci. U. S. A. 105, 10513–10518. https://doi.org/10.1073/pnas.0804549105

Moody, L., He, H., Pan, Y.-X., Chen, H., 2017. Methods and novel technology for microRNA quantification in colorectal cancer screening. Clin. Epigenetics 9. https://doi.org/10.1186/s13148-017-0420-9

Moss, E.G., Tang, L., 2003. Conservation of the heterochronic regulator Lin-28, its developmental expression and microRNA complementary sites. Dev. Biol. 258, 432–442. https://doi.org/10.1016/S0012-1606(03)00126-X

Nabet, B.Y., Qiu, Y., Shabason, J.E., Wu, T.J., Yoon, T., Kim, B.C., Benci, J.L., DeMichele, A.M., Tchou, J., Marcotrigiano, J., Minn, A.J., 2017. Exosome RNA Unshielding Couples Stromal Activation to Pattern Recognition Receptor Signaling in Cancer. Cell 170, 352-366.e13. https://doi.org/10.1016/j.cell.2017.06.031

Nagaoka, S., Murata, S., Kimura, K., Mori, T., Hojo, K., 2010. Antimicrobial activity of sodium citrate against Streptococcus pneumoniae and several oral bacteria: Antibacterial activity of citrate. Lett. Appl. Microbiol. 51, 546–551. https://doi.org/10.1111/j.1472-765X.2010.02932.x

Nath Neerukonda, S., Egan, N.A., Patria, J., Assakhi, I., Tavlarides-Hontz, P., Modla, S., Muñoz, E.R., Hudson, M.B., Parcells, M.S., 2019. Comparison of exosomes purified via ultracentrifugation (UC) and Total Exosome Isolation (TEI) reagent from the serum of Marek's disease virus (MDV)-vaccinated and tumor-bearing chickens. J. Virol. Methods 263, 1–9. https://doi.org/10.1016/j.jviromet.2018.10.004

Ng, E.K.O., Tsui, N.B.Y., Lam, N.Y.L., Chiu, R.W.K., Yu, S.C.H., Wong, S.C.C., Lo, E.S.F., Rainer, T.H., Johnson, P.J., Lo, Y.M.D., 2002. Presence of Filterable and

Nonfilterable mRNA in the Plasma of Cancer Patients and Healthy Individuals. Clin. Chem. 48, 1212–1217.

NucleoSpin miRNA Plasma [WWW Document], n.d. URL https://www.mn-net.com/ProductsBioanalysis/DNAandRNApurification/RNA/NucleoSpinmiRNAPlasma/tabid/11663/language/en-US/Default.aspx (accessed 3.6.19).

Oksvold, M.P., Neurauter, A., Pedersen, K.W., 2015. Magnetic bead-based isolation of exosomes. Methods Mol. Biol. Clifton NJ 1218, 465–481. https://doi.org/10.1007/978-1-4939-1538-5_27

Osteikoetxea, X., Németh, A., Sódar, B.W., Vukman, K.V., Buzás, E.I., 2016. Extracellular vesicles in cardiovascular disease: are they Jedi or Sith? J. Physiol. 594, 2881–2894. https://doi.org/10.1113/JP271336

Peng, Y., Croce, C.M., 2016. The role of MicroRNAs in human cancer. Signal Transduct. Target. Ther. 1, 15004. https://doi.org/10.1038/sigtrans.2015.4

Pérez-Bermúdez, P., Blesa, J., Soriano, J.M., Marcilla, A., 2017. Extracellular vesicles in food: Experimental evidence of their secretion in grape fruits. Eur. J. Pharm. Sci. Off. J. Eur. Fed. Pharm. Sci. 98, 40–50. https://doi.org/10.1016/j.ejps.2016.09.022

Piettre, M., Vila, A., 1920. On the separation of proteins of the serum. C R Hebd Seances Acad Sci 170, 1466–1468.

Polson, A., Potgieter, G.M., Largier, J.F., Mears, G.E., Joubert, F.J., 1964. THE FRACTIONATION OF PROTEIN MIXTURES BY LINEAR POLYMERS OF HIGH MOLECULAR WEIGHT. Biochim. Biophys. Acta 82, 463–475.

Posokhov, Y.O., Kyrychenko, A., 2013. Effect of acetone accumulation on structure and dynamics of lipid membranes studied by molecular dynamics simulations. Comput. Biol. Chem. 46, 23–31. https://doi.org/10.1016/j.compbiolchem.2013.04.005

Rajagopal, C., Harikumar, K.B., 2018. The Origin and Functions of Exosomes in Cancer. Front. Oncol. 8. https://doi.org/10.3389/fonc.2018.00066

Ramón-Núñez, L.A., Martos, L., Fernández-Pardo, Á., Oto, J., Medina, P., España, F., Navarro, S., 2017. Comparison of protocols and RNA carriers for plasma miRNA isolation. Unraveling RNA carrier influence on miRNA isolation. PLOS ONE 12, e0187005. https://doi.org/10.1371/journal.pone.0187005

Raposo, G., Stoorvogel, W., 2013. Extracellular vesicles: Exosomes, microvesicles, and friends. J. Cell Biol. 200, 373–383. https://doi.org/10.1083/jcb.201211138

Reinhart, B.J., Slack, F.J., Basson, M., Pasquinelli, A.E., Bettinger, J.C., Rougvie, A.E., Horvitz, H.R., Ruvkun, G., 2000. The 21-nucleotide *let-7* RNA regulates developmental timing in *Caenorhabditis elegans*. Nature 403, 901–906. https://doi.org/10.1038/35002607

Rider, M.A., Hurwitz, S.N., Jr, D.G.M., 2016. ExtraPEG: A Polyethylene Glycol-Based Method for Enrichment of Extracellular Vesicles. Sci. Rep. 6, 23978. https://doi.org/10.1038/srep23978

RNA Folding Form | mfold.rit.albany.edu [WWW Document], n.d. URL http://unafold.rna.albany.edu/?q=mfold/RNA-Folding-Form (accessed 3.6.19).

Roden, C., Gaillard, J., Kanoria, S., Rennie, W., Barish, S., Cheng, J., Pan, W., Liu, J., Cotsapas, C., Ding, Y., Lu, J., 2017. Novel determinants of mammalian primary microRNA processing revealed by systematic evaluation of hairpin-containing transcripts and human genetic variation. Genome Res. 27, 374–384. https://doi.org/10.1101/gr.208900.116

Sampey, G.C., Saifuddin, M., Schwab, A., Barclay, R., Punya, S., Chung, M.-C., Hakami, R.M., Zadeh, M.A., Lepene, B., Klase, Z.A., El-Hage, N., Young, M., Iordanskiy, S., Kashanchi, F., 2016. Exosomes from HIV-1-infected Cells Stimulate Production of Pro-inflammatory Cytokines through Trans-activating Response (TAR) RNA. J. Biol. Chem. 291, 1251–1266. https://doi.org/10.1074/jbc.M115.662171

Sansone, P., Savini, C., Kurelac, I., Chang, Q., Amato, L.B., Strillacci, A., Stepanova, A., Iommarini, L., Mastroleo, C., Daly, L., Galkin, A., Thakur, B.K., Soplop, N., Uryu, K., Hoshino, A., Norton, L., Bonafé, M., Cricca, M., Gasparre, G., Lyden, D., Bromberg, J., 2017. Packaging and transfer of mitochondrial DNA via exosomes regulate escape from dormancy in hormonal therapy-resistant breast cancer. Proc. Natl. Acad. Sci. U. S. A. 114, E9066–E9075. https://doi.org/10.1073/pnas.1704862114

Sanz-Rubio, D., Martin-Burriel, I., Gil, A., Cubero, P., Forner, M., Khalyfa, A., Marin, J.M., 2018. Stability of Circulating Exosomal miRNAs in Healthy Subjects. Sci. Rep. 8, 10306. https://doi.org/10.1038/s41598-018-28748-5

Schöneberg, J., Lee, I.-H., Iwasa, J.H., Hurley, J.H., 2017. Reverse-topology membrane scission by the ESCRT complexes. Nat. Rev. Mol. Cell Biol. 18, 5–17. https://doi.org/10.1038/nrm.2016.121

Schwarzenbach, H., 2017a. Clinical Relevance of Circulating, Cell-Free and Exosomal microRNAs in Plasma and Serum of Breast Cancer Patients. Oncol. Res. Treat. 40, 423–429. https://doi.org/10.1159/000478019

Schwarzenbach, H., 2017b. Methods for quantification and characterization of microRNAs in cell-free plasma/serum, normal exosomes and tumor-derived exosomes. Transl. Cancer Res. 7, S253-S263–S263. https://doi.org/10.21037/16263

Schwarzenbach, H., 2016a. Clinical significance of miR-15 and miR-16 in ovarian cancer. Transl. Cancer Res. 5, S50-S53–S53. https://doi.org/10.21037/7660

Schwarzenbach, H., 2016b. Diagnostic relevance of circulating cell-free and exosomal microRNAs and long non-coding RNAs in blood of cancer patients. LaboratoriumsMedizin 40. https://doi.org/10.1515/labmed-2016-0033

Schwarzenbach, H., 2015. The clinical relevance of circulating, exosomal miRNAs as biomarkers for cancer. Expert Rev. Mol. Diagn. 15, 1159–1169. https://doi.org/10.1586/14737159.2015.1069183

Schwarzenbach, H., Hoon, D.S.B., Pantel, K., 2011. Cell-free nucleic acids as biomarkers in cancer patients. Nat. Rev. Cancer 11, 426–437. https://doi.org/10.1038/nrc3066

Schwarzenbach, H., Nishida, N., Calin, G.A., Pantel, K., 2014. Clinical relevance of circulating cell-free microRNAs in cancer. Nat. Rev. Clin. Oncol. 11, 145–156. https://doi.org/10.1038/nrclinonc.2014.5

Shingara, J., Keiger, K., Shelton, J., Laosinchai-Wolf, W., Powers, P., Conrad, R., Brown, D., Labourier, E., 2005. An optimized isolation and labeling platform for accurate microRNA expression profiling. RNA N. Y. N 11, 1461–1470. https://doi.org/10.1261/rna.2610405

Shrestha, A., Mukhametshina, R.T., Taghizadeh, S., Vásquez-Pacheco, E., Cabrera-Fuentes, H., Rizvanov, A., Mari, B., Carraro, G., Bellusci, S., 2017. MicroRNA-142 is a multifaceted regulator in organogenesis, homeostasis, and disease. Dev. Dyn. 246, 285–290. https://doi.org/10.1002/dvdy.24477

Smith, G.S., Walter, G.L., Walker, R.M., 2013. Chapter 18 - Clinical Pathology in Non-Clinical Toxicology Testing, in: Haschek, W.M., Rousseaux, C.G., Wallig, M.A. (Eds.), Haschek and Rousseaux's Handbook of Toxicologic Pathology (Third Edition). Academic Press, Boston, pp. 565–594. https://doi.org/10.1016/B978-0-12-415759-0.00018-2

Sohel, M.H., 2016. Extracellular/Circulating MicroRNAs: Release Mechanisms, Functions and Challenges. Achiev. Life Sci. 10, 175–186. https://doi.org/10.1016/j.als.2016.11.007

Soreq, L., Salomonis, N., Bronstein, M., Greenberg, D.S., Israel, Z., Bergman, H., Soreq, H., 2013. Small RNA sequencing-microarray analyses in Parkinson leukocytes reveal deep brain stimulation-induced splicing changes that classify brain region transcriptomes. Front. Mol. Neurosci. 6. https://doi.org/10.3389/fnmol.2013.00010

Stein, E.V., Duewer, D.L., Farkas, N., Romsos, E.L., Wang, L., Cole, K.D., 2017. Steps to achieve quantitative measurements of microRNA using two step droplet digital PCR. PLoS ONE 12. https://doi.org/10.1371/journal.pone.0188085

Stevic, I., Müller, V., Weber, K., Fasching, P.A., Karn, T., Marmé, F., Schem, C., Stickeler, E., Denkert, C., van Mackelenbergh, M., Salat, C., Schneeweiss, A., Pantel, K., Loibl, S., Untch, M., Schwarzenbach, H., 2018. Specific microRNA signatures in exosomes of triple-negative and HER2-positive breast cancer patients undergoing neoadjuvant therapy within the GeparSixto trial. BMC Med. 16. https://doi.org/10.1186/s12916-018-1163-y

Stroun, M., Anker, P., Maurice, P., Gahan, P.B., 1977. Circulating nucleic acids in higher organisms. Int. Rev. Cytol. 51, 1–48.

Szatanek, R., Baj-Krzyworzeka, M., Zimoch, J., Lekka, M., Siedlar, M., Baran, J., 2017. The Methods of Choice for Extracellular Vesicles (EVs) Characterization. Int. J. Mol. Sci. 18. https://doi.org/10.3390/ijms18061153

Taha, M., Lee, M.-J., 2010. Interactions of TRIS [tris(hydroxymethyl)aminomethane] and related buffers with peptide backbone: Thermodynamic characterization. Phys. Chem. Chem. Phys. 12, 12840–12850. https://doi.org/10.1039/C0CP00253D

Takov, K., Yellon, D.M., Davidson, S.M., 2019. Comparison of small extracellular vesicles isolated from plasma by ultracentrifugation or size-exclusion

chromatography: yield, purity and functional potential. J. Extracell. Vesicles 8, 1560809. https://doi.org/10.1080/20013078.2018.1560809

Théry, C., Amigorena, S., Raposo, G., Clayton, A., 2006. Isolation and characterization of exosomes from cell culture supernatants and biological fluids. Curr. Protoc. Cell Biol. Chapter 3, Unit 3.22. https://doi.org/10.1002/0471143030.cb0322s30

Tiberio, P., Callari, M., Angeloni, V., Daidone, M.G., Appierto, V., 2015. Challenges in Using Circulating miRNAs as Cancer Biomarkers. BioMed Res. Int. 2015. https://doi.org/10.1155/2015/731479

Tietje, A., Maron, K.N., Wei, Y., Feliciano, D.M., 2014. Cerebrospinal Fluid Extracellular Vesicles Undergo Age Dependent Declines and Contain Known and Novel Non-coding RNAs. PLOS ONE 9, e113116. https://doi.org/10.1371/journal.pone.0113116

Trajkovic, K., Hsu, C., Chiantia, S., Rajendran, L., Wenzel, D., Wieland, F., Schwille, P., Brugger, B., Simons, M., 2008. Ceramide Triggers Budding of Exosome Vesicles into Multivesicular Endosomes. Science 319, 1244–1247. https://doi.org/10.1126/science.1153124

Tsui, N.B.Y., Ng, E.K.O., Lo, Y.M.D., 2002. Stability of Endogenous and Added RNA in Blood Specimens, Serum, and Plasma. Clin. Chem. 48, 1647–1653.

Turchinovich, A., Weiz, L., Langheinz, A., Burwinkel, B., 2011. Characterization of extracellular circulating microRNA. Nucleic Acids Res. 39, 7223–7233. https://doi.org/10.1093/nar/gkr254

Valadi, H., Ekström, K., Bossios, A., Sjöstrand, M., Lee, J.J., Lötvall, J.O., 2007. Exosome-mediated transfer of mRNAs and microRNAs is a novel mechanism of genetic exchange between cells. Nat. Cell Biol. 9, 654–659. https://doi.org/10.1038/ncb1596

Van Deun, J., Mestdagh, P., Sormunen, R., Cocquyt, V., Vermaelen, K., Vandesompele, J., Bracke, M., De Wever, O., Hendrix, A., 2014. The impact of disparate isolation methods for extracellular vesicles on downstream RNA profiling. J. Extracell. Vesicles 3. https://doi.org/10.3402/jev.v3.24858

Vickers, K.C., Palmisano, B.T., Shoucri, B.M., Shamburek, R.D., Remaley, A.T., 2011. MicroRNAs are Transported in Plasma and Delivered to Recipient Cells by High-Density Lipoproteins. Nat. Cell Biol. 13, 423–433. https://doi.org/10.1038/ncb2210

Vigneron, N., Meryet-Figuière, M., Guttin, A., Issartel, J.-P., Lambert, B., Briand, M., Louis, M.-H., Vernon, M., Lebailly, P., Lecluse, Y., Joly, F., Krieger, S., Lheureux, S., Clarisse, B., Leconte, A., Gauduchon, P., Poulain, L., Denoyelle, C., 2016. Towards a new standardized method for circulating miRNAs profiling in clinical studies: Interest of the exogenous normalization to improve miRNA signature accuracy. Mol. Oncol. 10, 981–992. https://doi.org/10.1016/j.molonc.2016.03.005

Wahid, F., Shehzad, A., Khan, T., Kim, Y.Y., 2010. MicroRNAs: Synthesis, mechanism, function, and recent clinical trials. Biochim. Biophys. Acta BBA - Mol. Cell Res. 1803, 1231–1243. https://doi.org/10.1016/j.bbamcr.2010.06.013

Wang, Z., Wu, H., Fine, D., Schmulen, J., Hu, Y., Godin, B., Zhang, J.X.J., Liu, X., 2013. Ciliated micropillars for the microfluidic-based isolation of nanoscale lipid vesicles. Lab. Chip 13, 2879–2882. https://doi.org/10.1039/c3lc41343h

Weng, Y., Sui, Z., Shan, Y., Hu, Y., Chen, Y., Zhang, L., Zhang, Y., 2016. Effective isolation of exosomes with polyethylene glycol from cell culture supernatant for in-depth proteome profiling. Analyst 141, 4640–4646. https://doi.org/10.1039/C6AN00892E

Witwer, K.W., Buzás, E.I., Bemis, L.T., Bora, A., Lässer, C., Lötvall, J., Nolte-‘t Hoen, E.N., Piper, M.G., Sivaraman, S., Skog, J., Théry, C., Wauben, M.H., Hochberg, F., 2013. Standardization of sample collection, isolation and analysis methods in extracellular vesicle research. J. Extracell. Vesicles 2. https://doi.org/10.3402/jev.v2i0.20360

Yamamoto, K.R., Alberts, B.M., Benzinger, R., Lawhorne, L., Treiber, G., 1970. Rapid bacteriophage sedimentation in the presence of polyethylene glycol and its application to large-scale virus purification. Virology 40, 734–744.

Yan, L., Liang, M., Hou, X., Zhang, Y., Zhang, H., Guo, Z., Jinyu, J., Feng, Z., Mei, Z., 2019. The role of microRNA-16 in the pathogenesis of autoimmune diseases: A comprehensive review. Biomed. Pharmacother. Biomedecine Pharmacother. 112, 108583. https://doi.org/10.1016/j.biopha.2019.01.044

Yassin, A.M., Abdel Hamid, M.I., Farid, O.A., Amer, H., Warda, M., 2016. Dromedary milk exosomes as mammary transcriptome nano-vehicle: Their isolation, vesicular and phospholipidomic characterizations. J. Adv. Res. 7, 749–756. https://doi.org/10.1016/j.jare.2015.10.003

Yoo, Y.K., Lee, J., Kim, H., Hwang, K.S., Yoon, D.S., Lee, J.H., 2018. Toward Exosome-Based Neuronal Diagnostic Devices. Micromachines 9. https://doi.org/10.3390/mi9120634

Zeugin, J.A., Hartley, J.L., 1985. Ethanol precipitation of DNA. Focus 7, 1–2.

Zhang, H., Freitas, D., Kim, H.S., Fabijanic, K., Li, Z., Chen, H., Mark, M.T., Molina, H., Martin, A.B., Bojmar, L., Fang, J., Rampersaud, S., Hoshino, A., Matei, I., Kenific, C.M., Nakajima, M., Mutvei, A.P., Sansone, P., Buehring, W., Wang, H., Jimenez, J.P., Cohen-Gould, L., Paknejad, N., Brendel, M., Manova-Todorova, K., Magalhães, A., Ferreira, J.A., Osório, H., Silva, A.M., Massey, A., Cubillos-Ruiz, J.R., Galletti, G., Giannakakou, P., Cuervo, A.M., Blenis, J., Schwartz, R., Brady, M.S., Peinado, H., Bromberg, J., Matsui, H., Reis, C.A., Lyden, D., 2018. Identification of distinct nanoparticles and subsets of extracellular vesicles by asymmetric flow field-flow fractionation. Nat. Cell Biol. 20, 332. https://doi.org/10.1038/s41556-018-0040-4

Zhang, L., Zhang, S., Yao, J., Lowery, F.J., Zhang, Q., Huang, W.-C., Li, P., Li, M., Wang, X., Zhang, C., Wang, H., Ellis, K., Cheerathodi, M., McCarty, J.H., Palmieri, D., Saunus, J., Lakhani, S., Huang, S., Sahin, A.A., Aldape, K.D., Steeg, P.S., Yu, D., 2015. Microenvironment-induced PTEN loss by exosomal microRNA primes brain metastasis outgrowth. Nature 527, 100–104. https://doi.org/10.1038/nature15376

Zijlstra, A., Di Vizio, D., 2018. Size matters in nanoscale communication. Nat. Cell Biol. 20, 228–230. https://doi.org/10.1038/s41556-018-0049-8

IX. ACKNOWLEDGMENTS

At first, I would like to express my sincere gratitude to my supervisor PD. Dr. Heidi Schwarzenbach, who helped me to plan and organize the workflow of my doctoral research, incessantly supported me with her brilliant ideas and gave me this great opportunity to work in her lab. Without her patience and motivational support, it would have been impossible to finish this thesis.

Besides my supervisor, I also own a debt of gratitude to Dr. Timo Hillebrand for giving me the opportunity to join his research and development team, as well as for providing an interesting research topic and laboratory facilities. Without his precious support, it would have not been possible to conduct this research.

I would like to thank my co-supervisor Prof. Dr. Julia Kehr for her time and support, as well as to the other members of my doctoral defense committee Prof. Wim Walter and PD Dr. Harwig Lüthen for their insightful comments.

My sincere thanks go to Dr. Elmara Graser and Vipulkumar Patel for the stimulating discussions, helpfulness, technical support and all the pleasure of working together last years.

My thanks also go to Robert Muirhead for proofreading of my thesis.

My special thanks go to Bettina Steinbach and Dr. Ines Stevic for their kind advices, help, technical support and time we spent together.

I would like to thank Dr. Antonio Virgilio Faila for his endless patience, expertise, and support by performing life imaging microscopy observations.

Many thanks to my colleagues: Jacqueline, Angela, Katjana, Thorsten, Kathrin, Uwe, Kristin, Wiebke, Stephan, Andreas and Rainer who by their kindness and support facilitated my first steps in Germany.

I would also like to say a heartfelt thank you to Federico who mentally supported me and constantly motivated to complete once started journey.

However, my biggest gratitude I direct to my parents, who as first taught me how important is the education, sacrificed so much to enable my studies and always were on my side during my ups and downs [Polish: Jednak moją największą wdzięczność kieruję do moich rodziców, którzy jako pierwsi nauczyli mnie, jak ważna jest edukacja, poświęcili tak wiele, aby umożliwić mi moje studia i zawsze byli przy mnie podczas moich wzlotów i upadków].

X. DECLARATION ON OATH

I hereby declare, on oath, that I have written the present dissertation by my own and have not used other than the acknowledged resources and aids.

Hamburg, 19.08.2019

XI. EIDESSTATTLICHE VERSICHERUNG

Hiermit erkläre ich an Eides statt, dass ich die vorliegende Dissertationsschrift selbst verfasst und keine anderen als die angegebenen Quellen und Hilfsmittel benutzt habe.

Hamburg, den 19.08.2019